

Hydrogen-Atom Transfer Photochemistry of  
Tetrakis( $\mu$ -pyrophosphito)diplatinate(II)

Thesis by Robert J. Sweeney

In Partial Fulfillment of the Requirements for the Degree of Doctor  
of Philosophy

California Institute of Technology

Pasadena, CA 1990

(Submitted May 23, 1990)

All my life I've been a blade of grass in the wind  
Or like a stubborn tree I let the wind shape me  
But now, I'm feeling bold enough to let go my hold  
And I'll not be a blade of grass again  
I'm gonna be the wind

-Laurie Lewis

## Acknowledgements

Harry Gray provided me with options, which at times are more valuable than almost anything else. Of course, Harry's also a great source of humor and perspective and he's taught me a lot of what I thought I came to Caltech to learn. Jack Beauchamp helped me learn lessons which I never intended to learn, but as it turns out, I'm glad I did. Tom Dunn seems like my third advisor. For four years, he was a most accessible and helpful guide through what I often thought of as a swamp of electronics and design.

The departmental staff members are consistently friendly and competent, which makes the life of a graduate student so much easier. Pat Bullard, Virginia Russell, Beth Kearns, Fran Bennett and John Seibert come to mind as people who have actually shocked me with their willingness and capacity to take care of things that I thought were going to become ordeals.

Of course, the men at the instrument shop are the epitome of quality and, at times, tolerance. Guy Duremberg, Ray Garcia, Delmer Dill and Tony Stark have always given their sound advice, pushed things through when I really needed them now, and put up with me when I got obnoxious.

The present and former members of the Beauchamp group helped me in many ways. Maggie I remember first for welcoming me into the group. And I guess Gary did too, in his own style. Seung-Koo, Dave and Bruce supported in a big-brotherly fashion; Pat stepped in occasionally as a much-needed big sister. Karl deserves much of the credit for keeping me going in lab when things would hit the bottom

and he also deserves a lot of thanks for when things were going well, too.

The Gray group turned out to be a valuable experience for many reasons, only one of which is academic. Mark, John, "crowbar" Julia, Wayne, Ramy, David and Jong-Ho make a fun and rather quirky group of co-workers (or, more often, co-nonworkers).

Although I came to Caltech for a "scientific experience," I certainly learned a lot more outside Noyes Lab than I did inside it. Thanks to my "other advisors" Ann, Scott, Claudia, Van, Bruce, Joseph, "Ram," Dave, Jonathan and Mark. They opened up whole new worlds to me and I certainly won't be the same again. I'll remember my time at Caltech most for the trips. Trips to the desert (for fun and protest), trips to concerts, trips around town. I've been lucky in having a sense of family while in Pasadena.

Of course, Erica's filled all the roles I've mentioned so far. I look forward to our future collaborations.

## Abstract

In many senses, the hydrogen-atom transfer reactions observed with the triplet excited state of pyrophosphito-bridged platinum(II) dimers resemble the reactions of organic ketone  $n\pi^*$  states. The first two chapters describe our attempts to understand the reactivity differences between these two chromophores. Reactivity of the metal dimers is strongly regulated by the detailed nature of the ligands that ring the axial site, the hydrogen-abstraction center. A hydrogen-bonded network linking the ligands facilitates H-atom transfer quenching with alcohols through the formation of a hydrogen-bonded complex between the alcohol and a dimer. For substrates of equal C-H bond strength that lack a hydroxyl group (e.g., benzyl hydrocarbons), the quenching rate is several orders of magnitude slower.

The shape and size of the axial site, as determined by the ligands, also discriminate among quenchers by their steric characteristics. Very small quenchers quench slowly because of high entropies of activation, while very large ones have large enthalpic barriers. The two effects find a balance with quenchers of "just the right size."

The third chapter discusses the design of a mass spectrometer that uses positron annihilation to ionize neutral molecules. The mass spectrometer creates positron-molecule adducts whose annihilation produces fragmentation products that may yield information on the bonding of positrons in such complexes.

**Table of Contents**

	<b>Page</b>
Dedication	ii
Acknowledgements	iii
Abstract	v
Table of Contents	vi
List of Tables	vii
List of Figures	ix
Chapter 1 Introduction	2
Experimental Details	5
Results and Discussion	9
Appendix 1	26
Appendix 2	29
References	41
Chapter 2 Introduction	44
Experimental Details	47
Results and Discussion	52
References	64
Appendix	66
Chapter 3 Introduction	109
Mass Spectrometer Design	116
Data Analysis	125
Instrumental Details	130
References	145

## List of Tables

<b>Chapter 1</b>	<b>Page</b>
Table 1 $^3\text{Pt}_2^*$ Stern-Volmer quenching rate constants for organic H-atom donors Alcohols RR'CHOH	11
Table 2 $^3\text{Pt}_2^*$ phosphorescence quenching parameters for selected alcohols RR'CHOH	16
Table 3.     Arrhenius parameters for $^3\text{Pt}_2^*$ phosphorescence quenching by alcohols RR'CHOH	18
Table 4     Product formation rates and reaction efficiencies for selected quenchers	24
 <b>Chapter 2</b>	
Table 1.     Selected bond distances for $\text{BF}_2\text{Pt}_2$ and $\text{Pt}_2$	53
Table 2.     Selected bond angles for $\text{BF}_2\text{Pt}_2$ and $\text{Pt}_2$ .	53
Table 3.     Selected geometric parameters for $\text{BF}_2\text{Pt}_2$ and other $\text{BF}_2$ -bridged square-planar, platinum phosphito complexes.	55
Table 4.     Emission parameters for $\text{BF}_2\text{Pt}_2$ and $\text{Pt}_2$	59
Table 5.     Photophysical parameters for axial dihydrides	59
Table 6.     Stern-Volmer quenching rate constants for the reaction of excited platinum dimers and organic H-atom donors	62
Table A1     Crystal and Intensity Collection Data for Tetrakis(tetra- <i>n</i> -butylammonium) tetrakis(bis (difluoroborato)- $\mu$ -pyrophosphito)diplatinate(II)	67

Table A2	Final Anion Parameters for Tetrakis(tetra- <i>n</i> -butylammonium) tetrakis(bis(difluoroborato)- $\mu$ -pyrophosphito)diplatinate(II)	68
Table A3	Final Cation Parameters for Tetrakis(tetra- <i>n</i> -butylammonium) tetrakis(bis(difluoroborato)- $\mu$ -pyrophosphito)diplatinate(II)	70
Table A4	Assigned Hydrogen Parameters for Tetrakis(tetra- <i>n</i> -butylammonium) tetrakis(bis(difluoroborato)- $\mu$ -pyrophosphito)diplatinate(II)	71
Table A5	Anisotropic Parameters for Tetrakis(tetra- <i>n</i> -butylammonium) tetrakis(bis(difluoroborato)- $\mu$ -pyrophosphito)diplatinate(II)	73
Table A6	Complete Distances and Angles for Tetrakis (tetra- <i>n</i> -butylammonium) tetrakis(bis (difluoroborato)- $\mu$ -pyrophosphito)diplatinate(II)	74
Table A7	Observed and Calculated Structure Factors for Tetrakis(tetra- <i>n</i> -butylammonium) tetrakis(bis (difluoroborato)- $\mu$ -pyrophosphito)diplatinate(II)	80

### Chapter 3

Table 1	Critical charges for the attachment of positrons to free atoms.	112
---------	---	-----



## List of Figures

Chapter	1	Page
Figure 1	The structure of the tetrakis( $\mu$ -pyrophosphito) diplatinate(II) tetraanion	3
Figure 2	The dependence of the $^3\text{Pt}_2^*$ quenching rate constant on the C-H bond strength for a variety of organic H-atom donor quenchers. Squares represent data for sterically hindered alcohols.	10
Figure 3	A proposed view of alcohol "docking" onto $\text{Pt}_2$ ligands.	13
Figure 4	The Stern-Volmer quenching plot for the quenching of $^3\text{Pt}_2^*$ phosphorescence with $\alpha$ -methylbenzyl alcohol.	15
Figure 5	Quenching data for the reaction of $\alpha$ -methylbenzyl alcohol with $^3\text{Pt}_2^*$ plotted according to Equation (3).	17
Figure 6	The variation of the Stern-Volmer quenching rate $k_q$ as a function of the cone angle of $\alpha$ -substituents on benzyl alcohols.	20
Figure 7	Absorption of the 313 nm $\text{Pt}_2\text{H}_2$ band as a function of the time of irradiation into the $\text{Pt}_2$ absorption band at 372 nm. The H-atom donor quencher is benzyl alcohol (0.077M).	23
Figure 8	Calibration plot for the quantitative determination of bibenzyl using biphenyl as an internal GC standard.	30

Figure 9	Stern-Volmer plot for the quenching of ${}^3\text{Pt}_2^*$ phosphorescence by ethylbenzene	31
Figure 10	Stern-Volmer plot for the quenching of ${}^3\text{Pt}_2^*$ phosphorescence by $\alpha$ -deuterio- $\alpha$ -methylbenzyl alcohol	32
Figure 11	Stern-Volmer plot for the quenching of ${}^3\text{Pt}_2^*$ phosphorescence by ethylene glycol	33
Figure 12	Michaelis-Menten plot for the quenching of ${}^3\text{Pt}_2^*$ phosphorescence by ethylene glycol	34
Figure 13	Temperature dependence of the rate of ${}^3\text{Pt}_2^*$ phosphorescence quenching by ethylene glycol (9.0M)	35
Figure 14	Temperature dependence of the rate of ${}^3\text{Pt}_2^*$ phosphorescence quenching by $\alpha$ -methylbenzyl alcohol (0.24M)	36
Figure 15	Temperature dependence of the rate of ${}^3\text{Pt}_2^*$ phosphorescence quenching by $\alpha$ -methylbenzyl alcohol (6.0M)	37
Figure 16	Stern-Volmer plot for the quenching of ${}^3\text{Pt}_2^*$ phosphorescence by 3-methyl-2-butanol	38
Figure 17	Michaelis-Menten plot for the quenching of ${}^3\text{Pt}_2^*$ phosphorescence by 3-methyl-2-butanol	39
Figure 18	Temperature dependence of the rate of ${}^3\text{Pt}_2^*$ phosphorescence quenching by 3-methyl-2-butanol (7.4M)	40

**Chapter 2**

- Figure 1 Structure of one face of the tetrakis( $\mu$ -pyrophosphito)diplatinate(II) tetraanion. 45
- Figure 2 An ORTEP drawing of tetrakis(bis(difluoroborato)- $\mu$ -pyrophosphito)diplatinate(II). Thermal ellipsoids are shown at the 20% probability level; the  $\text{BF}_2$  groups are one-tenth scale. 46
- Figure 3 An ORTEP drawing of one face of the tetrakis(bis(difluoroborato)- $\mu$ -pyrophosphito)diplatinate(II) tetraanion shown at the 10% probability level. 54
- Figure 4 Structures of previously reported difluoroborato-substituted, square-planar, phosphito platinum complexes. 57
- Figure 5 Quenching rates for  $^3\text{Pt}_2^*$  and  $^3\text{BF}_2\text{Pt}_2^*$  phosphorescence with H-atom donors in acetonitrile solutions at room temperature. 61

**Chapter 3**

- Figure 1 A schematic diagram of the Positron Annihilation Mass Spectrometer. 117
- Figure 2 The PEPICO diagram for ethylene. 127
- Figure 3 The photoelectron spectrum for ethylene. 128
- Figure 4 A flowchart describing the electronic controls of the Positron Annihilation Mass Spectrometer. 137
- Figure 5 The Gate circuit. 139
- Figure 6 The Switch circuit. 140

Figure 7	The Inverter circuit.	141
Figure 8	The Extract circuit.	142

---

---

**Chapter 1**Hydrogen-Atom Transfer Reactions of  ${}^3\text{Pt}_2^*$  with Alcohols and  
Aromatic Hydrocarbons

---

---

Robert J. Sweeney, Erica L. Harvey, Harry B. Gray

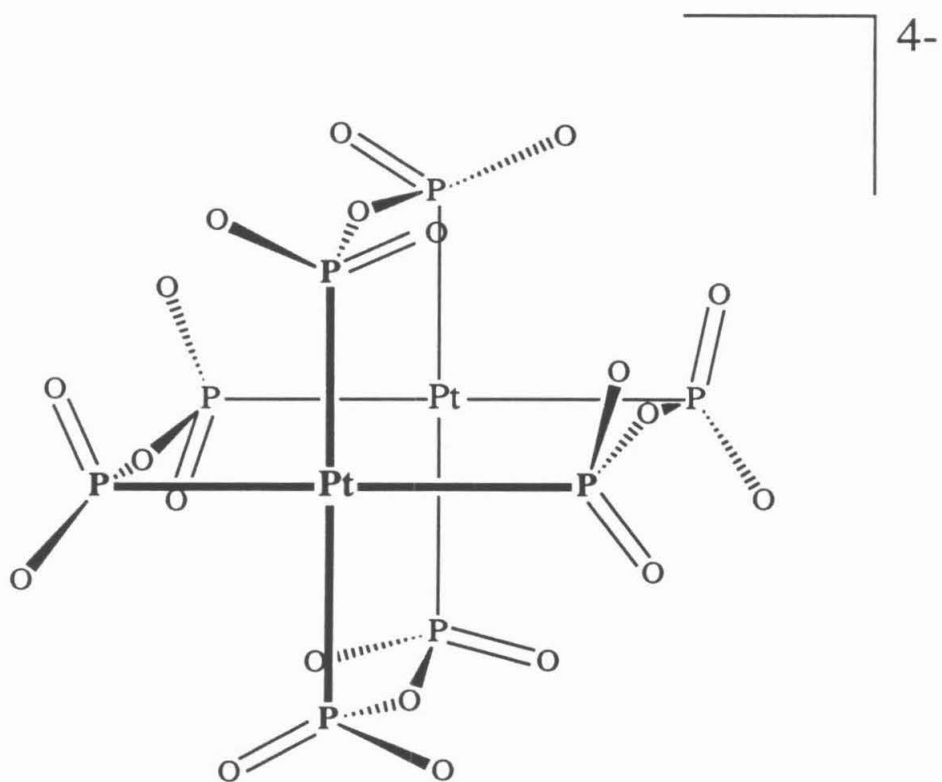
## Introduction

The triplet excited state of tetrakis( $\mu$ -pyrophosphito) diplatinate(II) (Figure 1, ground state abbreviated Pt<sub>2</sub>) is deactivated by reaction with a variety of hydrogen-donating organic species,<sup>1, 2</sup> including alcohols,<sup>3-5</sup> benzyl hydrocarbons,<sup>4</sup> alkenes<sup>3, 6</sup> and main-group hydrides.<sup>7</sup> The initial photoproducts are organic radicals, and the monohydride Pt<sub>2</sub>H;<sup>3, 5, 8</sup> subsequent, poorly understood, steps lead to formation of the stable axial dihydride Pt<sub>2</sub>H<sub>2</sub><sup>9</sup> and typical organic radical products (e.g., dimers from alkanes, ketones from alcohols).<sup>4</sup> In contrast to other hydrogen-abstraction reactions, the hydrogenated product Pt<sub>2</sub>H<sub>2</sub> is efficiently photoconverted back to Pt<sub>2</sub> with the evolution of H<sub>2</sub>, thus completing a catalytic cycle.<sup>9</sup>



The vast range of rate constants<sup>3</sup> for the C-H activation step (2) suggests that Pt<sub>2</sub> may be useful in selective functionalization of organic substrates. The utility of Pt<sub>2</sub> as a photo-dehydrogenation catalyst depends on several factors that are not well understood,

**Figure 1.** The structure of the tetrakis( $\mu$ -pyrophosphito) diplatinate(II) tetraanion.



Note: Protons (not shown) bridge neighboring P=O and P-O groups

namely, dehydrogenation selectivity and overall reaction efficiencies.

In an effort to address these questions, we have examined in detail the reactions of alcohols and aromatic hydrocarbons with  $^3\text{Pt}_2^*$ . In contrast to previous work on  $^3\text{Pt}_2^*$  dehydrogenations, the rates of both the initial abstraction step and the stable product formation have been determined.

Several excellent reviews of  $\text{Pt}_2^{1, 2}$  and its photochemistry<sup>10</sup> have recently been published. An extensive background will not be presented here, and readers are referred to these articles for further information.



## Experimental Details

**Materials.** The tetra-*n*-butylammonium (TBA) salt of Pt<sub>2</sub> was prepared from the potassium salt as described previously.<sup>11</sup> The tetra-*n*-octylammonium (TOA) salt is prepared by vigorous mixing of ethyl ether with an aqueous mixture of K<sub>4</sub>Pt<sub>2</sub> and TOABr (Aldrich 98%), followed by drying and evaporation of the ether phase. [TOA]<sub>4</sub>Pt<sub>2</sub> is a yellow, viscous oil that resisted attempts at crystallization. Calculated 54.1%C, 9.88%H, 2.0%N. Found 54.4%C, 9.81%H, 1.55%N. [TOA]<sub>4</sub>Pt<sub>2</sub> dissolves in diethyl ether, toluene, methylene chloride and acetonitrile, but not in water.

Burdick and Jackson High-Purity, UV grade acetonitrile was used as received as solvent for all experiments. Isopropanol, 2-butanol (Aldrich Gold Label 99+%), 3-methyl-2-butanol (Aldrich 99%), toluene (Burdick and Jackson High-Purity Solvent) and ethylene glycol (Aldrich 99+%) were used as received. Benzyl alcohol, 1-phenyl-1-ethanol (methylbenzyl alcohol), 1-phenyl-1-propanol and diphenylmethane were purchased from Aldrich, reagent grade; 2-methyl-1-phenyl-1-propanol was purchased from Wiley, 97%. Purification of ethylbenzene, cumene and *tert*-butylbenzene is detailed elsewhere.<sup>12</sup> The liquid alcohols and hydrocarbons were purified by fractional distillation under vacuum or a nitrogen atmosphere and stored under nitrogen or argon. The solid quencher 2,2-dimethyl-1-phenyl-1-propanol (Wiley 97%) was sublimed under vacuum two times immediately prior to use. The monodeuterated alcohol PhCD(OH)CH<sub>3</sub> was synthesized by reducing acetophenone with NaBD<sub>4</sub> and quenching the reaction with H<sub>2</sub>O.

**Quenching studies.** Acetonitrile solutions containing  $[\text{TBA}]_4\text{Pt}_2$  ( $1\text{-}3 \times 10^{-4}$  M) plus incrementally varied quencher concentrations were degassed with at least 5 freeze-pump-thaw cycles on a vacuum line with a limiting pressure of  $\sim 10^{-5}$  torr. Quenchers were added directly to the quenching cell (roundbottom flask connected by two arms to 1 mm and 1 cm cuvettes and sealed by teflon vacuum valves), using a syringe of the appropriate volume (between 10  $\mu\text{L}$  and 1 mL); the solution was opened to air for the addition of each quencher aliquot. Alternatively, relatively concentrated quencher solutions were successively diluted by additions of acetonitrile. Excited-state lifetimes ( $\tau$ ) were measured with a Quanta Ray Nd:YAG (8 ns fwhm; 355 nm excitation) laser system described elsewhere.<sup>13</sup> Emission was monitored at 518 nm. Quenching rate constants and the quantities derived from them have estimated associated errors of <10%.

Cumene and ethylbenzene react rapidly with  $\text{Pt}_2$  in the presence of air with loss of  $\text{Pt}_2$ , requiring mixing of the two during quenching studies only after degassing.  $[\text{TOA}]_4\text{Pt}_2$  in neat toluene also degrades rapidly in the presence of air.

Normal quenching studies were performed at room temperature. For activation parameter studies, temperature was controlled in the range 6°C to 80°C through immersion of the quenching cell in a water bath. The lifetime of  ${}^3\text{Pt}_2^*$  in  $\text{CH}_3\text{CN}$  remains constant throughout the temperature range studied. Thus, changes in the  ${}^3\text{Pt}_2^*$  lifetime as temperature varies, in the presence of a given quencher concentration, directly reflect changes in the quenching rate.

Kinetic data were analyzed by either linear Stern-Volmer plots of  $(1/\tau - 1/\tau_0)$  versus quencher concentration  $[Q]$ , or linear Michaelis-Menten plots of  $(1/\tau - 1/\tau_0)^{-1}$  versus  $[Q]^{-1}$ .

The lifetime  $\tau$  of  $[\text{TOA}]_4\text{Pt}_2$  phosphorescence in toluene is 7.3  $\mu\text{sec}$ . An unquenched  $\tau_0$  of 10.3  $\mu\text{sec}$  in toluene is calculated if  $k_q$  is assumed to be the same as that found in  $\text{CH}_3\text{CN}$  solutions ( $k_q = 4.2 \times 10^3 \text{M}^{-1}\text{s}^{-1}$ ). Therefore,  $\tau_0$  is approximately invariant in acetonitrile, methanol and toluene! In quenching studies that employ high quencher concentrations, the quenchers may begin to alter the solvent's properties and therefore may change the unquenched lifetime of excited states, which may be sensitive to solvent viscosity or other properties. Since changes in the solvent medium do not significantly alter the natural lifetime  $\tau_0$  of  $\text{Pt}_2$ , such effects are negligible and lifetime changes can be attributed solely to changes in the quenching rate.

**Bulk photolyses.** Acetonitrile solutions of  $[\text{TBA}]_4\text{Pt}_2$  ( $\sim 3 \times 10^{-4} \text{M}$ ) were degassed with at least 5 freeze-pump-thaw cycles. Solutions were irradiated in a 1 cm cell, and the absorption changes were measured in an attached 1 mm cell. Cary 14 and Shimadzu UV-260 absorption spectrometers were used. For the irradiation source, a 1000W Hg-Xe lamp with cutoff and band-pass optical filters provided a photon flux of  $\sim 10^{-7} \text{Ei s}^{-1}$  for the wavelength range 340 nm to 400 nm. Actinometry was performed with Aberchrome 540, or *trans*-2-(2,5-dimethyl-3-furanyl)ethylidene-3-(1-methylethylidene)succinic anhydride, dissolved in degassed toluene (Burdick and Jackson High-Purity Solvent). Absorptions of both the actinometer and  $\text{Pt}_2$  solutions are

sufficiently high that all photons reaching the solutions are absorbed.

**Product Identification.** Products were identified by gas chromatography and their retention times compared to those of authentic samples. In some cases the products were also identified through  $^1\text{H}$  NMR. Prior to GC analysis,  $\text{KPF}_6$  was added to photolyzed solutions to precipitate the platinum complex. Both Carbowax and glass columns were used with a flame ionization detector on the Hewlett-Packard 8410 GC. GC peak areas are proportional to moles of carbon detected; this relationship was verified for the bibenzyl/biphenyl system. Biphenyl was used as the internal standard. Although the  $k_q$  for biphenyl with  $\text{Pt}_2$  is  $\sim 10^5 \text{M}^{-1}\text{s}^{-1}$ , quenching does not lead to product formation and biphenyl is present at such low concentrations (less than 0.01 M) that its quenching is not significant.

## Results and Discussion

### H-atom transfer quenching of $^3\text{Pt}_2^*$

The reaction between  $^3\text{Pt}_2^*$  and organic substrates has typically been monitored by determining the rate with which the organic compound (Q) quenches the luminescence of the  $^3\text{Pt}_2^*$  excited state. The Stern-Volmer equation (Equation 1) describes the dependence of the excited state lifetime on the quencher concentration when deactivation of the excited state occurs via bimolecular reactions with a quencher.

$$1/\tau - 1/\tau_0 = k_q [Q] \quad (1)$$

The quenched and unquenched lifetimes of the luminescent excited state are given by  $\tau$  and  $\tau_0$ , respectively;  $k_q$  is the Stern-Volmer quenching rate constant determined from the slope of a linear plot of  $(1/\tau - 1/\tau_0)$  versus  $[Q]$ .

The rate of hydrogen-atom abstraction by  $^3\text{Pt}_2^*$ , as measured by the quenching rate  $k_q$ , is given for a variety of organic H-atom donors in Table 1. Figure 2 shows the correlation of quenching rate constants with C-H homolytic bond strength.

Benzyl alcohols quench  $^3\text{Pt}_2^*$  mainly through H-atom transfer, as demonstrated by the large kinetic isotope effect observed for quenching with methylbenzyl alcohol ( $k_H/k_D=5$ ) and the observation of ketones and  $\text{Pt}_2\text{H}_2$  as photolysis products in reasonably high yields (*vide infra*). Also,  $k_q$  tends to decrease with increasing  $D(\text{C-H})$  for the alcohols, as observed in photoabstraction reactions by the  $n\pi^*$  excited states of ketones.<sup>14-16</sup>

**Figure 2.** The dependence of the  $^3\text{Pt}_2^*$  quenching rate constant on the C-H bond strength for a variety of organic H-atom donor quenchers. Squares represent data for sterically hindered alcohols.

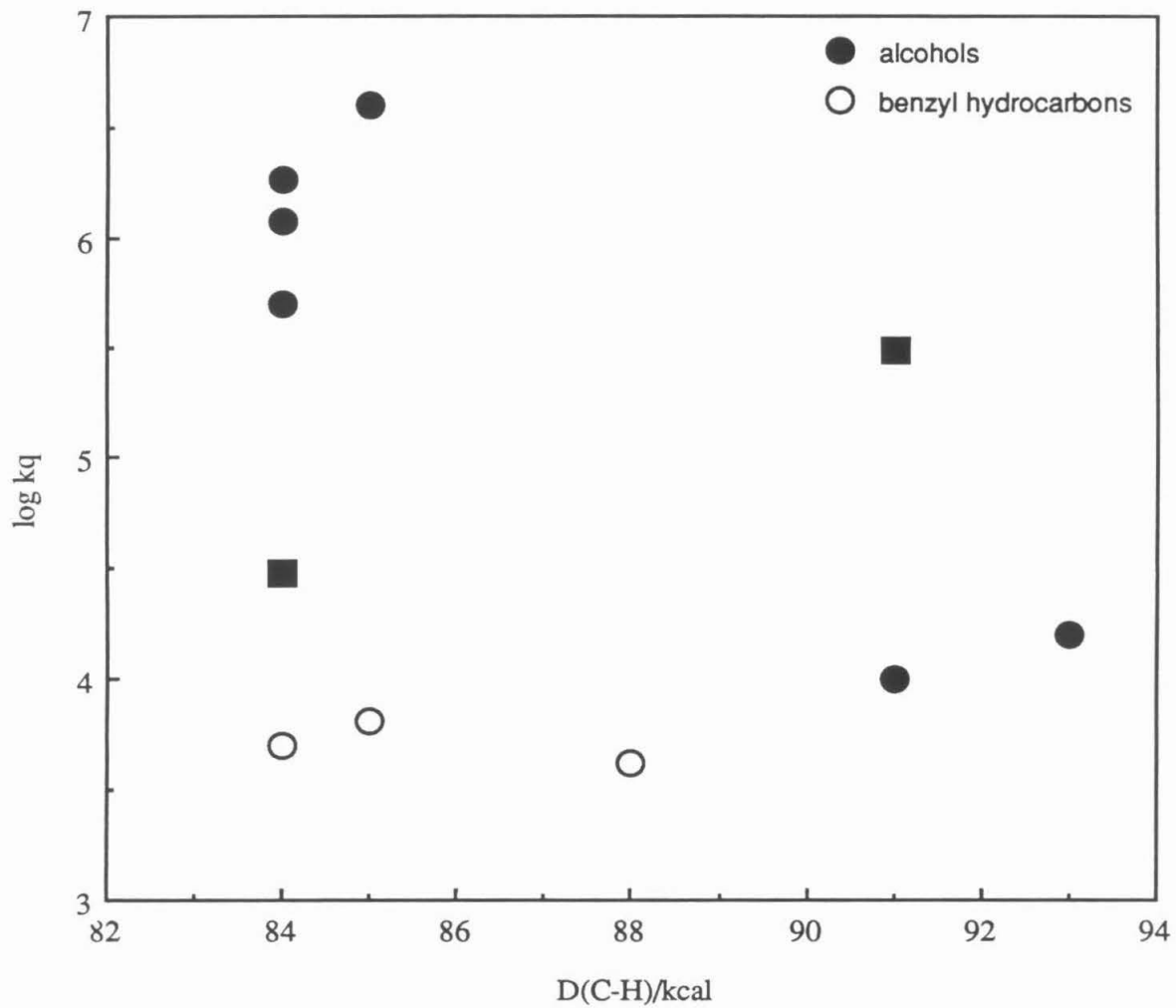


Table 1  $^3\text{Pt}_2^*$  Stern-Volmer quenching rate constants for organic H-atom donors Alcohols  $\text{RR}'\text{CHOH}^{17}$

R	R'	$k_q$ ( $\text{M}^{-1}\text{s}^{-1}$ )	D(C-H) (kcal/mol)
Ph	H	$4 \times 10^6$	85
Ph	$\text{CH}_3$	$1.8 \times 10^6$	84
Ph $\alpha$ -D	$\text{CH}_3$	$3.6 \times 10^5$	
Ph	$\text{CH}_2\text{CH}_3$	$1.2 \times 10^6$	84
Ph	$\text{CH}(\text{CH}_3)_2$	$5 \times 10^5$	84
Ph	$\text{C}(\text{CH}_3)_3$	$3 \times 10^4$	84
$\text{CH}_3$	$\text{CH}_3$	$\sim 10^4$	91
$\text{CH}_3$	$\text{CH}_2\text{CH}_3$	$\sim 10^4$	91
$\text{CH}_3$	$\text{CH}(\text{CH}_3)_2$	$3 \times 10^5$	91
$\text{CH}_2\text{OH}$	H	$1.6 \times 10^4$	93
Benzyl Hydrocarbons			
$\text{PhCH}_3$		$4.2 \times 10^3$	88
$\text{PhCD}_3$		$2.8 \times 10^3$	
$\text{PhCH}_2\text{CH}_3$		$6.4 \times 10^3$	85
$\text{PhCH}(\text{CH}_3)_2$		$5.0 \times 10^3$	84
$\text{PhC}(\text{CH}_3)_3$		$7.4 \times 10^3$	

Benzyl hydrocarbons also quench  $^3\text{Pt}_2^*$  through H-atom abstraction, as confirmed by the formation of  $\text{Pt}_2\text{H}_2$  and radical coupling products (e.g., bibenzyl from toluene). However, the main route of quenching by benzyl hydrocarbons apparently is not H-atom transfer, since the quenching rate remains approximately constant from toluene to *tert*-butylbenzene, although the latter has no easily abstractable hydrogen atoms. Also, radical coupling products are detected in low yield (*vide infra*) and the isotope effect for toluene ( $k_H/k_D = 1.5$ ) is much lower than for the alcohols. Therefore, we report the  $k_q$  values as upper limits on the actual H-atom-transfer

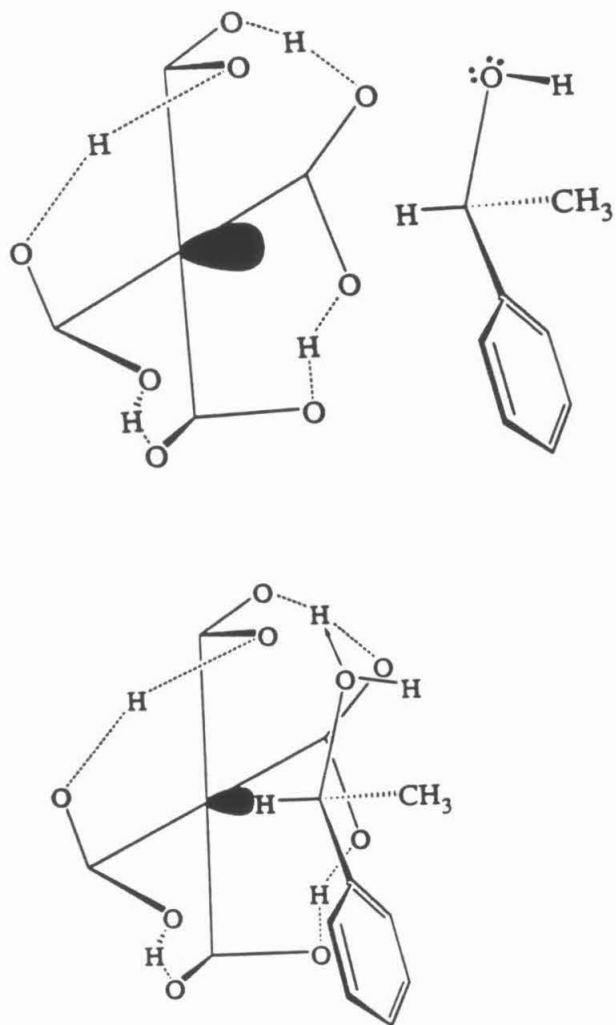
quenching rate for these substrates. Clearly, atom-transfer quenching rates for  $^3\text{Pt}_2^*$  with benzyl alcohols are much faster than the rates for hydrocarbons with comparable benzylic C-H bond strengths.

Steric interactions are a very plausible source of the unusual reactivity patterns observed for reactions of  $^3\text{Pt}_2^*$  with organic substrates. In the triplet excited state of  $\text{Pt}_2$  responsible for H-atom transfer reactions, an electron has been promoted from a  $d\sigma^*$  orbital directed out along the Pt-Pt axis to a  $p\sigma$  orbital localized between the two platinum atoms.<sup>11, 18</sup> This leaves a hole/radical in the  $d\sigma^*$  orbital, localized in the axial site. This situation is similar to the hole left in the oxygen-localized  $n$  orbital in the  $n\pi^*$  state of organic ketones, which also abstract H atoms from suitable substrates.<sup>14</sup> The high kinetic isotope effect for H-atom transfer suggests that the C-H bond forms a linear transition state along the Pt-H-C coordinate during H-atom transfer. The presence of OH moieties in alcohols gives rise to the possibility of H-bonding interactions between the substrate and the H-bonded terminal oxygens on the  $\text{Pt}_2$  ligands. Such interactions may specifically facilitate the approach of alcohol substrates to the axial sites on the metal complex, preparatory to abstraction by the metal center (Figure 3).

Alcohols exhibit unusual quenching behavior when present at high concentrations. The rate of quenching,  $1/\tau - 1/\tau_0$ , reaches a limiting value as more alcohol is added (i.e., the Stern-Volmer plot becomes horizontal, Figure 4). The initial linear region is used to extract  $k_q$ . Nonlinearity has previously been attributed to self-



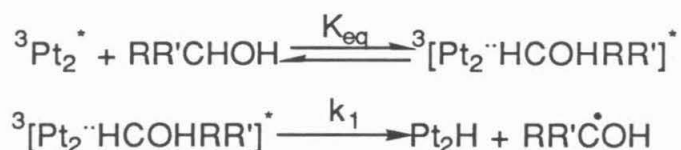
**Figure 3.** A proposed view of alcohol "docking" onto Pt<sub>2</sub> ligands.



dimerization of alcohol quenchers,<sup>19</sup> but this model does not predict the limiting quenching rate observed.

A hydrogen-bonded intermediate alters the previously assumed bimolecular reaction model by dividing the quenching reaction into two steps. The first step is formation of an H-bonded precursor complex between the metal dimer and the alcohol substrate, followed by unimolecular H-atom transfer.

### Scheme 2



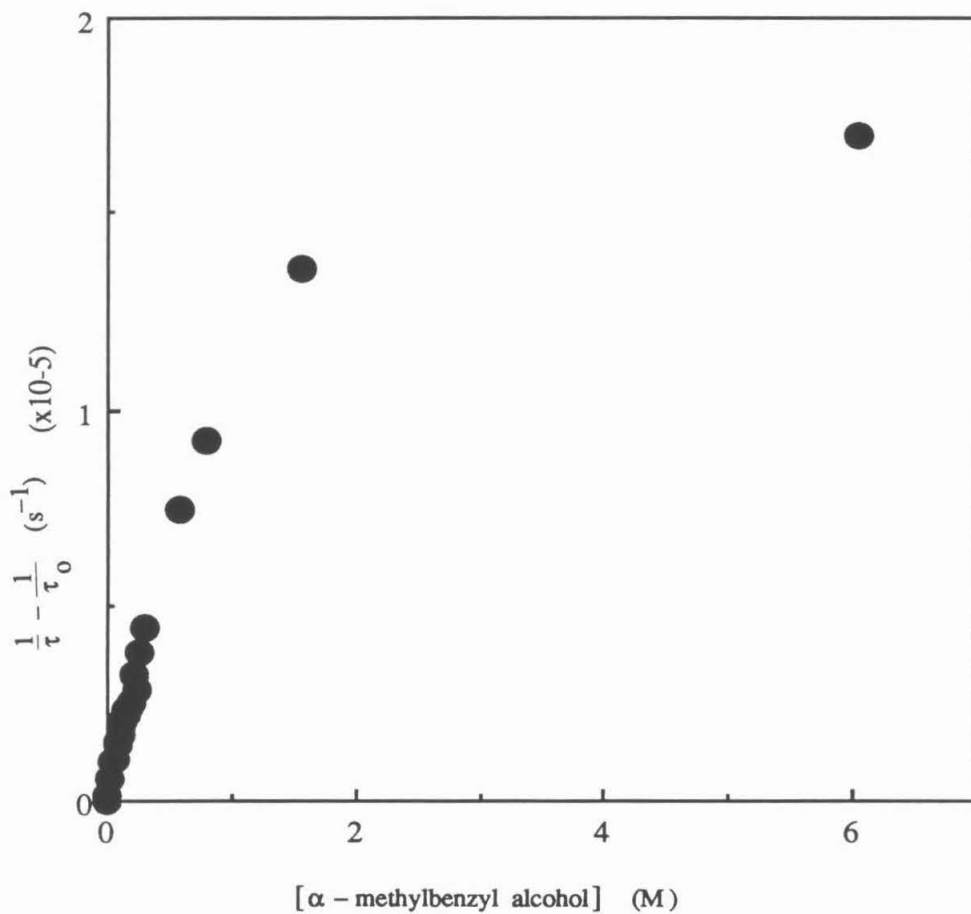
The pre-equilibrium step is consistent with pressure-dependent quenching studies that find a large negative  $\Delta V^\ddagger$  for the reaction of  ${}^3\text{Pt}_2^*$  with benzyl alcohols.<sup>19</sup>

The kinetic treatment for this pre-equilibrium model, which is directly analogous to Michaelis-Menten enzyme catalysis kinetics, predicts Equation 2.

$$1/\tau_0 - 1/\tau = \frac{K_{\text{eq}}k_1}{K_{\text{eq}} + 1/[\text{ROH}]} \quad (2)$$

In contrast to Stern-Volmer bimolecular kinetics, quenching of the excited state should not be linear with quencher concentration except in the low-concentration limit where  $k_q$  experiments are normally performed. At high concentrations, the Stern-Volmer plot should begin to flatten out, as observed (Figure 4). Similar pre-

**Figure 4.** The Stern-Volmer quenching plot for the quenching of  ${}^3\text{Pt}_2^*$  phosphorescence with  $\alpha$ -methylbenzyl alcohol.



equilibrium reactions are important in electron-transfer reactions between bipyridyl complexes and copper proteins.<sup>20</sup>

Rearrangement of Equation 2 predicts a linear relationship between  $1/k_q$  and  $1/[ROH]$  for quenchers that form a precursor complex (Equation 3).

$$(1/\tau - 1/\tau_0)^{-1} = 1/k_1 + 1/K_{eq}k_1[ROH] \quad (3)$$

Plotting alcohol quenching data in this manner does indeed give a straight line (Figure 5).

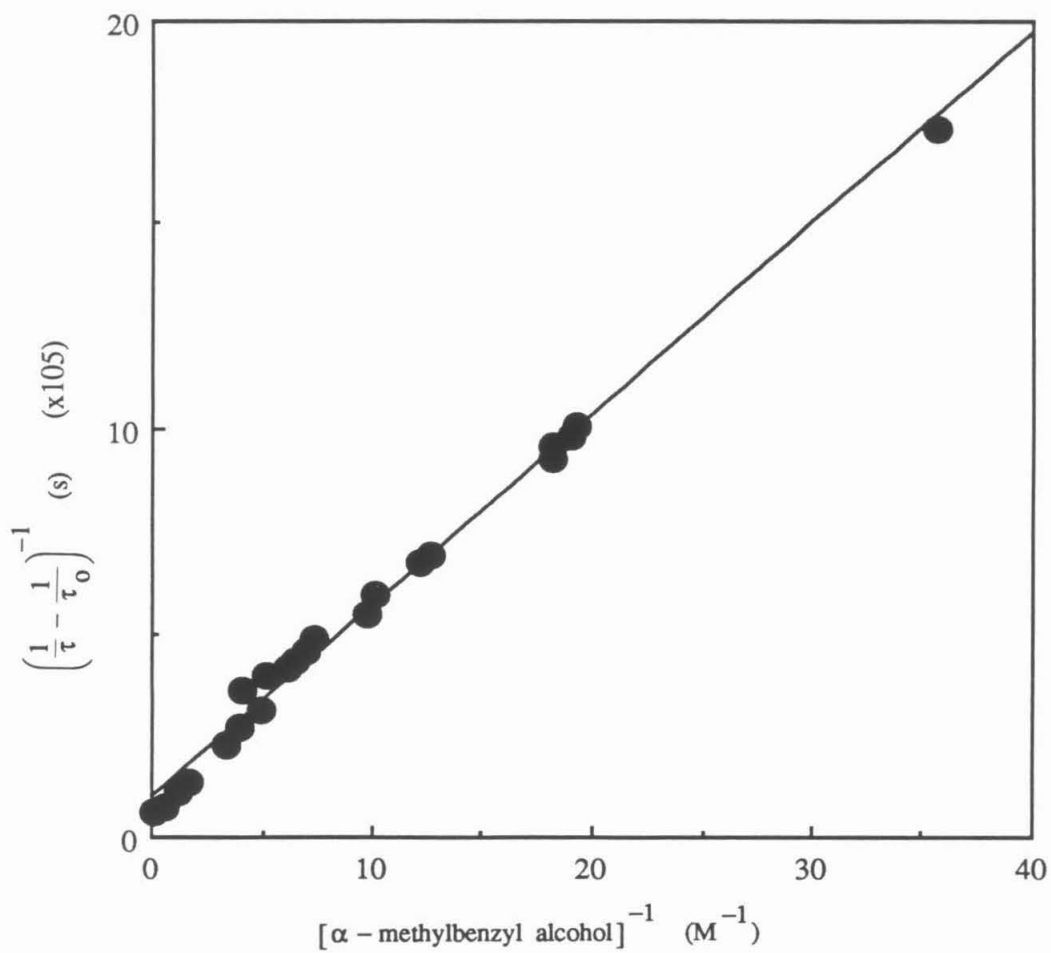
Values of  $K_{eq}$  and  $k_1$  can be extracted from both types of plots. The slope of the Stern-Volmer plot at low alcohol concentrations is equal to  $K_{eq}k_1$ , which corresponds to the  $k_q$  reported previously. At high concentrations,  $k_q$  reaches a limiting value equivalent to the unimolecular rate constant,  $k_1$ . The slope of the linear Michaelis-Menten plot equals  $(K_{eq}k_1)^{-1}$ ; the high-concentration intercept is  $k_1^{-1}$ .

Table 2  ${}^3\text{Pt}_2^*$  phosphorescence quenching parameters for selected alcohols  $\text{RR}'\text{CHOH}$

R	R'	$K_{eq}$ ( $\text{M}^{-1}$ )	$k_1$ ( $\text{s}^{-1}$ )
Ph	$\text{CH}_3$	1.0	$2.1 \times 10^6$
Ph	$\text{CH}(\text{CH}_3)_2$	0.2	$2.1 \times 10^6$
$\text{CH}_2\text{OH}$	H	0.5	$3.5 \times 10^4$
$\text{CH}_3$	$\text{CH}(\text{CH}_3)_2$	0.5	$5.0 \times 10^5$

$K_{eq}$  and  $k_1$  values were determined for a series of alcohols (Table 2). The fact that  $K_{eq}$  is relatively invariant with respect to substitution on the  $\alpha$  carbon is consistent with a docking interaction

**Figure 5.** Quenching data for the reaction of  $\alpha$ -methylbenzyl alcohol with  $^3\text{Pt}_2^*$  plotted according to Equation (3).



involving only the hydroxyl group, since variation of alkyl groups on the  $\alpha$  carbon should not affect the hydroxyl group significantly. The  $\Delta S_{rxn}$  associated with  $K_{eq}$  is -66 e.u., as determined by variable-temperature quenching experiments with methylbenzyl alcohol. The high degree of organization implied agrees with our formulation of this step as a bimolecular association. The  $\Delta H_{rxn}$  of -1.8 kcal/mol is reasonable for the strength of a hydrogen bond.

Since  $K_{eq}$  varies little, large changes in  $k_q$  are due mainly to differences in the unimolecular rate  $k_1$ . Therefore, in order to understand and predict the relative reactivities of alcohols with  ${}^3Pt_2^*$ , the factors that determine  $k_1$  must be understood. As alcohol substituents are varied, the effect of such substitutions on  $k_1$  can be determined by following changes in  $k_1$ 's activation parameters. Arrhenius parameters for the  $k_1$  constants of selected alcohols are listed in Table 3.

Table 3. Arrhenius parameters for  ${}^3Pt_2^*$  phosphorescence quenching by alcohols  $RR'CHOH$

R	R'	$\Delta S^\ddagger$ (e.u.)	$E_a$ (kcal/mol)
Ph	CH <sub>3</sub>	-20	2.9
Ph	CH(CH <sub>3</sub> ) <sub>2</sub>	-12	5.5
CH <sub>2</sub> OH	H	-23	4.4
CH <sub>3</sub>	CH(CH <sub>3</sub> ) <sub>2</sub>	-10	6.8

Entropic barriers in this unimolecular quenching step are reasonably large and reflect the highly organized nature of the presumably linear H-atom-transfer transition state. For comparison,

the  $\Delta S^\ddagger$  for cyclopentadiene dimerization, is -34 e.u.<sup>21</sup> and corresponds to a highly ordered bimolecular condensation. The primary variable responsible for the range in  $\Delta S^\ddagger$  appears to be steric bulk of substituents  $\alpha$  to the hydroxyl group. Being anchored to Pt<sub>2</sub> via the hydroxyl group, alcohols have a limited number of available orientations that are further limited by steric requirements of the substituents. The entropy of activation reflects the proportion of these conformations that can lead to atom transfer. Large substituents reduce the number of nonreactive conformations and therefore make the reaction more facile entropically. For example, replacement of an  $\alpha$ -methyl group with an *iso*-propyl group drastically decreases the magnitude of  $\Delta S^\ddagger$  for both benzyl and aliphatic alcohols.

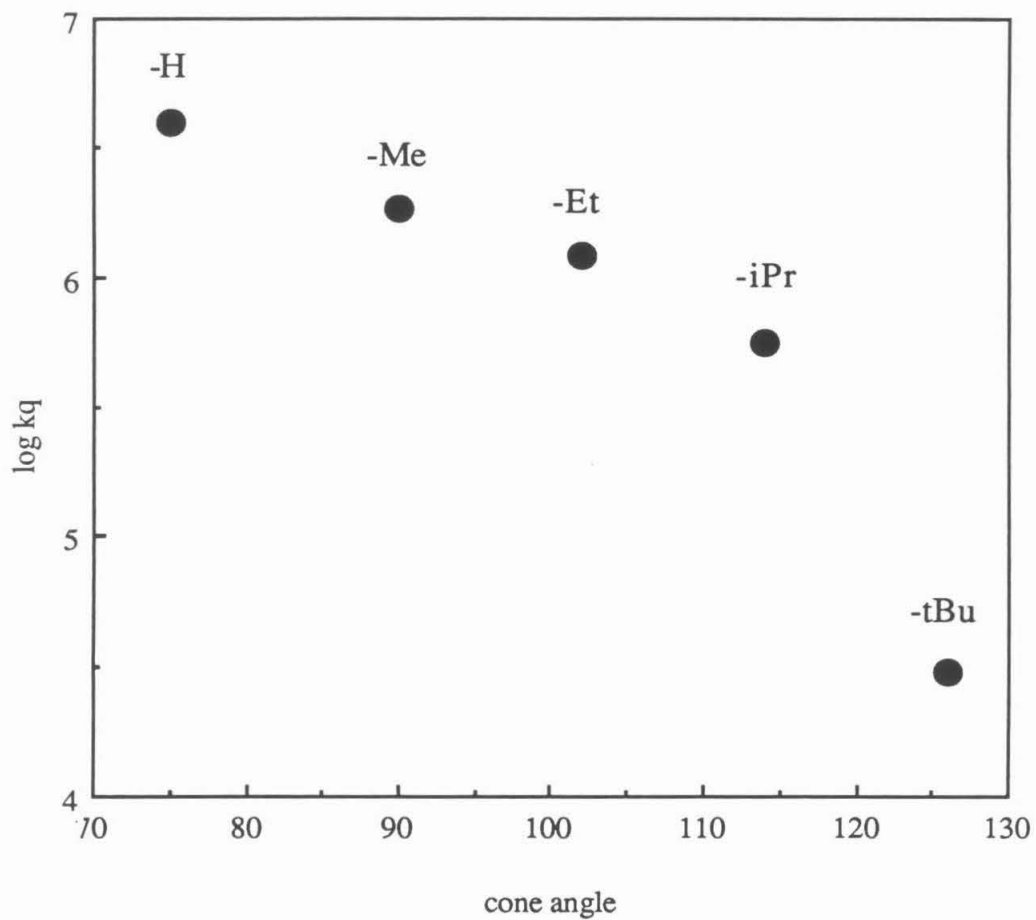
For compounds with similar  $\Delta S^\ddagger$  values, the activation energy  $E_a$  follows the  $\alpha$ C-H bond strength, as expected.  $E_a$  increases  $\sim 1.5$  kcal/mol between benzyl and aliphatic alcohols. For both types of alcohols, increasing steric bulk actually increases  $E_a$ . Presumably, the transition state for atom transfer is not a low-energy conformation and the measured  $E_a$  is some combination of the barrier to atom abstraction and the energy required to reach the linear transition state. Thus, the overall contribution of increased steric bulk depends on the balance between changes in  $\Delta S^\ddagger$  and  $E_a$ .

For the series of aliphatic alcohols including isopropanol, 2-butanol and 3-methyl-2-butanol, the increase in substituent size dramatically increases the quenching rate from the technique's lower measurement limits ( $10^4 \text{ M}^{-1}\text{s}^{-1}$ ) to rates near those of the benzyl alcohols. Within a series of benzyl alcohols (Figure 6),

increasing substituent size decreases the quenching rate  $k_q$ . In the case of *tert*-butyl benzyl alcohol, the reactive transition state itself is one of the conformations disallowed by sterics and  $k_q$  plummets.



**Figure 6.** The variation of the Stern-Volmer quenching rate  $k_q$  as a function of the cone angle of  $\alpha$ -substituents on benzyl alcohols.



### Product formation rates

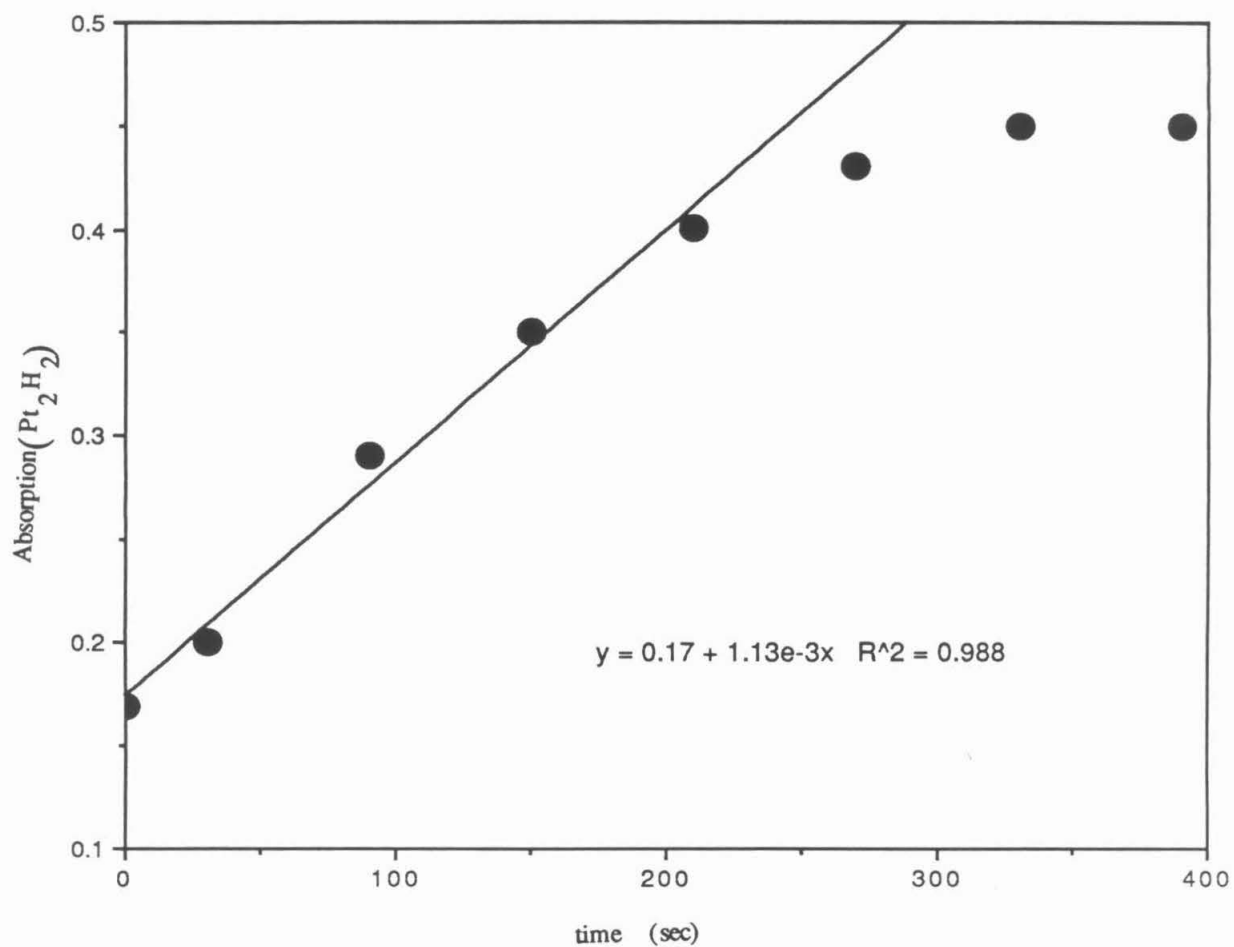
Stern-Volmer quenching constants provide useful information about factors that control the selectivity of the initial H-atom abstraction by  $^3\text{Pt}_2^*$ , but yield no information regarding formation of the eventual stable products. Although the quenching of  $^3\text{Pt}_2^*$  with alcohols has been studied thoroughly, deactivation of the excited state is only the first step in a sequence of reactions that leads to the observed stable products  $\text{Pt}_2\text{H}_2$ ,  $\text{H}_2$ , and ketones. The relationship between effective rate constants for product formation ( $k_p$ ) and the rate constant of the quenching step ( $k_q$ ) can be expressed through the efficiency parameter  $\Phi_p$ , where  $\Phi_p$  is necessarily less than 1.

$$k_p/k_q = \Phi_p \quad (4)$$

A  $\Phi_p$  value of unity (100%) implies that every deactivation reaction leads to the formation of one molecule of a stable atom-transfer product. The growth of the distinctive ultraviolet absorption band for  $\text{Pt}_2\text{H}_2$  at 313 nm proved to be a useful handle for following product formation with alcohols in  $\text{CH}_3\text{CN}$ .

At high conversions to  $\text{Pt}_2\text{H}_2$ , the system appeared to approach a photostationary state; i.e., the absorption spectrum showed no change upon further irradiation (Figure 7). The low-energy tail of the  $\text{Pt}_2\text{H}_2$  band presumably absorbs some of the excitation light ( $\lambda > 350$  nm) and photoeliminates dihydrogen. When the growth in  $\text{Pt}_2\text{H}_2$  that is due to abstraction from alcohols is exactly balanced by its photochemical decomposition, a steady state of the dihydride is established.

**Figure 7.** Absorption of the 313 nm Pt<sub>2</sub>H<sub>2</sub> band as a function of the time of irradiation into the Pt<sub>2</sub> absorption band at 372 nm. The H-atom donor quencher is benzyl alcohol (0.077M).



For reactions with benzyl hydrocarbons, long-term photolyses yielded benzyl dimers as products, which were quantitatively analyzed by gas chromatography. The amount of product formed and the photon flux ( $I$ ) combine to give  $k_p$ , through the equation  
 moles RH consumed = 2(moles dimer  $R_2$  produced) =  $I\tau k_p[RH]$ .

A small amount of the dihydride was also formed in photolyses with cumene and ethylbenzene, but the  $k_p$  values were not determined. Toluene solutions were not found to yield the dihydride. This may merely reflect the slow hydrogen-transfer rate of toluene relative to cumene and ethylbenzene. Photolyses of  $[TOA]_4Pt_2$  in tert-butylbenzene yielded only trioctylamine, presumably via electron-transfer reactions from  $^3Pt_2^*$  to the tetraoctylammonium cation.

Table 4 Product formation rates and reaction efficiencies for selected quenchers

Quencher	[ROH] (M)	$k_p$ ( $M^{-1}s^{-1}$ )	$\Phi_p$
Pt <sub>2</sub> H <sub>2</sub> product			
benzyl alcohol	0.058	$5.9 \times 10^5$	0.15
	0.077	$4.0 \times 10^5$	0.10
isopropanol	6.53	820	~0.08
Dimer product			
toluene	4.7	25	0.006
ethylbenzene	4.1	400	0.06
cumene	3.6	600	0.1

The  $\Phi_p$  (Table 4) values of about 10% reveal that the H-atom-transfer reaction is reasonably efficient for many substrates. However, the rates of product formation span nearly three orders of magnitude among the alcohols, demonstrating remarkable reaction selectivity. From these data, one would predict that given a choice of isopropanol and benzyl alcohol in the same solution, 99.8% of  $^3\text{Pt}_2^*$  would dehydrogenate benzyl alcohol.

In a more practical test of dehydrogenation selectivity,  $\text{Pt}_2$  was irradiated in the presence of two alcohols to compare the relative yields of the corresponding ketones. Photolysis of  $\text{Pt}_2$  in an approximately equimolar (0.5M) solution of benzyl alcohol and cyclohexanol demonstrated a reaction selectivity for the benzyl alcohol over cyclohexanol of 15:1. A similar experiment with 2-cyclohexen-1-ol and cyclohexanol yielded no cyclohexenol but showed 365 turnovers in the dehydrogenation of the cyclohexanol to cyclohexanone.

## Conclusions

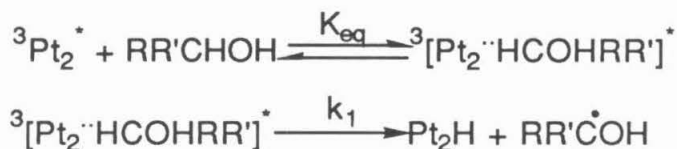
The H-atom-transfer reaction selectivity of  $^3\text{Pt}_2^*$  is governed more by the chemical and physical structure of its ligands than by the inherent activity of the abstraction center. The hydrophilic nature of the ligands selects alcohols preferentially over hydrophobic substrates, and the steric constraints of the ligands moderate reactivities according to the steric properties of the substrate.

## Appendix 1

### Extraction of Activation Parameter for a Complex Reaction

The pre-equilibrium quenching model requires the measurement of four activation parameters rather than two, as are needed for simple bimolecular reactions. The activation parameters for the equilibrium step are the enthalpy,  $\Delta H^{eq}$ , and the entropy of the reaction,  $\Delta S^{eq}$ . The unimolecular quenching step has an energy,  $E_a$ , and an entropy of activation,  $\Delta S^\ddagger$ , which describe the transition state of the reaction. These four terms can be extracted from the apparent Arrhenius parameters at high- and low-quencher concentrations, as determined by following the reaction at various temperatures.

The quenching of emission for the reaction



obeys the rate law

$$-\frac{d[{}^3\text{Pt}_2^*]}{dt} = \frac{K_{eq} k_1}{K_{eq} + 1/[\text{ROH}]} \quad (1)$$

Equation (1) can be contrasted to the analogous Stern-Volmer equation

$$-\frac{d[{}^3\text{Pt}_2^*]}{dt} = \left(\frac{1}{\tau} - \frac{1}{\tau_0}\right) = k_q[\text{Q}] \quad (2)$$

When coupled to the rate expressions

$$K_{\text{eq}} = A^{\text{eq}} \exp(-\Delta H^{\text{eq}}/RT) \quad (3)$$

$$k_1 = A^1 \exp(-E_a/RT), \quad (4)$$

the quenching rate can be expressed as

$$\left(\frac{1}{\tau} - \frac{1}{\tau_0}\right) = \frac{A^{\text{eq}} A^1 \exp(-E_a/RT) \exp(-\Delta H^{\text{eq}}/RT)}{A^{\text{eq}} \exp(-\Delta H^{\text{eq}}/RT) + 1/[\text{ROH}]} \quad (5)$$

The two limiting cases of quencher concentrations simplify this equation considerably.

**A)** High-concentration limit,  $[\text{ROH}]^{-1} \gg K_{\text{eq}}$ . Equations (1) and (5) reduce to

$$k_{\text{obs}} = k_1 = A^1 \exp(-E_a/RT), \quad (6)$$

and  $k_{\text{obs}}$  can be treated as if it represented a simple, one-step reaction.

$$\log k_1 = \log A^1 - \frac{E_a}{2.303RT} \quad (7)$$

$$\Delta S^\ddagger = R \ln \left( \frac{A^1 h c^\circ}{kT} \right) \quad (8)$$

$$R = 1.987 \text{ cal mol}^{-1} \text{ K}^{-1}$$

$$h = 6.626 \times 10^{-34} \text{ J sec}$$

$$c^\circ = 1 \text{ M}$$

$$k = 1.38 \times 10^{-23} \text{ J K}^{-1}$$

$$T = 298 \text{ K}$$

**B)** Low-concentration limit,  $[\text{ROH}]^{-1} \ll K_{\text{eq}}$ . Equations (1) and (5) reduce to

$$k_{\text{obs}} = K_{\text{eq}} k_1 [\text{ROH}] = [\text{ROH}] A^{\text{eq}} A^1 \exp(-E_a/RT) \exp(-\Delta H^{\text{eq}}/RT), \quad (9)$$

which requires a more complicated but still reasonable treatment. We can still treat these data with equations similar to (7) and (8), but we find that

$$E_{\text{obs}} = E_a + \Delta H^{\text{eq}} \quad (10)$$

and

$$A_{\text{obs}} = A^1 A^{\text{eq}} [\text{ROH}]. \quad (11)$$

Equation (11) produces the sum of the entropic parameters through

$$\Delta S^\ddagger + \Delta S^{\text{eq}} = R \ln \left[ \left( \frac{hc^0}{kT} \right)^2 A^1 A^{\text{eq}} \right]. \quad (12)$$

The activation parameters for the equilibrium follow from knowledge of results from the two limiting cases.



**Appendix 2**

**Representative Data**

**Figure 8** Calibration plot for the quantitative determination of bibenzyl using biphenyl as an internal GC standard.

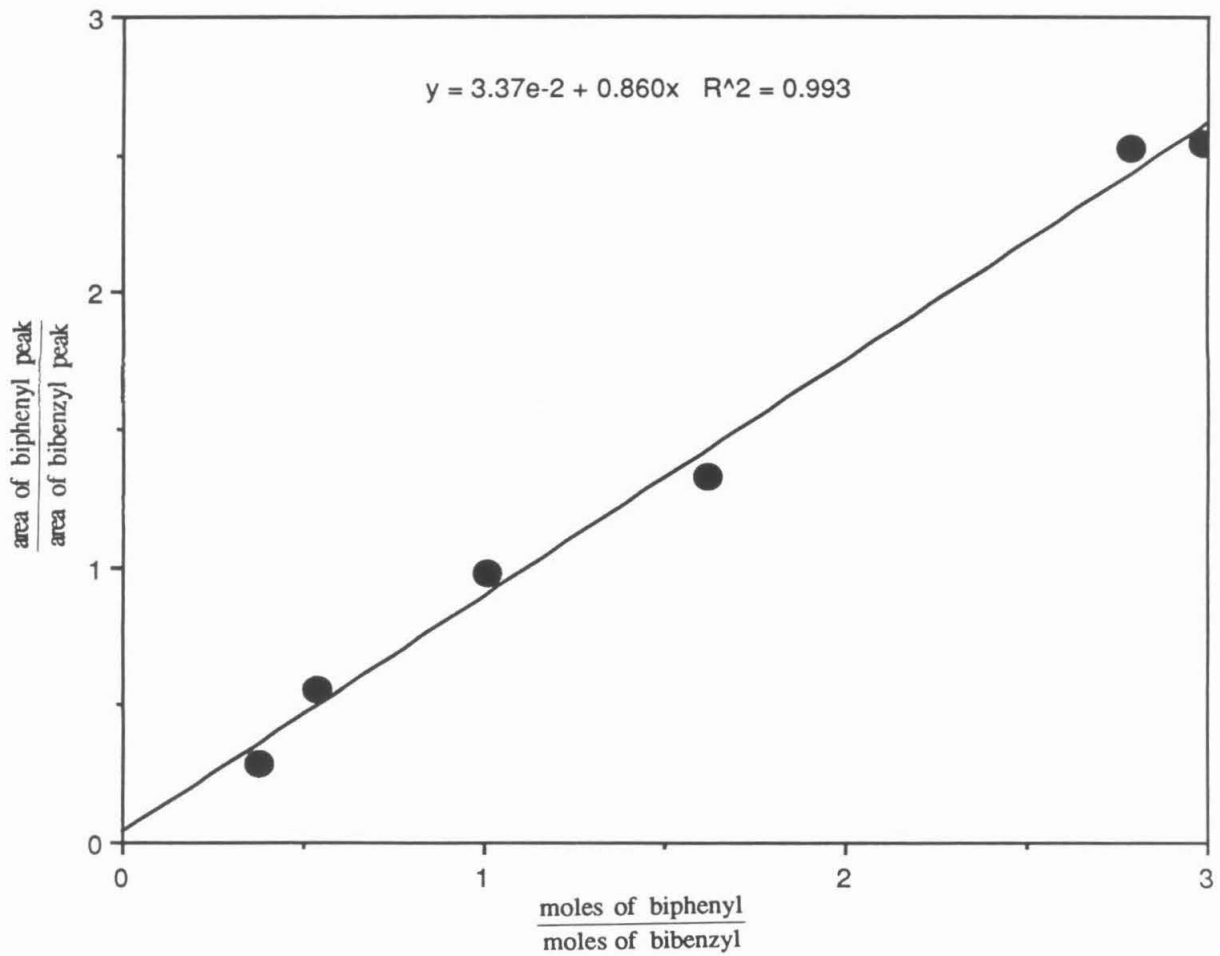


**Figure 9** Stern-Volmer plot for the quenching of  ${}^3\text{Pt}_2^*$  phosphorescence by ethylbenzene

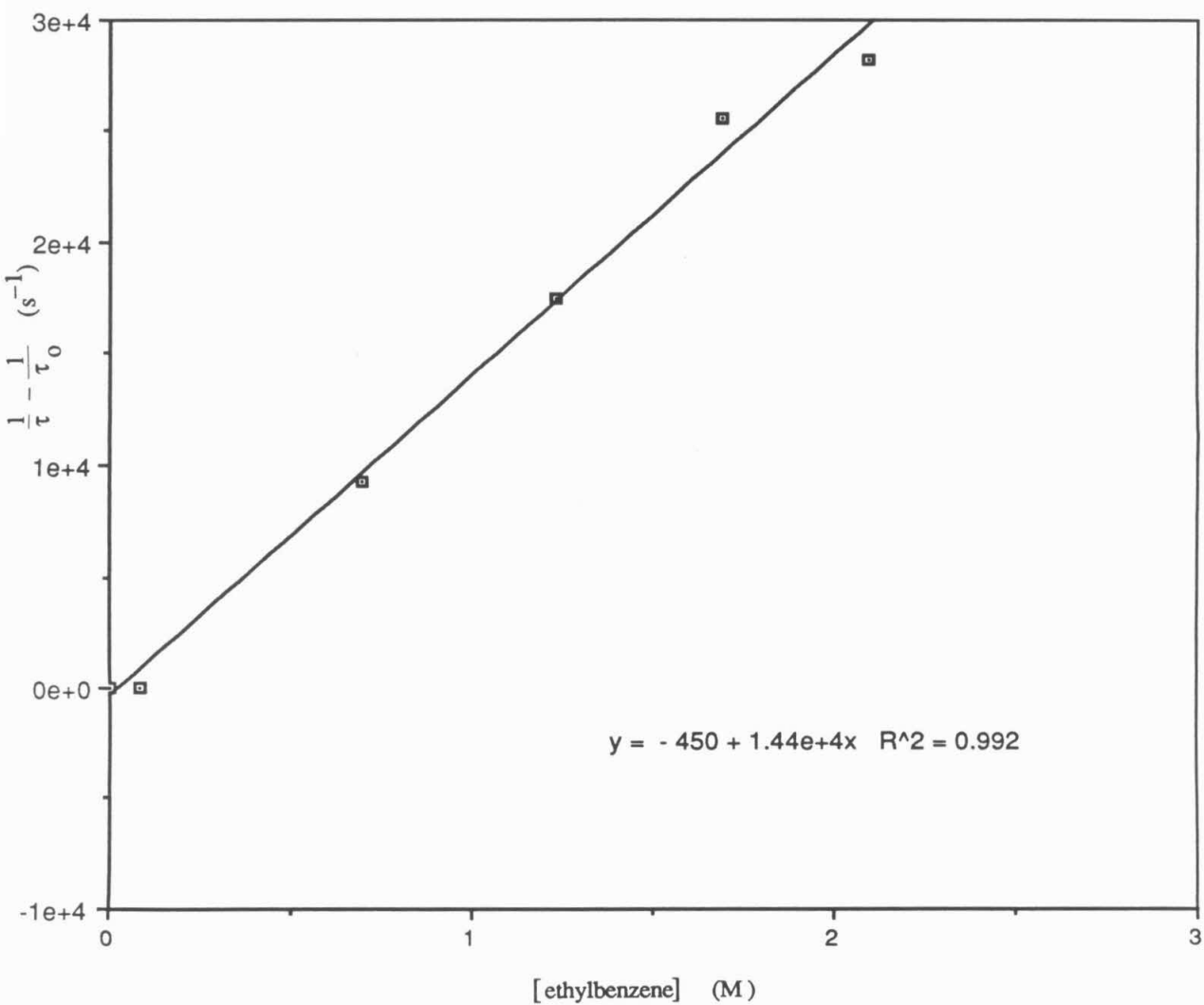


**Figure 10** Stern-Volmer plot for the quenching of  $^3\text{Pt}_2^*$  phosphorescence by  $\alpha$ -deuterio- $\alpha$ -methylbenzyl alcohol

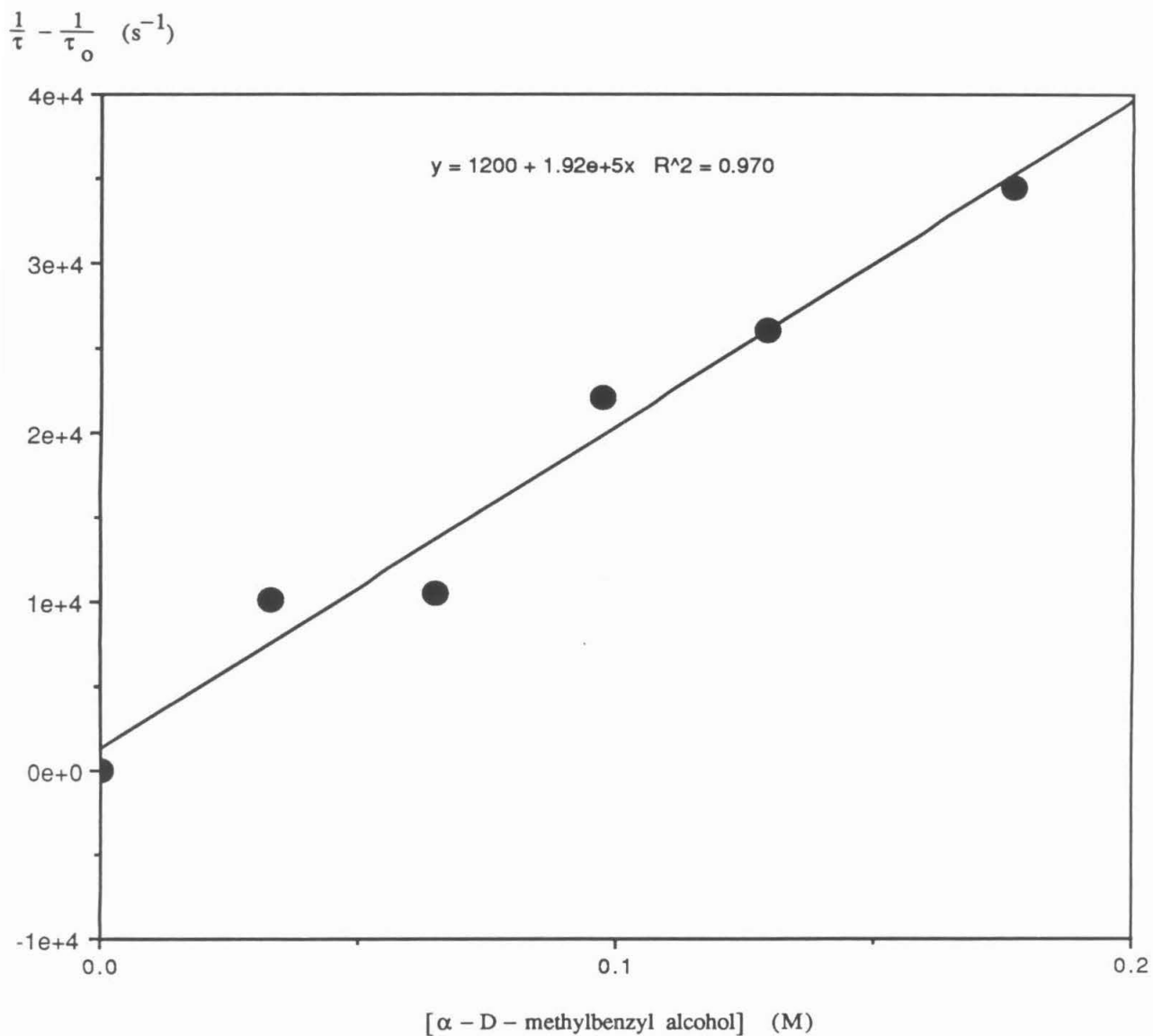


**Figure 11** Stern-Volmer plot for the quenching of  $^3\text{Pt}_2^*$  phosphorescence by ethylene glycol

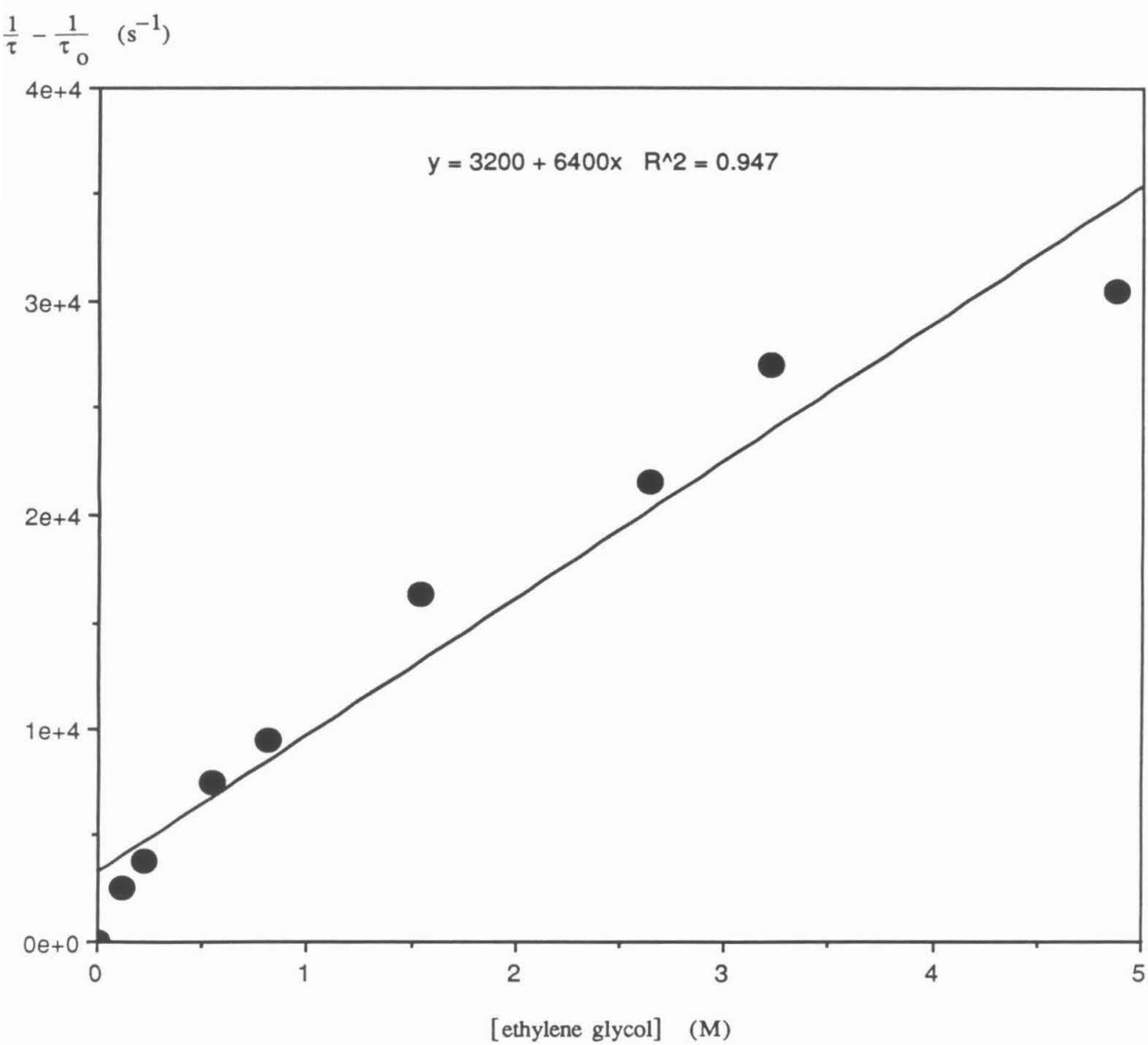


**Figure 12** Michaelis-Menten plot for the quenching of  $^3\text{Pt}_2^*$  phosphorescence by ethylene glycol

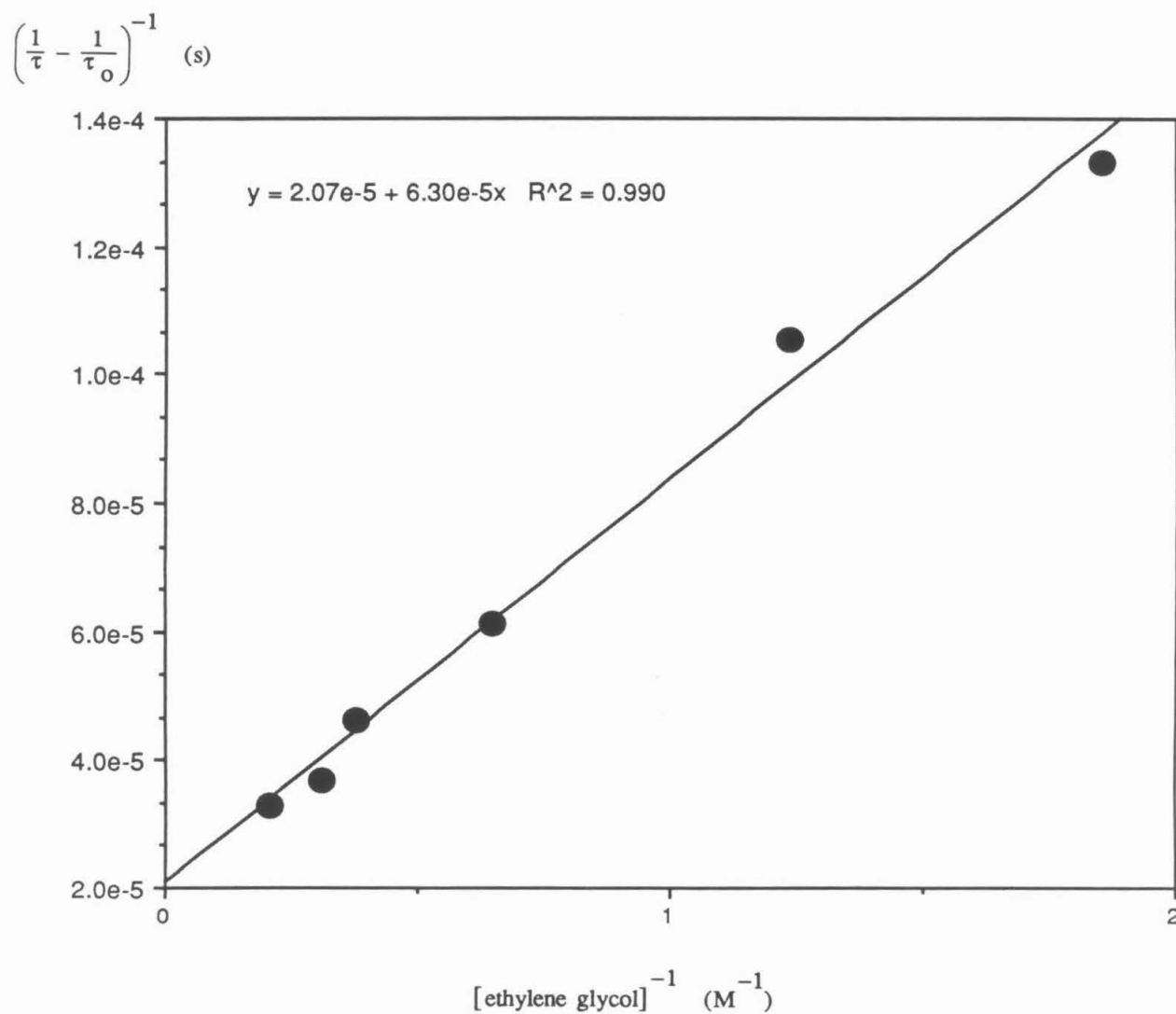


**Figure 13** Temperature dependence of the rate of  $^3\text{Pt}_2^*$  phosphorescence quenching by ethylene glycol (9.0M)

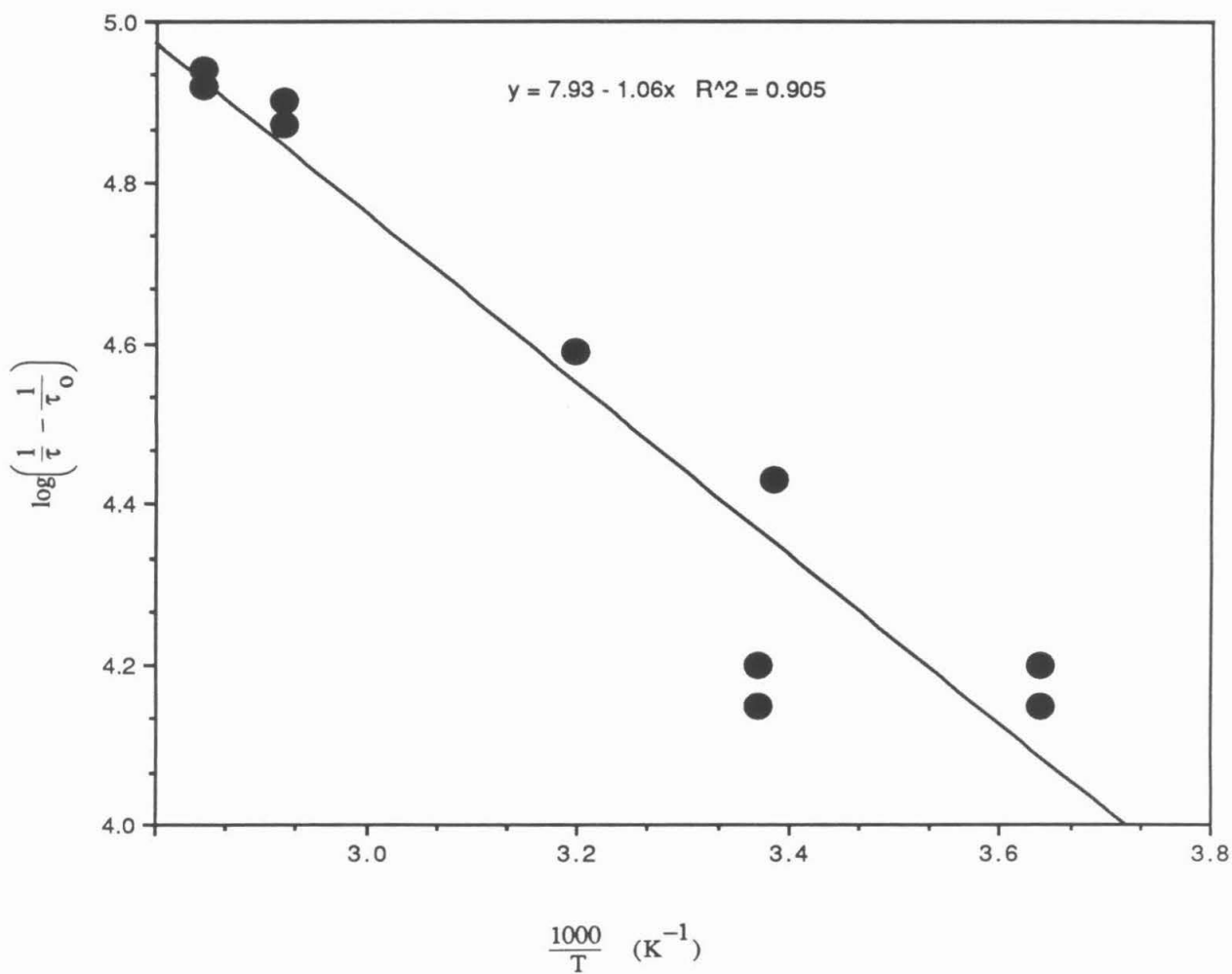


**Figure 14** Temperature dependence of the rate of  ${}^3\text{Pt}_2^*$  phosphorescence quenching by  $\alpha$ -methylbenzyl alcohol (0.24M)

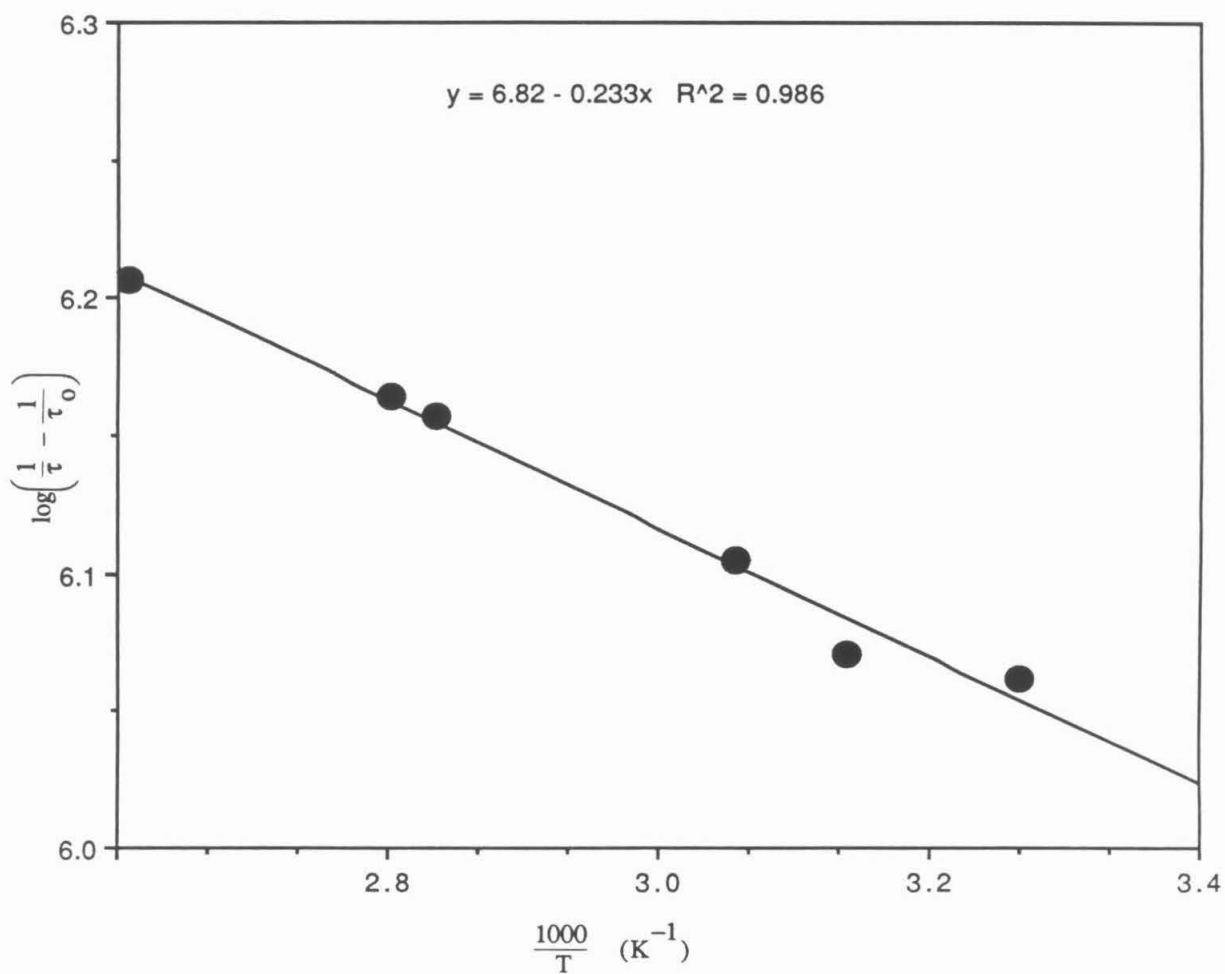




**Figure 15** Temperature dependence of the rate of  $^3\text{Pt}_2^*$  phosphorescence quenching by  $\alpha$ -methylbenzyl alcohol (6.0M)

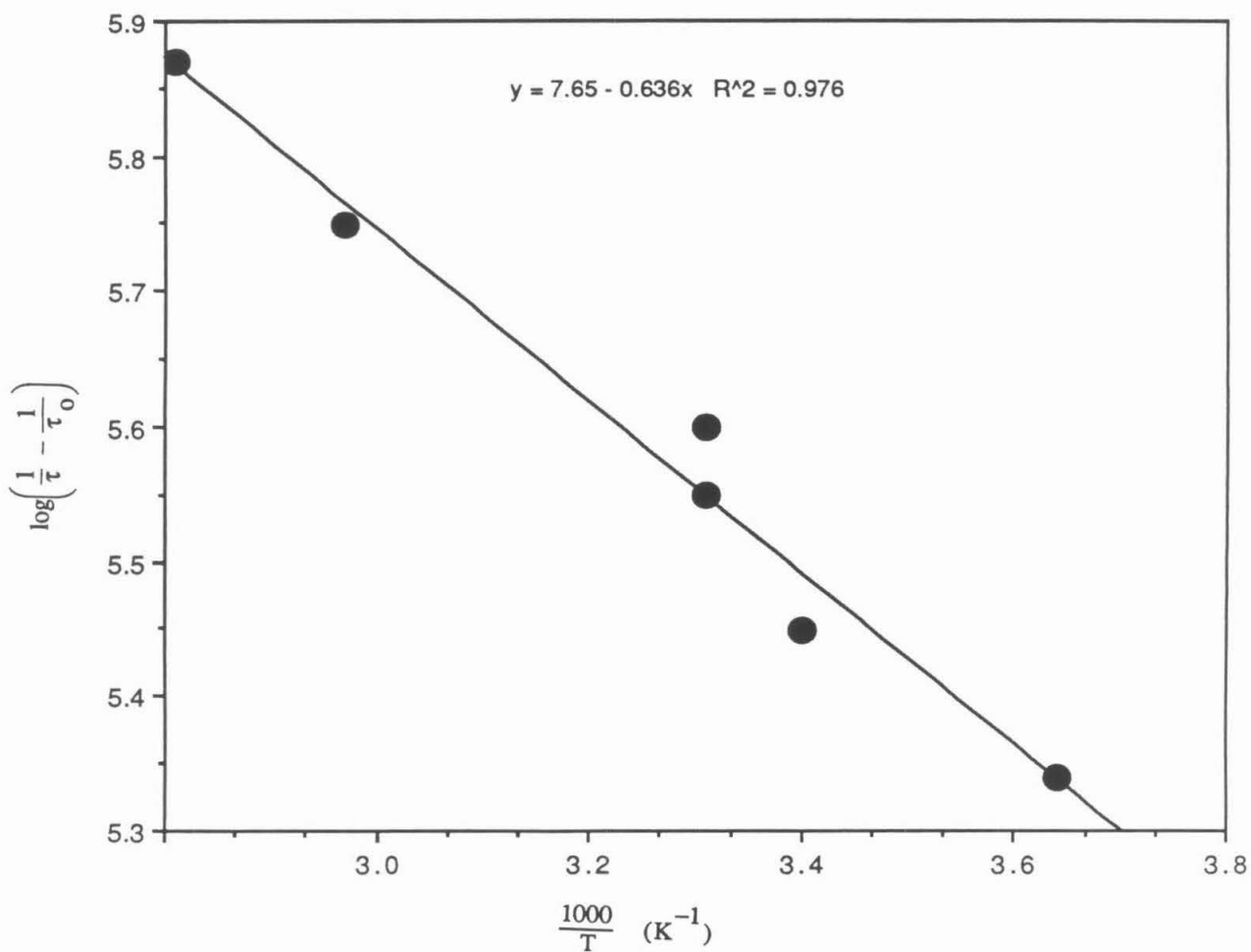


**Figure 16** Stern-Volmer plot for the quenching of  $^3\text{Pt}_2^*$  phosphorescence by 3-methyl-2-butanol

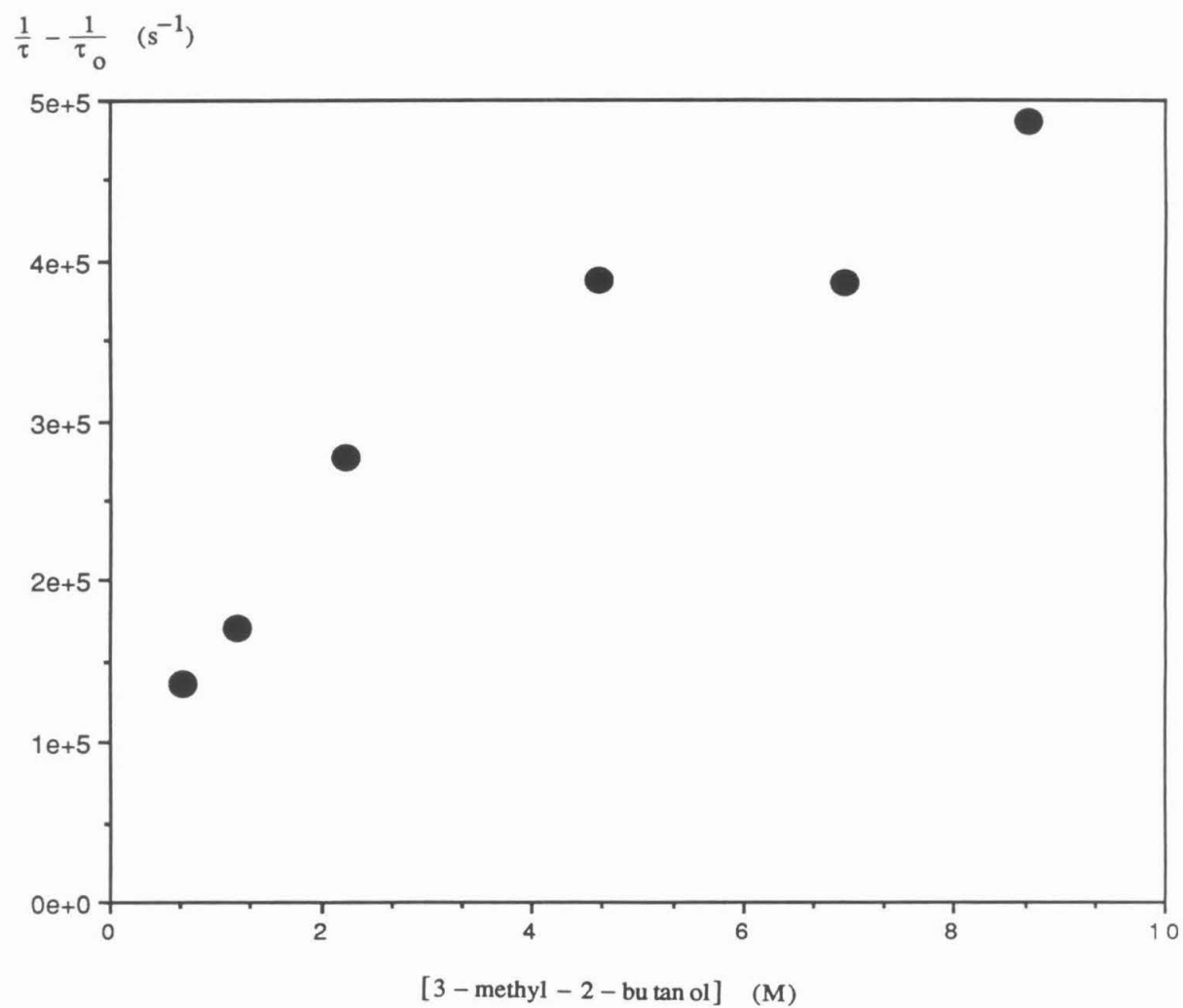


**Figure 17** Michaelis-Menten plot for the quenching of  ${}^3\text{Pt}_2^*$  phosphorescence by 3-methyl-2-butanol

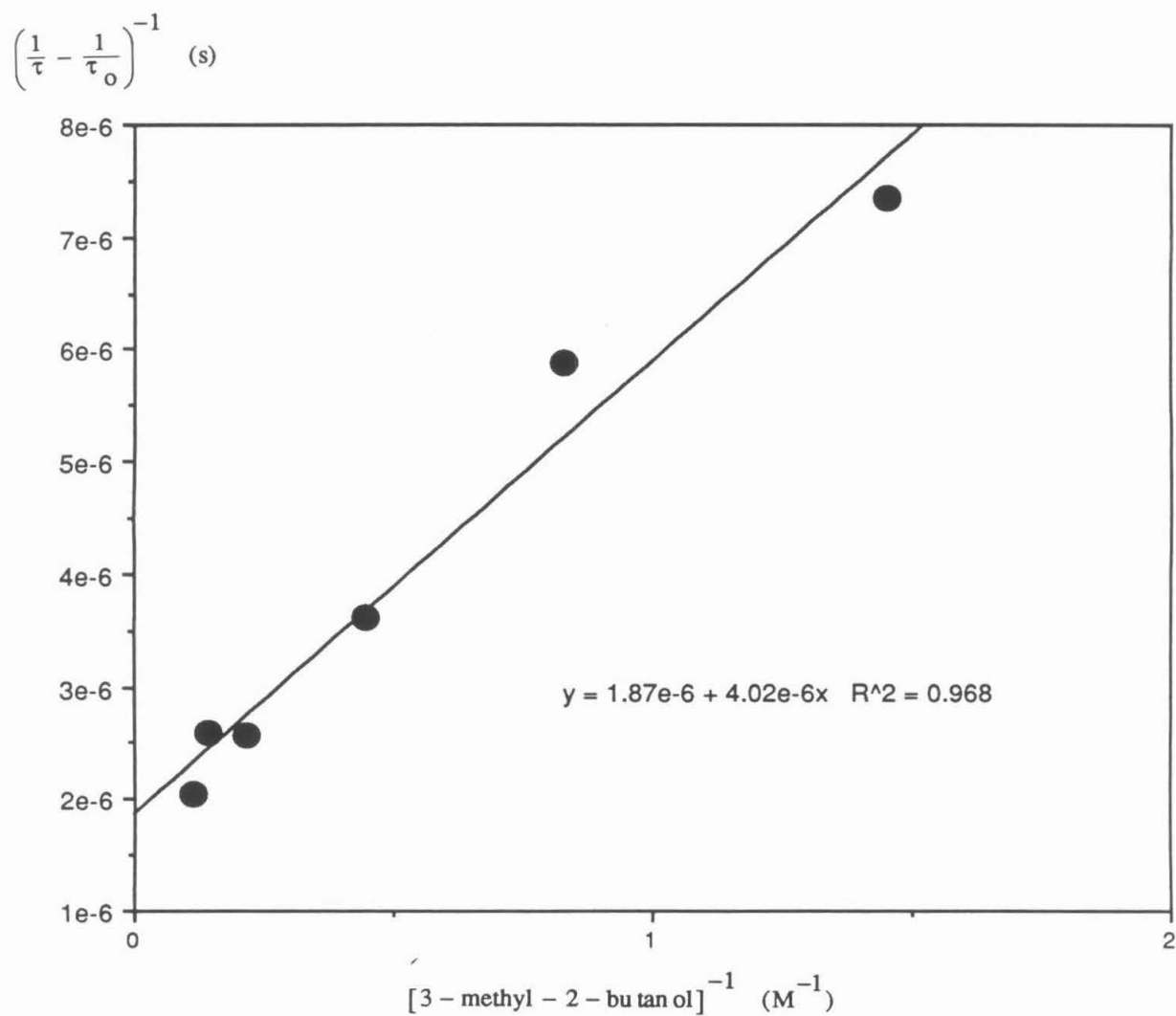
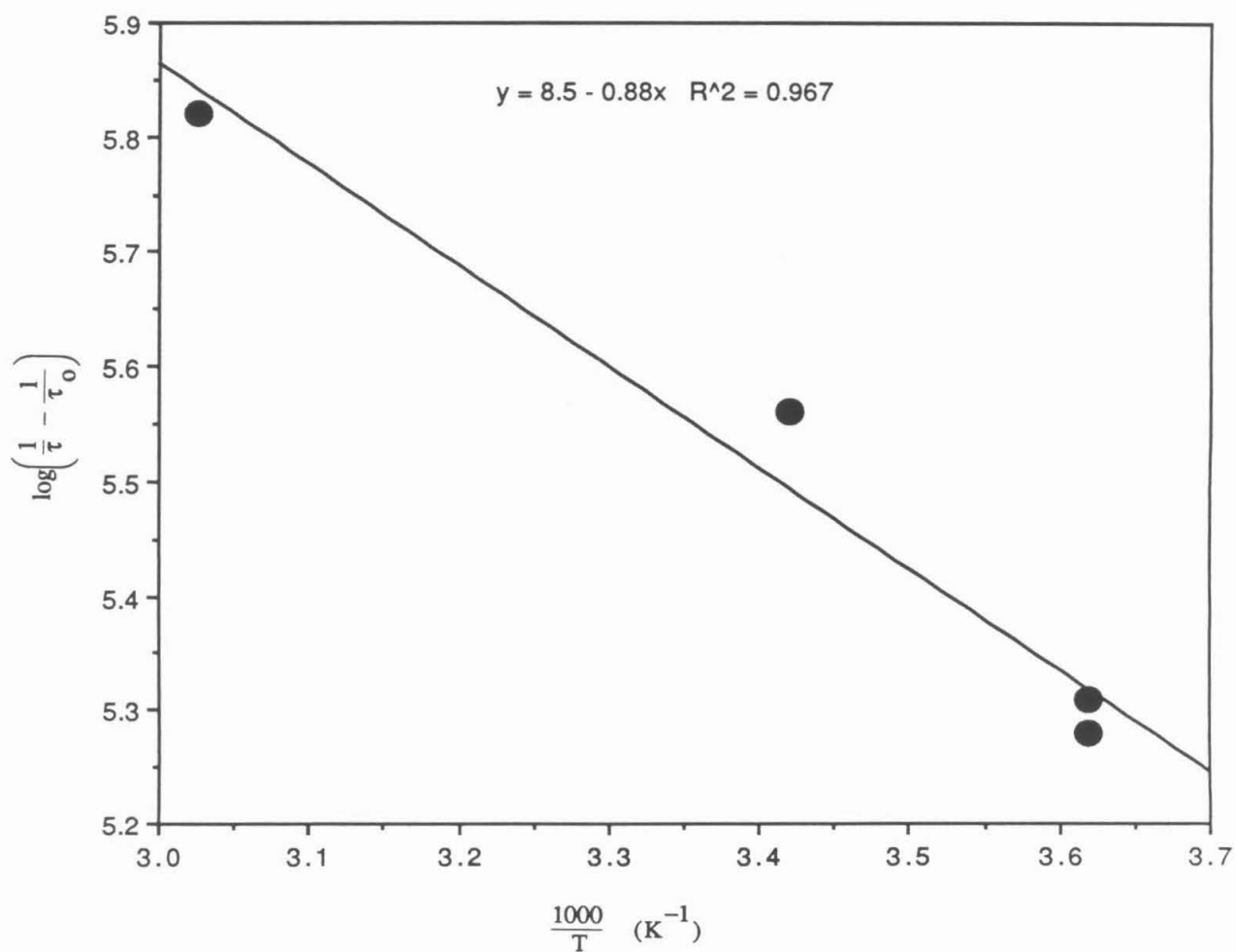


**Figure 18** Temperature dependence of the rate of  $^3\text{Pt}_2^*$  phosphorescence quenching by 3-methyl-2-butanol (7.4M)



## References

- (1) Roundhill, D. M.; Gray, H. B.; Che, C.-M. *Acc. Chem. Res.* **1989**, *22*, 55.
- (2) Zipp, A. P. *Coord. Chem. Rev.* **1988**, *84*, 47.
- (3) Roundhill, D. M.; Shen, Z.; King, C.; Atherton, S. J. *J. Phys. Chem.* **1988**, *92*, 4088.
- (4) Marshall, J. L.; Stiegman, A. E.; Gray, H. B. in *Photochemistry of Dinuclear  $d^8$ - $d^8$  Iridium and Platinum Complexes*; Lever, A. B. P.; American Chemical Society, Washington, D.C., 1986; pp. 166-176.
- (5) Che, C.-M.; Lee, W.-M.; Cho, K.-C.; Harvey, P. D.; Gray, H. B. *J. Phys. Chem.* **1989**, *93*, 3095.
- (6) Smith, D. C., Ph. D. Thesis, California Institute of Technology, 1989.
- (7) Vlcek, A., Jr.; Gray, H. B. *Inorg. Chem.* **1987**, *26*, 1997.
- (8) Roundhill, D. M.; Atherton, S. J.; Shen, Z.-P. *J. Am. Chem. Soc.* **1987**, *109*, 6076.
- (9) Harvey, E. L.; Stiegman, A. E.; Vlcek, A., Jr.; Gray, H. B. *J. Am. Chem. Soc.* **1987**, *109*, 5233.
- (10) Harvey, E. L., Ph. D. Thesis, California Institute of Technology, 1989.
- (11) Stiegman, A. E.; Rice, S. F.; Gray, H. B.; Miskowski, V. M. *Inorg. Chem.* **1987**, *26*, 1112.
- (12) Perrin, D. D.; Armarego, W. L. F.; Perrin, D. R. *Purification of Laboratory Chemicals*; Pergamon Press: Oxford, 1966.
- (13) Nocera, D. G.; Winkler, J. R.; Yocom, K. M.; Bordignon, E.; Gray, H. B. *J. Am. Chem. Soc.* **1984**, *106*, 5145.

- (14) Turro, N. J. *Modern Molecular Photochemistry*; Benjamin/Cummings: Menlo Park, NJ, 1978.
- (15) Formosinho, S. J. *J. C. Faraday II* **1976**, *72*, 1313.
- (16) Ayscough, P. B.; Sealy, R. C. *J. C. S. Perkin II* **1974**, 1402.
- (17) Bond strengths either provided in, or estimated from, McMillen, D. F.; Golden, D. M. *Ann. Rev. Phys. Chem.* **1982**, *33*, 493.
- (18) Rice, S. F.; Gray, H. B. *J. Am. Chem. Soc.* **1983**, *105*, 4571.
- (19) Crane, D. R.; Ford, P. C. **1990**, unpublished results.
- (20) Brunschwig, B. S.; DeLaive, P. J.; English, A. M.; Goldberg, M.; Gray, H. B.; Mayo, S. L.; Sutin, N. *Inorg. Chem.* **1985**, *24*, 3743.
- (21) Wasserman, A. *Monatsh. Chem.* **1952**, *83*, 543.

---

---

**Chapter 2**

Characterization and Reactivity of  
Tetrakis(bis(difluoroborato)- $\mu$ -pyrophosphito)diplatinate(II)

---

---

Robert J. Sweeney, Larry Henling, Harry B. Gray

## Introduction

To test the postulate that H-atom abstraction reactivity of the triplet state of tetrakis( $\mu$ -pyrophosphito)diplatinate(II)  ${}^3\text{Pt}_2^*$  with alcohol substrates is governed by interaction of the substrate with the  $\text{Pt}_2$  ligands, an attempt was made to perturb the interligand OH network in the metal complex. Close examination of the H-bonding arrangement around an axial site in  $\text{Pt}_2$  reveals four 6-membered rings fused together around a central Pt atom (Figure 1). The arrangement of atoms within each 6-membered ring resembles the arrangement of atoms in the enol tautomer of a  $\beta$ -diketone complex. In analogy to  $\beta$ -diketonates, the bridging protons in  $\text{Pt}_2$  are susceptible to replacement with  $\text{BF}_2^+$ .

Reaction of  $[\text{TBA}]_4\text{Pt}_2$  with  $\text{BF}_3$  or  $\text{BF}_3\cdot\text{OEt}_2$  produces a new compound that bears a striking physical and photophysical resemblance to  $\text{Pt}_2$ , but is much harder to oxidize.<sup>1</sup> This new complex, tetrakis(bis(difluoroborato)- $\mu$ -pyrophosphito)diplatinate(II), has the structure shown in Figure 2; the complex will be abbreviated as  $\text{BF}_2\text{Pt}_2$ .

In analogy to the products of oxidative addition to  $\text{Pt}_2$ , a series of axially substituted  $\text{BF}_2\text{Pt}_2\text{X}_2$  ( $\text{X}=\text{Cl}, \text{Br}, \text{I}$ ) complexes are available through direct reaction of  $\text{BF}_2\text{Pt}_2$  and  $\text{X}_2$ . H-atom-transfer quenching reactivity of  ${}^3\text{BF}_2\text{Pt}_2^*$  is also similar to that of the parent compound.



**Figure 1.** Structure of one face of the tetrakis( $\mu$ -pyrophosphito)diplatinate(II) tetraanion.

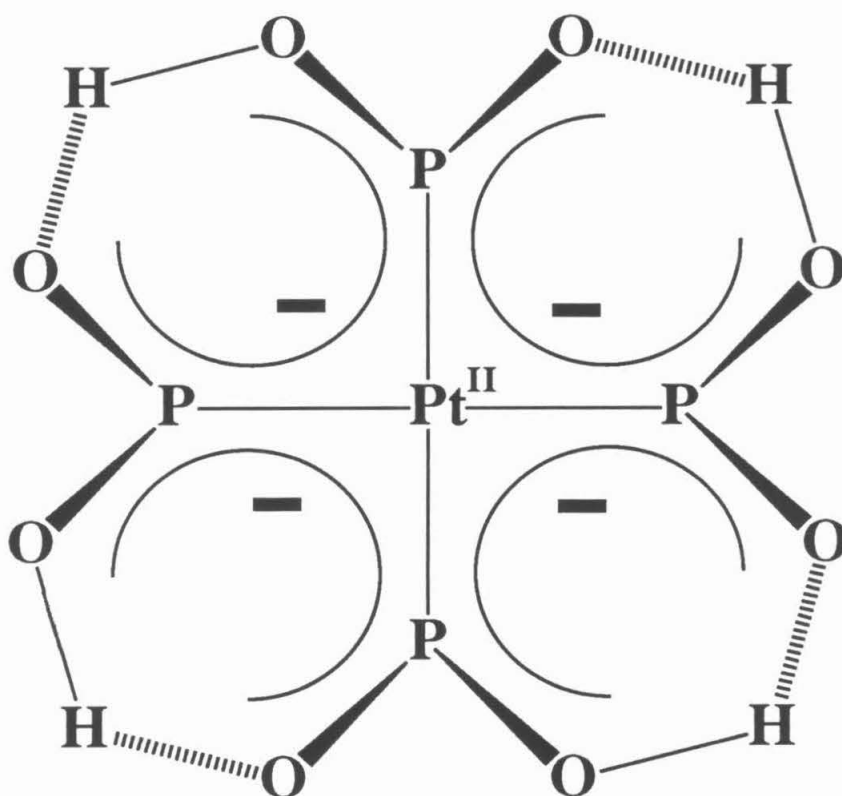
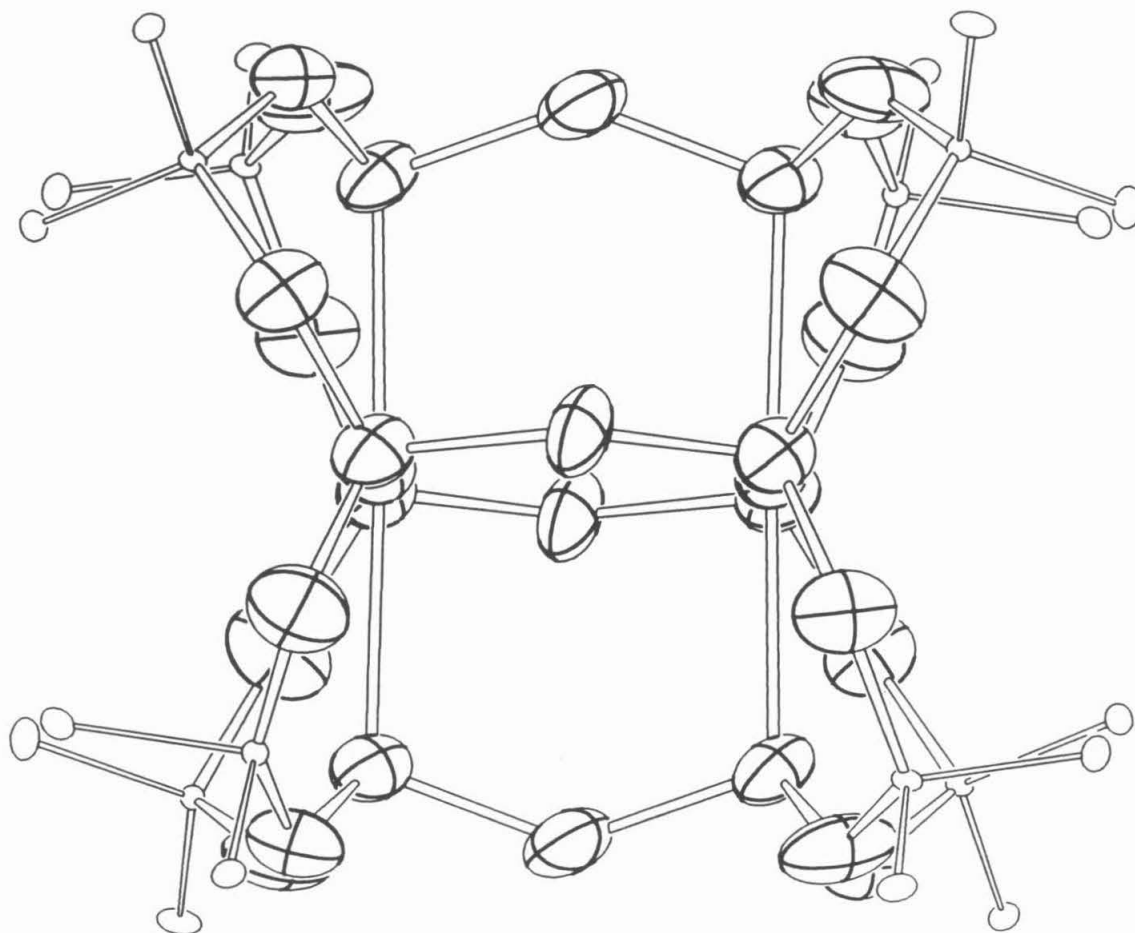


**Figure 2** An ORTEP drawing of tetrakis(bis(difluoroborato)- $\mu$ -pyrophosphito)diplatinate(II). Thermal ellipsoids are shown at the 20% probability level; the  $\text{BF}_2$  groups are one-tenth scale.



## Experimental Details

### Instrumentation

All spectroscopic measurements were made in Burdick and Jackson High-Purity acetonitrile.

UV-Visible absorption spectra were measured on a Cary 14 UV-Visible spectrometer; all spectra were run against solvent baselines.

Emission spectra were recorded on a previously described<sup>2</sup> emission spectrometer; 366 nm excitation light from an Oriel 200W Hg/Xe lamp was selected with a Spex 1670 monochromator and an Oriel 366 nm(#5643) interference filter. Emitted light was sent through a cutoff filter into a Spex 1870 monochromator connected to a Hamamatsu R955 photomultiplier tube and EG & G 182-A lock-in amplifier. Uncorrected spectra were printed out on a chart recorder. Quantum yields were measured relative to quinine sulfate in 1M H<sub>2</sub>SO<sub>4</sub> as a standard ( $\Phi_f=0.546$ ).<sup>3</sup> Relative emission intensities were measured by cutting out the emission bands from photocopies of emission spectra and weighing the paper.

Excited-state lifetimes ( $\tau$ ) were measured with a Quanta Ray Nd:YAG (8 ns fwhm; 355 nm excitation) laser system described elsewhere.<sup>4</sup>  $^3\text{Pt}_2^*$  emission was monitored at 518 nm. Quenching rate constants  $k_q$  were determined using the Stern-Volmer kinetics outlined in Chapter 1. Quenching rate constants and the quantities derived from them have estimated associated errors of <10%.

## Synthesis and Purification

Alcohol and hydrocarbon quenchers and solvents were purified as described in Chapter 1.  $[\text{TBA}]_4\text{BF}_2\text{Pt}_2$  and  $[\text{TBA}]_4\text{BF}_2\text{Pt}_2\text{X}_2$  ( $\text{X}=\text{Cl}$ ,  $\text{Br}$ ,  $\text{I}$ ) were prepared as previously described.<sup>1</sup>

In an attempt to synthesize the  $\text{BCl}_2^+$ -substituted compound, 1 ml of  $\text{BCl}_3$  in hexanes (1M, Aldrich) was added to 11 mg  $[\text{TBA}]_4\text{Pt}_2$  under an argon atmosphere. After a few minutes, all volatiles were removed under vacuum, leaving behind a yellow powder that demonstrated a bright yellow emission under a black light. UV-Vis spectra were taken of this solid dissolved in 10 ml acetonitrile and exposed to air. The yellow solution had UV  $\lambda_{\text{max}}$  values of 239 and 367 nm. From comparison with the  $\text{BF}_2^+$ -substituted dimer, this could well be " $\text{BCl}_2\text{Pt}_2$ ." Exposed to air overnight, a new UV spectrum appeared, with  $\lambda_{\text{max}}$  values similar to those for  $\text{Pt}_2\text{Cl}_2$  (283 and 356 nm). A yellow precipitate also began to form, and the emission turned greener. Hydrolysis by atmospheric moisture probably accounted for the decomposition.

## Crystal Structure

Small, transparent, green crystals of  $[\text{TBA}]_4\text{BF}_2\text{Pt}_2$  were obtained by enclosing an open vial containing an acetonitrile solution of  $[\text{TBA}]_4\text{BF}_2\text{Pt}_2$  in a larger chamber of ethyl ether. As the ether transferred onto the acetonitrile solution, a yellow-green oil came out of the solution, and crystals began to form slowly on the walls of the vial. Several crystals were examined and found to be inadequate before a twinned but usable crystal was found. Crystals also formed from methylene chloride/diethyl ether solutions, but

these samples clouded and lost order rapidly, once they were removed from the solution.

All crystallographic measurements and calculations were performed by Larry Henling at Caltech.

A flat fragment was broken off a twinned crystal, mounted on a fiber and centered on a CAD-4 diffractometer. Unit cell parameters and an orientation cell matrix were obtained by a least-squares calculation from the setting angles of 24 reflections with  $26^\circ < 2\theta < 31^\circ$ . Two equivalent data sets out to a  $2\theta$  of  $45^\circ$  were collected at a  $\chi$  angle calculated to minimize absorption. The data were corrected for absorption and decay. An average background as a function of  $2\theta$  was calculated but not used. Lorentz and polarization factors were applied and the two data sets were then merged to yield the final data set. Preliminary Weissenberg photographs and absences in the diffractometer data revealed the space group to be  $P2_1/n$ . The platinum dimer has a center of symmetry and therefore only one half of the dimer was located in a unit cell.

A Patterson map gave the platinum atom coordinates. The remaining non-hydrogen atoms in the dianion were located via successive structure factor-Fourier calculations. One of the two tetra-*n*-butyl ammonium cations was disordered and defied attempts at construction of a refinable model. As a result, four of the carbon atoms (the last two atoms on two of the arms) were fixed in positions derived from electron density maps calculated from the end of the least-squares refinement process. One terminal atom was placed in three sites with populations based on relative peak heights. Isotropic temperature factors were estimated from

the refined atoms. All parameters for these four atoms were then held constant for the remainder of the refinement.

In the early stages of refinement, the thermal parameters of the BF<sub>2</sub> group adjacent to the disordered cation were larger than those of the other three groups. Additionally, the BF<sub>2</sub> and the cation were unusually close. On the assumption that this site was partially occupied by both a BF<sub>2</sub> bridge and a hydrogen atom, population factors were introduced for all four BF<sub>2</sub> groups, with the three atoms in each group constrained to the same population. In the final cycle of least squares, the populations of three of the groups converged to within  $2\sigma$  ( $\sigma < 0.02$ ) of unity. However, the site near the cation had a population of only 0.73(2). The boron atom in this group, and all refined carbon atoms, were treated isotropically. Anisotropic displacement parameters were used for the remaining non-hydrogen atoms. The fractional hydrogen atom was ignored in the calculations.

The position of the tetra-*n*-butyl ammonium cation apparently depends on the nature of the bridging group. The hydrogen atoms of the cations were introduced as constant contributions of the structure factors at calculated positions (C-H=0.95Å), assuming staggered geometry. They were repositioned before the final three cycles. The complete least-squares full matrix, consisting of coordinates, displacement parameters, and a scale factor, contained 373 variables. A final difference Fourier map showed deviations ranging from  $-2.41\text{e}\text{\AA}^{-3}$  to  $+3.44\text{e}\text{\AA}^{-3}$ . The largest features were near the platinum and were attributed to deficiencies in the absorption correction. The refinement converged with an R-factor of 0.1196 (0.0774 for  $F_0^2 > 3\sigma(F_0^2)$ ) and a goodness of fit of 2.00 for all

6557 reflections. The R-factors for various subsets of reflections revealed nothing unusual. Crystallographic data, including associated error estimates, are given in the appendix.

Calculations were done with programs of the CRYM Crystallographic Computing System and ORTEP. Scattering factors and corrections for anomalous scattering were taken from a standard reference.  $R = \frac{\sum |F_o - |F_c||}{\sum F_o}$ , for only  $F_o^2 > 0$ , and goodness of fit =  $[\sum w(F_o^2 - F_c^2)^2 / (n - p)]^{1/2}$ , where n is the number of data and p the number of parameters refined. The function minimized in least squares was  $\sum w(F_o^2 - F_c^2)^2$ , where  $w = 1/\sigma^2(F_o^2)$ . Variances of the individual reflections were assigned based on counting statistics plus an additional term,  $0.014|l|^2$ . Variances of the merged reflections were determined by standard propagation of error plus another additional term,  $0.014\langle l \rangle^2$ . The absorption correction was done by Gaussian integration over an 8x8x8 grid. Transmission factors varied from 0.56 to 0.79.

## Results and Discussion

### Crystal Structure

Like the parent compound Pt<sub>2</sub>, BF<sub>2</sub>Pt<sub>2</sub> consists of two rigorously eclipsed, square-planar platinum(II) ions bridged by four bidentate pyrophosphito ligands (Figure 3). Difluoroborato groups replace the protons between terminal oxygen atoms in the parent compound Pt<sub>2</sub>. The two halves of the dimer are related by a center of symmetry. The eclipsed phosphorus atoms have torsional angles of 0.1(2) and 0.3(2)°. The platinum atom lies 0.04Å from the plane that passes closest to the four coordinated phosphorus atoms, and the Pt-Pt-P angles range from 90.6(1) to 91.4(1)°. There are no significant interactions between different ions in the crystal.

Tables 1 and 2 contain selected distances and angles for both BF<sub>2</sub>Pt<sub>2</sub> and Pt<sub>2</sub>.<sup>5-7</sup>

As predicted by Harvey and Gray<sup>1</sup> from UV absorption data, the Pt-P bond distances shorten in BF<sub>2</sub>Pt<sub>2</sub>. The electron-withdrawing BF<sub>2</sub><sup>+</sup> groups increase the π-acidity of the phosphorus atoms, strengthening the backbonding interactions. Electron density transfers from the π/π\* Pt-Pt orbitals to the phosphorus centers, leading to less repulsive interactions between the metals. The decrease in intermetallic repulsion shortens the Pt-Pt bond (by 0.041Å), and the increase in backbonding shortens the Pt-P bond (by 0.015-0.040Å).



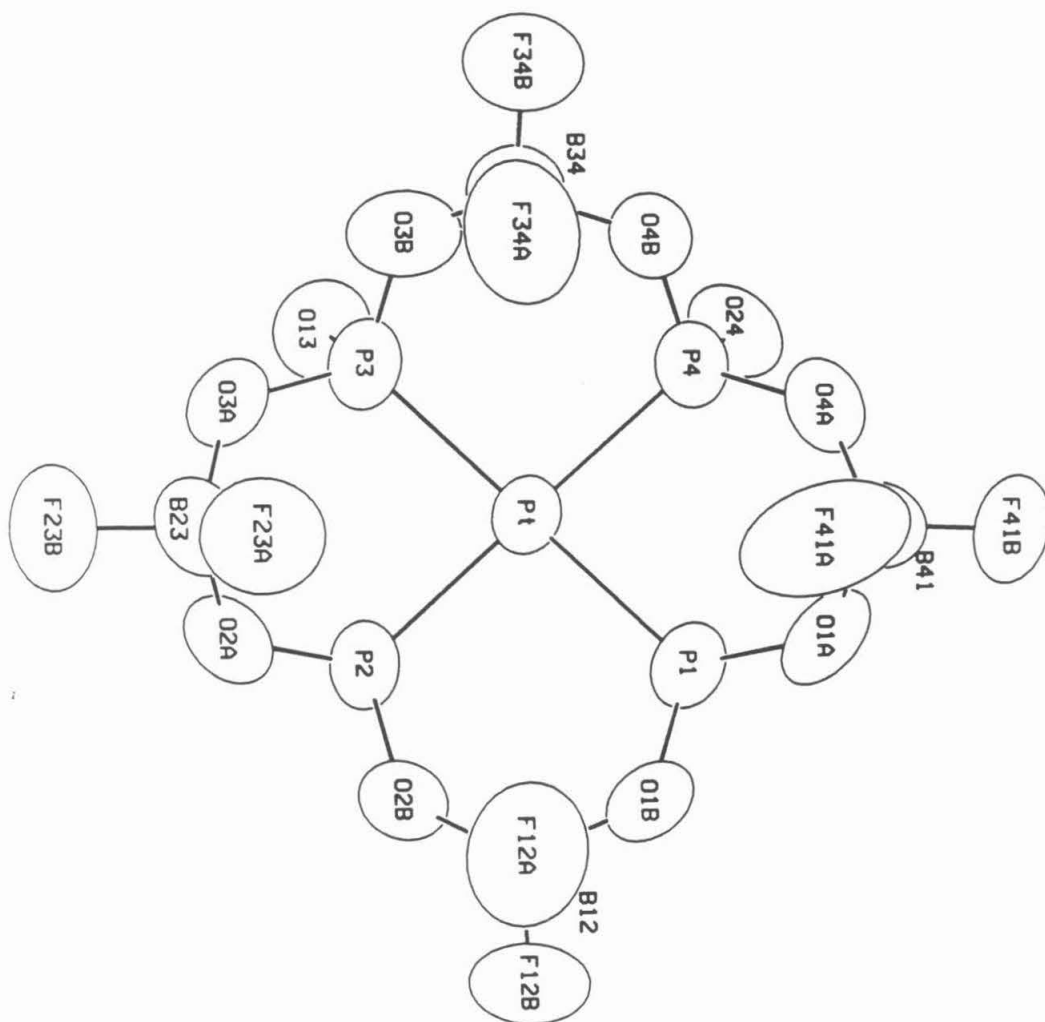
Table 1. Selected bond distances for BF<sub>2</sub>Pt<sub>2</sub> and Pt<sub>2</sub>.

Bond Distance (Å)	[TBA] <sub>4</sub> BF <sub>2</sub> Pt <sub>2</sub>	K <sub>4</sub> Pt <sub>2</sub>
Pt-Pt	2.884	2.925
Pt-P	2.278-2.305	2.320
P-O <sub>term</sub>	1.51-1.56	1.52, 1.58
P-O <sub>bridge</sub>	1.56-1.64	1.62

Table 2. Selected bond angles for BF<sub>2</sub>Pt<sub>2</sub> and Pt<sub>2</sub>.

Bond Angle (°)	[TBA] <sub>4</sub> BF <sub>2</sub> Pt <sub>2</sub>	K <sub>4</sub> Pt <sub>2</sub>
Pt-Pt-P	90.6, 91.4	90.7
P-Pt-P	90.8, 88.9	
P-O-P <sub>bridge</sub>	137	133
O-P-O <sub>term</sub>	107	

**Figure 3** An ORTEP drawing of one face of the tetrakis(bis(difluoroborato)- $\mu$ -pyrophosphito)diplatinate(II) tetraanion shown at the 10% probability level.



The terminal P-O bonds, which alternate between double and single bonds in hydrogen-bonded Pt<sub>2</sub>, have equivalent lengths in BF<sub>2</sub>Pt<sub>2</sub>, reflecting the covalent nature of B-O bonds.

Table 3 Selected geometric parameters for BF<sub>2</sub>Pt<sub>2</sub> and other BF<sub>2</sub>-bridged square-planar, platinum phosphito complexes.

	[TBA] <sub>4</sub> BF <sub>2</sub> Pt <sub>2</sub>	Reference Compounds
Bond Distance (Å)		
B-F	1.33-1.43	1.31-1.40
B-O	1.44	1.46-1.49
Bond Angle (°)		
O-B-O	116-119	107-110
F-B-F	103-110	112

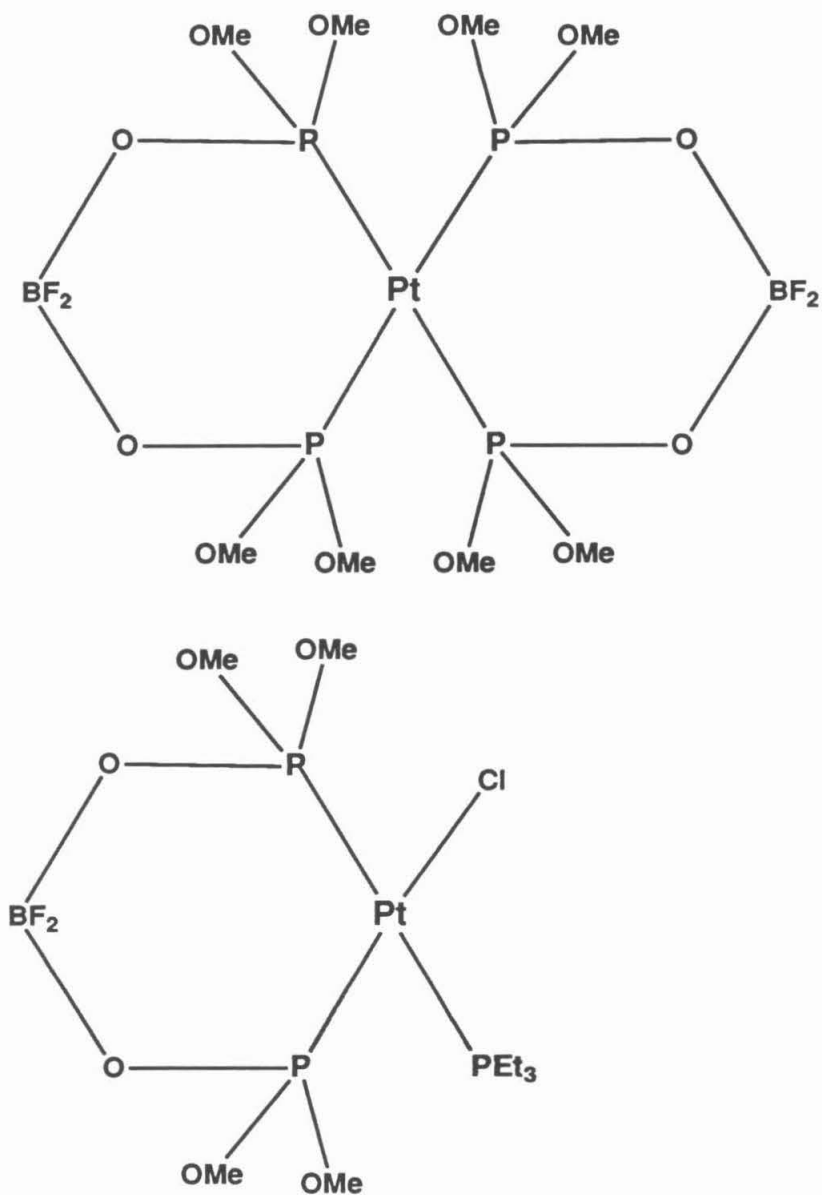
The O-B and B-F bond lengths (Table 3) are in agreement with those found for other BF<sub>2</sub>-bridged phosphito ligands on square-planar platinum centers<sup>8, 9</sup> (Figure 4). The O-B-O angles in BF<sub>2</sub>Pt<sub>2</sub> are larger, and the F-B-F angles smaller, than in those same compounds, a difference that may reflect ring strain in BF<sub>2</sub>Pt<sub>2</sub>.

On average, the crystal structure predicts 7.5 BF<sub>2</sub> groups per platinum dimer unit. This population may reflect either the actual solution composition of BF<sub>2</sub>Pt<sub>2</sub> or merely the fraction of solution species that crystallize. Either way, reaction with BF<sub>3</sub>·OEt<sub>2</sub> effectively replaces all eight protons on the original dimer with BF<sub>2</sub><sup>+</sup> groups. The dimers pack in the crystal so that any protons left on the dimer concentrate in the cramped region of the unit cell

where the TBA cation is very close to the ligands, since protons take up less space than BF<sub>2</sub> groups. This accounts for the reduced population in only one crystallographic BF<sub>2</sub> site.

The BF<sub>2</sub> group with a low population density is excluded from Tables 1,2 and 3. The bond angles ( $\angle\text{O-B-O}=132^\circ$ ,  $\angle\text{F-B-F}=97^\circ$ ) and distances ( $d(\text{B-F})=1.36\text{\AA}$ ,  $1.53\text{\AA}$ ,  $d(\text{B-O})=1.23\text{\AA}$ ,  $1.43\text{\AA}$ ) for this group are not within the range of values found for the other BF<sub>2</sub> groups. Because crystallographic calculations ignore the (assumed) partial population of the proton in that position when the BF<sub>2</sub> is absent, the position of the boron atom is subject to errors in excess of the calculated standard deviations. Therefore, the strange distances and angles may or may not reflect the actual geometry of the BF<sub>2</sub> moiety. If the geometry is accurate, it indicates that ring-induced strain could account for the difficulty in fully populating this position.

**Figure 4** Structures of previously reported difluoroborato-substituted, square-planar, phosphito platinum complexes.



## Photophysics

Photophysical properties of  $\text{BF}_2\text{Pt}_2$  are startlingly similar to those of  $\text{Pt}_2$ . The emission band maxima, excited triplet-state lifetime (10  $\mu\text{sec}$ ) and phosphorescence quantum yields are nearly identical within experimental resolution. In contrast, a large increase is observed in the fluorescence quantum yield of  $\text{BF}_2\text{Pt}_2$  (Table 4). This increase may reflect the extra rigidity forced on  $\text{BF}_2\text{Pt}_2$  by the new 6-membered covalently bound rings introduced through  $\text{BF}_2$  substitution. A decrease in the the number of accessible vibrational modes may eliminate deactivational motions important to the singlet state. High-energy O-H vibrational modes, which are eliminated in the modified complex, may be responsible for this effect.

Heuer, et al.<sup>10</sup> reported the phosphorescence quantum yield for  $\text{Pt}_2$  in water as 0.52, but they report the unquenched lifetime to be only 6.2 msec. Assuming that the decrease in lifetime is due to quenching, the unquenched quantum yield can be calculated, using  $\tau_0=10$  msec. The resulting value of 0.83 agrees with our results.

The axial dihalides  $\text{BF}_2\text{Pt}_2\text{X}_2$  ( $\text{X}=\text{Cl}, \text{Br}, \text{I}$ ) have electronic absorption spectra that closely resemble those of the  $\text{Pt}_2$  derivatives. Absorption and emission data for the dihalides are presented in Table 5.

Table 4 Emission parameters for BF<sub>2</sub>Pt<sub>2</sub> and Pt<sub>2</sub>

Emission	[TBA] <sub>4</sub> Pt <sub>2</sub>	[TBA] <sub>4</sub> BF <sub>2</sub> Pt <sub>2</sub>
Phosphorescence $\lambda_{\max}$ (nm), 77K	518	521
Fluorescence $\lambda_{\max}$ (nm), 77K	409	409
Phosphorescence $\lambda_{\max}$ (nm), RT	524	521
$\Phi_p$ , RT	0.8	0.8
Fluorescence $\lambda_{\max}$ (nm), RT	416	413
$\Phi_f$ , RT	$1 \times 10^{-4}$	$7 \times 10^{-3}$

Table 5 Photophysical parameters for axial dihydrides

X <sub>2</sub>	Pt <sub>2</sub> X <sub>2</sub> absorption $\lambda_{\max}$ (nm)	BF <sub>2</sub> Pt <sub>2</sub> X <sub>2</sub> absorption $\lambda_{\max}$ (nm) <sup>a</sup>	Pt <sub>2</sub> X <sub>2</sub> emission $\lambda_{\max}$ (nm) <sup>b</sup>	BF <sub>2</sub> Pt <sub>2</sub> X <sub>2</sub> emission $\lambda_{\max}$ (nm) <sup>c</sup>
Cl <sub>2</sub>	285	276 (4.66)	685	628
	349	321 (4.05)		
Br <sub>2</sub>	308	301 (4.64)	715	685
	349	336 (4.43)		
I <sub>2</sub>	338	364 (4.60)	-----	-----
	438	455 (3.73)		

a  $\log(\epsilon)$  is in parentheses

b Ph<sub>4</sub>As<sup>+</sup> salt in ethanol/methanol glass<sup>11</sup>

c measured in acetonitrile solutions at 77K.

## H-atom Transfer

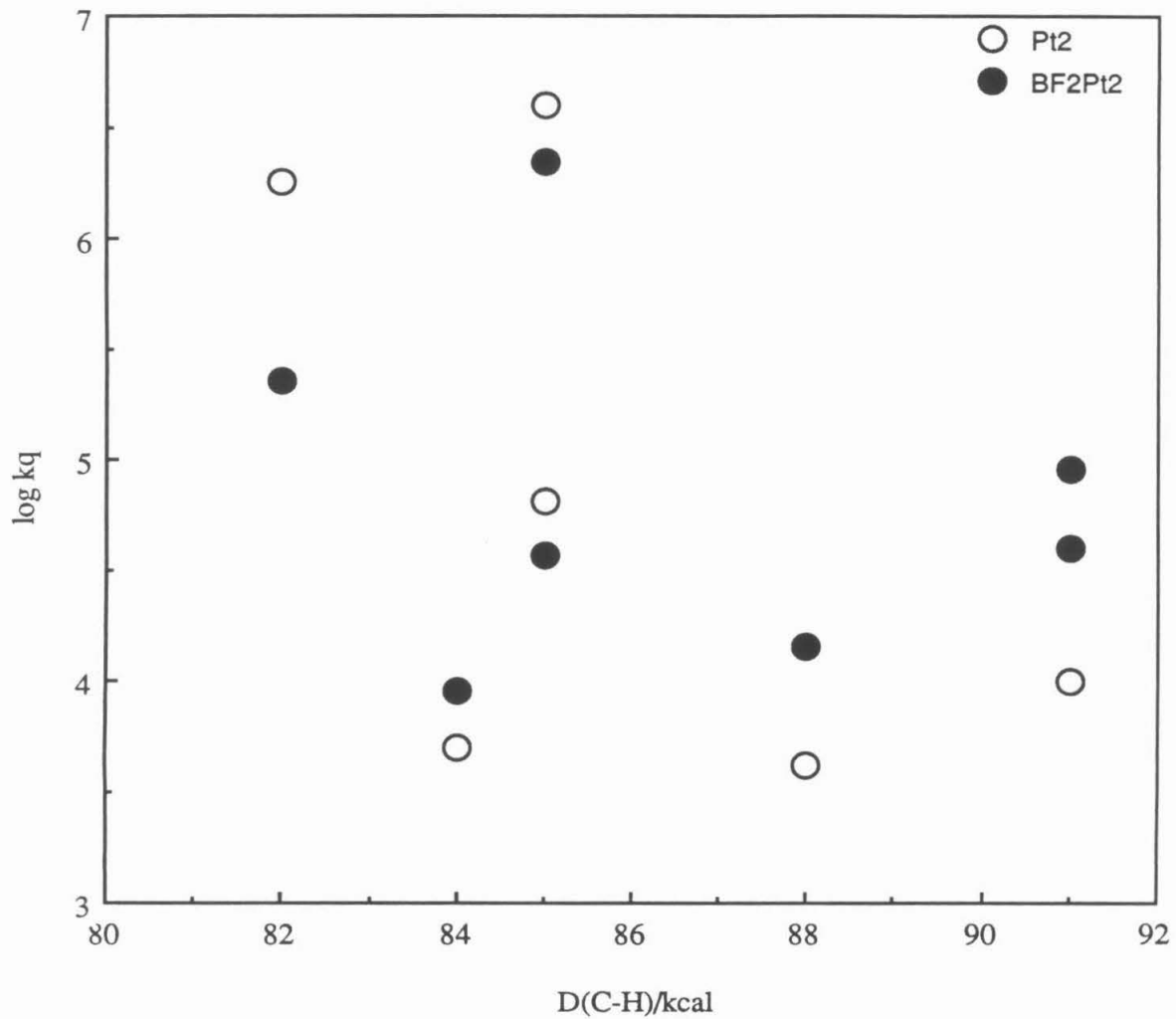
In contrast to differences of several orders of magnitude observed in electron-transfer reactivity,<sup>1, 12</sup> quenching rates for  $^3\text{Pt}_2^*$  and  $^3\text{BF}_2\text{Pt}_2^*$  with a given H-atom donor are all within an order of magnitude<sup>13</sup> (Table 6 and Figure 5). Although differences in reactivities between  $^3\text{Pt}_2^*$  and  $^3\text{BF}_2\text{Pt}_2^*$  with alcohols are expected because of the loss of protons available for hydrogen bonding and the stronger Pt-H bond in  $\text{BF}_2\text{Pt}_2\text{H}_2$ , the steric bulk introduced by  $\text{BF}_2$  groups can account for reactivity differences with alcohols. As demonstrated in Chapter 1, increasing steric bulk of the substrate increases  $k_q$  with small aliphatic alcohols but decreases  $k_q$  with the larger benzyl alcohols. This same trend is observed when steric bulk is increased at the axial site, as with the substitution of  $\text{BF}_2^+$  groups for protons. The quenching of aliphatic alcohols is faster with  $\text{BF}_2\text{Pt}_2$  than with  $\text{Pt}_2$ . The opposite is true for the benzyl alcohols.

The similarity in quenching rates of alcohols with  $\text{Pt}_2$  and  $\text{BF}_2\text{Pt}_2$  also implies that the ligands' oxygen atoms participate in the hydrogen-bonding of the alcohols to  $\text{Pt}_2$ , since the ligand protons have been removed. On the other hand, the large quenching rate for benzyl methyl ether<sup>14</sup> with  $^3\text{Pt}_2^*$  indicates that the ligand protons, when present, also help in docking.

Reactivity differences with benzyl hydrocarbons are not easily rationalized, since the quenching is not well understood (see Chapter 1). However, an electron-transfer mechanism may be ruled out since the  $k_q$  change with  $\text{BF}_2$  substitution is much smaller than the large



**Figure 5** Quenching rates for  $^3\text{Pt}_2^*$  and  $^3\text{BF}_2\text{Pt}_2^*$  phosphorescence with H-atom donors in acetonitrile solutions at room temperature.



changes consistently observed for both reductive and oxidative electron transfer.

The efficiency of the dehydrogenation of isopropanol as measured by formation of  $\text{BF}_2\text{Pt}_2\text{H}_2$  ( $k_p=1 \times 10^4 \text{ M}^{-1}\text{s}^{-1}$ ,  $F=0.1$ ) is identical to that for the reaction of  $\text{Pt}_2$  with isopropanol, a counter-intuitive result since the axial dihydride is thought to result from disproportionation of the monohydride.<sup>15</sup> Changing the sterics and hydrophilicity of the axial site should affect the efficiency of dihydride formation if this mechanism reflects reality.

Table 6 Stern-Volmer quenching rate constants for the reaction of excited platinum dimers and organic H-atom donors

Substrate	$^3\text{Pt}_2^*$ Quenching Rate $k_q$ ( $\text{M}^{-1}\text{s}^{-1}$ )	$^3\text{BF}_2\text{Pt}_2^*$ Quenching Rate $k_q$ ( $\text{M}^{-1}\text{s}^{-1}$ )	C-H Bond Strength <sup>16</sup> (kcal/mol)
cumene	$5.0 \times 10^3$	$9 \times 10^3$	84
ethylbenzene	$6.4 \times 10^4$	$3.7 \times 10^4$	85
toluene	$4.2 \times 10^3$	$1.4 \times 10^4$	88
$\alpha$ -methylbenzyl alcohol	$1.8 \times 10^6$	$2.3 \times 10^5$	82
benzyl alcohol	$4 \times 10^6$ $2.2 \times 10^6$ <sup>a</sup>	$2.2 \times 10^6$	85
sec-butanol	$\sim 10^4$	$4 \times 10^4$	91
isopropanol	$\sim 10^4$	$9 \times 10^4$	91

a static quenching as measured by emission intensity quenching.

## Conclusions

The emissive product of the reaction between  $\text{BF}_3$  and  $\text{Pt}_2$  is a species with a general structure identical to  $\text{Pt}_2$  except for replacement of  $\text{BF}_2^+$  groups for the eight ligand protons. The substantial changes in bond lengths that are due to this substitution are consistent with expectations and reflect an increase in the  $\pi$ -acidity of the pyrophosphito ligands. Evidence suggests ring strain in  $\text{BF}_2\text{Pt}_2$ 's polycyclic ligand's structure.

Considering the changes in bond lengths, the photophysical properties of  $\text{BF}_2\text{Pt}_2$  and  $\text{Pt}_2$  are remarkably similar. The rates of emission quenching with H-atom donors also vary little between the two compounds, and those differences that exist are easily rationalized through previous results with the parent system.

**References**

- (1) Harvey, E. L., Ph. D. Thesis, California Institute of Technology, 1989.
- (2) Rice, S. F.; Gray, H. B. *J. Am. Chem. Soc.* **1983**, *105*, 4571.
- (3) Demas, J. N.; Crosby, G. A. *J. Phys. Chem.* **1971**, *75*, 991.
- (4) Nocera, D. G.; Winkler, J. R.; Yocom, K. M.; Bordignon, E.; Gray, H. B. *J. Am. Chem. Soc.* **1984**, *106*, 5145.
- (5) Pinto, M. A. F. D. R.; Sadler, P. J.; Neidler, S.; Sanderson, M. R.; Subbiah, A.; Kuroda, R. *J. Chem. Soc., Chem. Comm.* **1980**, 13.
- (6) Marsh, R. E.; Herbstein, F. H. *Acta. Cryst.* **1983**, *B39*, 280.
- (7) Che, C.-M.; Herbstein, F. H.; Schaefer, W. P.; Marsh, R. E.; Gray, H. B. *J. Am. Chem. Soc.* **1983**, *105*, 4604.
- (8) Berry, D. E.; Bushnell, G. W.; Dixon, K. R. *Inorg. Chem.* **1982**, *21*, 957.
- (9) Roundhill, S. G. N.; Roundhill, D. M. *Acta. Cryst.* **1982**, *B38*, 2479.
- (10) Heuer, W. B.; Totten, M. D.; Rodman, G. S.; Hebert, E. J.; Tracy, H. J.; Nagle, J. K. *J. Am. Chem. Soc.* **1984**, *106*, 1163.
- (11) Stiegman, A. E.; Miskowski, V. M.; Gray, H. B. *J. Am. Chem. Soc.* **1986**, *108*, 2781.
- (12) Julia Hodge, unpublished results.
- (13) Some quenching rates determined by Erica Harvey, Reference 1.
- (14) Crane, D. R.; Ford, P. C. **1990**, Manuscript submitted for publication.
- (15) Roundhill, D. M.; Atherton, S. J.; Shen, Z.-P. *J. Am. Chem. Soc.* **1987**, *109*, 6076.

- (16) Bond strengths found in, or estimated from, McMillen, D. F. & Golden, D. M. *Ann. Rev. Phys. Chem.* **1982**, *33*, 493.

**Appendix: Crystallographic Data for  
Tetrakis(tetra-*n*-butylammonium)  
tetrakis(bis(difluoroborato)- $\mu$ -  
pyrophosphito)diplatinate(II)**

Table A1	Crystal and Intensity Collection Data for Tetrakis(tetra- <i>n</i> -butylammonium) tetrakis(bis(difluoroborato)- $\mu$ -pyrophosphito)diplatinate(II)
Table A2	Final Anion Parameters for Tetrakis(tetra- <i>n</i> -butylammonium) tetrakis(bis(difluoroborato)- $\mu$ -pyrophosphito)diplatinate(II)
Table A3	Final Cation Parameters for Tetrakis(tetra- <i>n</i> -butylammonium) tetrakis(bis(difluoroborato)- $\mu$ -pyrophosphito)diplatinate(II)
Table A4	Assigned Hydrogen Parameters for Tetrakis(tetra- <i>n</i> -butylammonium) tetrakis(bis(difluoroborato)- $\mu$ -pyrophosphito)diplatinate(II)
Table A5	Anisotropic Parameters for Tetrakis(tetra- <i>n</i> -butylammonium) tetrakis(bis(difluoroborato)- $\mu$ -pyrophosphito)diplatinate(II)
Table A6	Complete Distances and Angles for Tetrakis(tetra- <i>n</i> -butylammonium) tetrakis(bis(difluoroborato)- $\mu$ -pyrophosphito)diplatinate(II)
Table A7	Observed and Calculated Structure Factors for Tetrakis(tetra- <i>n</i> -butylammonium) tetrakis(bis(difluoroborato)- $\mu$ -pyrophosphito)diplatinate(II)

**Table A1** Crystal and Intensity Collection Data for  
Tetrakis(tetra-*n*-butylammonium) tetrakis(bis(difluoroborato)- $\mu$ -  
pyrophosphito)diplatinat(II)

Formula:  $\text{Pt}_2\text{P}_8\text{O}_{20}\text{B}_{7.46}\text{F}_{14.92}\text{N}_4\text{C}_{64}\text{H}_{144.54}$

Crystal color: Lime-green

Habit: Bladed

Crystal size:  $0.07 \times 0.21 \times 0.56$  mm

Space group:  $P2_1/n$  (#14)

$a = 16.678(7)\text{\AA}$

$b = 16.751(9)\text{\AA}$

$\beta = 99.58(8)^\circ$

$c = 18.131(24)\text{\AA}$

$\rho_{\text{calc}} = 1.52 \text{ g cm}^{-3}$

$\mu = 31.65 \text{ cm}^{-1}$  ( $\mu_{\text{r,max}} = 1.91$ )

Transmission coeff. =  $0.56 - 0.79$

$\omega$  scan

$\lambda = 0.7107\text{\AA}$

Graphite monochromator

$2\theta$  range:  $2^\circ - 45^\circ$

Octants collected:  $h, \pm k, \pm l$

$T = 294^\circ\text{K}$

Number of reflections measured: 14269

Number of independent reflections: 6557

Number with  $F_o^2 > 0$ : 5401

Number with  $F_o^2 > 3\sigma(F_o^2)$ : 3299

Number of reflections used in refinement: 6557

Goodness of fit for merging data: 1.46

Final R-index: 0.1196 for 5401 reflections with  $F_o^2 > 0$

Final R-index: 0.0774 for 3299 reflections with  $F_o^2 > 3\sigma(F_o^2)$

Final goodness of fit: 2.00 for 373 parameters and 6557 reflections

**Table A2** Final Anion Parameters for Tetrakis(tetra-*n*-butylammonium) tetrakis(bis(difluoroborato)- $\mu$ -pyrophosphito)diplatinate(II)

Atom	$x, y, z$ and $U_{eq}^a \times 10^4$			
	$x$	$y$	$z$	$U_{eq}$ or $B$
Pt	218(.5)	677(.5)	483(.4)	658(2)
P1	-806(3)	389(3)	1129(3)	801(17)
P2	-625(4)	1497(3)	-309(3)	808(17)
P3	1257(4)	999(3)	-138(3)	844(18)
P4	1074(4)	-112(3)	1309(3)	803(17)
O1a	-552(9)	211(8)	1981(7)	1141(51)
O1b	-1516(7)	985(9)	1057(7)	1032(43)
O13	1240(7)	408(7)	-858(6)	985(44)
O2a	-254(9)	2190(7)	-659(6)	899(43)
O2b	-1382(8)	1802(8)	-40(7)	1208(47)
O24	1009(8)	-1007(7)	1050(7)	1056(45)
O3a	1215(7)	1827(8)	-508(6)	908(40)
O3b	2138(8)	899(9)	299(9)	1219(54)
O4a	876(8)	-164(8)	2095(6)	1146(50)
O4b	1993(7)	80(8)	1377(6)	946(42)
B12	-1678(18)	1722(20)	628(15)	985(98)
F12a	-1320(9)	2315(7)	1140(8)	1616(56)
F12b	-2487(8)	1878(8)	569(7)	1546(50)
B23	599(20)	2417(19)	-447(13)	971(107)
F23a	738(7)	2731(7)	256(7)	1325(46)



Atom	<i>x</i>	<i>y</i>	<i>z</i>	<i>U<sub>eq</sub></i> or <i>B</i>
F23b	736(7)	3042(6)	-944(6)	1309(44)
B34	2377(27)	599(26)	913(24)	7.8(9) *
F34a	2360(12)	1323(12)	1420(9)	1689(80)
F34b	3191(9)	453(9)	1078(9)	1385(65)
B41	241(17)	166(17)	2443(18)	896(96)
F41a	439(8)	946(9)	2617(9)	1759(61)
F41b	165(7)	-232(9)	3061(6)	1570(53)

$$^{\circ} U_{eq} = \frac{1}{3} \sum_i \sum_j [U_{ij}(a_i^* a_j^*)(\vec{a}_i \cdot \vec{a}_j)]$$

\* Isotropic displacement parameter, *B*

**Table A3** Final Cation Parameters for  
Tetrakis(tetra-*n*-butylammonium) tetrakis(bis(difluoroborato)- $\mu$ -  
pyrophosphito)diplatinate(II)

Atom	$x, y, z$ and $U_{eq}^a \times 10^4$			$U_{eq}$ or $B$
	$x$	$y$	$z$	
N1	6514(10)	1775(9)	7595(9)	980(54)
C1	6720(12)	2611(12)	7741(11)	7.9(5) *
C2	7490(13)	2823(13)	8273(11)	9.2(6) *
C3	7611(14)	3696(14)	8443(12)	10.5(6) *
C4	8340(15)	3935(14)	8999(14)	12.9(8) *
C5	7181(12)	1348(12)	7279(11)	8.4(5) *
C6	7367(13)	1699(13)	6564(12)	10.5(6) *
C7	7968(16)	1150(15)	6251(15)	13.5(8) *
C8	8201(18)	1539(18)	5540(17)	18.0(11) *
C9	6428(12)	1334(12)	8324(11)	8.5(5) *
C10	5777(13)	1653(12)	8735(12)	10.0(6) *
C11	5757(14)	1132(13)	9436(13)	11.6(7) *
C12	5143(16)	1450(15)	9858(15)	15.5(9) *
C13	5721(13)	1732(13)	7041(12)	8.8(6) *
C14	5391(13)	921(13)	6788(11)	9.8(6) *
C15	4604(14)	926(14)	6233(13)	11.7(7) *
C16	4315(15)	109(17)	6025(14)	13.6(8) *
N2	1829(10)	1850(11)	7285(9)	1127(58)
C17	2408(13)	2555(13)	7435(12)	8.8(5) *
C18	2511(15)	2919(16)	8255(14)	13.2(8) *
C19	3149(18)	3623(17)	8395(14)	14.2(9) *
C20	3903(19)	3265(18)	8419(16)	17.1(10) *
C21	1829(12)	1661(12)	6451(11)	8.9(5) *
C22	1248(13)	1013(13)	6134(12)	10.8(6) *
C25	2109(15)	1158(15)	7761(13)	11.0(7) *
C26	2923(15)	823(15)	7684(13)	13.4(8) *
C29	971(15)	2086(14)	7409(12)	10.1(6) *
C30	572(17)	2741(17)	7037(15)	14.3(9) *
C31	-328(23)	2812(23)	7239(20)	19.1(13) *
C32	-509(27)	3503(28)	7043(25)	26.7(19) *
C23	1494	873	5361	16.0 *
C24	1000	1423	4809	20.0 *
C27	3209	197	8280	17.0 *
C28A	4059	-132	8173	19.1 *
C28B	3458	-564	7909	19.1 *
C28C	3333	593	9054	19.1 *

$$^a U_{eq} = \frac{1}{3} \sum_i \sum_j [U_{ij}(a_i^* a_j^*)(\bar{a}_i \cdot \bar{a}_j)]$$

\* Isotropic displacement parameter,  $B$

**Table A4** Assigned Hydrogen Parameters for  
Tetrakis(tetra-*n*-butylammonium) tetrakis(bis(difluoroborato)- $\mu$ -  
pyrophosphito)diplatinate(II)

Atom	$x, y$ and $z \times 10^4$			<i>B</i>
	<i>x</i>	<i>y</i>	<i>z</i>	
HC1A	6281	2841	7934	9.0
HC1B	6764	2844	7272	9.0
HC2A	7942	2643	8062	11.0
HC2B	7480	2555	8733	11.0
HC3A	7147	3880	8628	13.0
HC3B	7655	3956	7988	13.0
HC4A	8344	4503	9054	15.0
HC4B	8314	3696	9469	15.0
HC4C	8822	3773	8829	15.0
HC5A	7025	807	7190	9.0
HC5B	7665	1368	7644	9.0
HC6A	7603	2211	6661	11.0
HC6B	6882	1739	6213	11.0
HC7A	7723	646	6136	13.0
HC7B	8443	1087	6620	13.0
HC8A	8573	1185	5355	15.0
HC8B	7726	1591	5181	15.0
HC8C	8446	2031	5665	15.0
HC9A	6934	1373	8655	9.0
HC9B	6308	793	8208	9.0
H10A	5264	1633	8418	11.0
H10B	5897	2189	8886	11.0
H11A	6272	1129	9743	13.0
H11B	5605	600	9285	13.0
H12A	5138	1132	10286	15.0
H12B	5300	1983	10008	15.0
H12C	4633	1453	9550	15.0
H13A	5805	2017	6608	9.0
H13B	5320	1992	7267	9.0
H14A	5300	639	7215	11.0
H14B	5787	663	6557	11.0
H15A	4680	1200	5793	13.0
H15B	4192	1186	6451	13.0
H16A	3821	140	5674	15.0
H16B	4714	-158	5795	15.0
H16C	4227	-172	6453	15.0
H17A	2984	2395	7387	9.0
H17B	2299	3001	7102	9.0
H18A	2675	2498	8607	11.0

Atom	<i>x</i>	<i>y</i>	<i>z</i>	<i>B</i>
H18B	1990	3104	8322	11.0
H19A	3114	3880	8858	13.0
H19B	3046	3998	8002	13.0
H20A	4305	3670	8505	15.0
H20B	3982	2892	8816	15.0
H20C	3915	3010	7960	15.0
H21A	2386	1461	6431	9.0
H21B	1749	2121	6168	9.0
H22A	697	1196	6076	11.0
H22B	1296	534	6417	11.0
H23A	1393	334	5209	13.0
H23B	2056	988	5389	13.0
H24A	1148	1350	4330	15.0
H24B	439	1307	4784	15.0
H24C	1101	1960	4964	15.0
H25A	1724	704	7612	9.0
H25B	2103	1258	8264	9.0
H26A	3298	1263	7745	11.0
H26B	2912	600	7202	11.0
H27A	2827	-228	8233	13.0
H27B	3249	430	8763	13.0
H28A	4233	-524	8544	15.0
H28B	4019	-365	7691	15.0
H28C	4441	293	8220	15.0
H28D	3633	-954	8282	15.0
H28E	3006	-764	7571	15.0
H28F	3890	-447	7645	15.0
H28G	3508	204	9427	15.0
H28H	3733	1000	9075	15.0
H28J	2835	820	9139	15.0
H29A	1030	2172	7941	9.0
H29B	649	1617	7291	9.0
H30A	543	2663	6520	11.0
H30B	874	3206	7195	11.0
H31A	-318	2752	7755	13.0
H31B	-677	2441	6962	13.0
H32A	-1048	3617	7127	15.0
H32B	-144	3876	7306	15.0
H32C	-502	3565	6514	15.0

**Table A5** Anisotropic Parameters for  
Tetrakis(tetra-*n*-butylammonium) tetrakis(bis(difluoroborato)- $\mu$ -  
pyrophosphito)diplatinate(II)

Atom	$U_{11}$	$U_{22}$	$U_{33}$	$U_{12}$	$U_{13}$	$U_{23}$
Pt	851(5)	656(5)	525(4)	108(6)	288(3)	23(5)
P1	1007(45)	830(45)	647(37)	69(37)	372(32)	39(31)
P2	1202(50)	608(37)	713(38)	194(35)	450(36)	123(32)
P3	1070(51)	750(43)	781(38)	28(35)	356(36)	144(32)
P4	1039(50)	811(43)	610(35)	197(37)	283(32)	115(31)
O1a	1022(112)	1836(149)	685(93)	-30(101)	489(83)	66(92)
O1b	972(103)	1321(127)	937(97)	262(94)	551(81)	181(90)
O13	1403(116)	679(98)	947(98)	39(81)	414(82)	-293(75)
O2a	928(104)	828(97)	880(105)	124(90)	-32(86)	157(76)
O2b	1373(126)	1345(125)	1058(109)	810(101)	642(99)	401(94)
O24	1357(120)	763(97)	1048(105)	426(82)	202(87)	84(83)
O3a	959(102)	914(104)	956(98)	7(84)	467(79)	146(82)
O3b	809(106)	1513(145)	1307(126)	22(98)	91(92)	51(113)
O4a	1292(118)	1613(133)	561(81)	529(102)	236(81)	340(83)
O4b	810(101)	1206(108)	805(88)	26(83)	81(74)	271(80)
B12	941(233)	1272(274)	757(200)	30(208)	181(177)	280(190)
F12a	2174(161)	1185(113)	1536(129)	-370(103)	443(109)	-152(96)
F12b	1208(110)	1744(130)	1788(128)	627(99)	544(95)	313(99)
B23	1369(291)	1203(247)	368(145)	419(226)	225(170)	29(158)
F23a	1545(118)	1409(112)	1029(100)	110(84)	234(83)	-292(82)
F23b	1821(127)	932(89)	1233(102)	-93(84)	423(86)	283(79)
F34a	2068(208)	1778(194)	1140(156)	-237(159)	29(132)	137(139)
F34b	1039(135)	1207(151)	1888(168)	-30(108)	184(112)	205(120)
B41	716(222)	815(206)	1099(245)	-184(184)	-18(192)	-15(191)
F41a	1267(122)	1643(145)	2460(175)	-432(104)	584(108)	-779(124)
F41b	1283(110)	2465(170)	1053(96)	168(100)	461(81)	881(105)
N1	1203(146)	745(118)	1029(126)	157(104)	298(112)	32(98)
N2	1184(146)	1328(156)	920(128)	-255(128)	325(107)	-160(120)

$U_{i,j}$  values have been multiplied by  $10^4$

The form of the displacement factor is:

$$\exp -2\pi^2(U_{11}h^2a^{*2} + U_{22}k^2b^{*2} + U_{33}l^2c^{*2} + 2U_{12}hka^*b^* + 2U_{13}hla^*c^* + 2U_{23}klb^*c^*)$$

**Table A6** Complete Distances and Angles for  
Tetrakis(tetra-*n*-butylammonium) tetrakis(bis(difluoroborato)- $\mu$ -  
pyrophosphito)diplatinate(II)

	Distance(Å)		Distance(Å)
Pt -Pt	2.884(1)	C2 -C3	1.50(3)
Pt -P1	2.278(5)	C2 -HC2A	0.949
Pt -P2	2.291(6)	C2 -HC2B	0.951
Pt -P3	2.281(6)	C3 -C4	1.50(3)
Pt -P4	2.305(5)	C3 -HC3A	0.943
P1 -O1a	1.562(15)	C3 -HC3B	0.948
P1 -O1b	1.537(14)	C4 -HC4A	0.956
P1 -O13	1.558(13)	C4 -HC4B	0.948
P2 -O2a	1.505(14)	C4 -HC4C	0.947
P2 -O2b	1.515(14)	C5 -C6	1.50(3)
P2 -O24	1.613(14)	C5 -HC5A	0.949
P3 -O13	1.635(13)	C5 -HC5B	0.955
P3 -O3a	1.539(13)	C6 -C7	1.54(3)
P3 -O3b	1.558(16)	C6 -HC6A	0.948
P4 -O24	1.570(14)	C6 -HC6B	0.945
P4 -O4a	1.518(14)	C7 -C8	1.55(4)
P4 -O4b	1.549(13)	C7 -HC7A	0.946
O1a -B41	1.45(3)	C7 -HC7B	0.954
O1b -B12	1.46(3)	C8 -HC8A	0.958
O2a -B23	1.46(3)	C8 -HC8B	0.941
O2b -B12	1.39(3)	C8 -HC8C	0.931
O3a -B23	1.44(3)	C9 -C10	1.51(3)
O3b -B34	1.23(5)	C9 -HC9A	0.952
O4a -B41	1.43(3)	C9 -HC9B	0.943
O4b -B34	1.43(5)	C10 -C11	1.55(3)
B12 -F12a	1.42(3)	C10 -H10A	0.948
B12 -F12b	1.36(3)	C10 -H10B	0.950
B23 -F23a	1.36(3)	C11 -C12	1.48(4)
B23 -F23b	1.43(3)	C11 -H11A	0.943
B34 -F34a	1.53(5)	C11 -H11B	0.954
B34 -F34b	1.36(5)	C12 -H12A	0.942
B41 -F41a	1.37(3)	C12 -H12B	0.957
B41 -F41b	1.33(3)	C12 -H12C	0.936
N1 -C1	1.46(3)	C13 -C14	1.51(3)
N1 -C5	1.51(3)	C13 -H13A	0.949
N1 -C9	1.54(3)	C13 -H13B	0.947
N1 -C13	1.52(3)	C14 -C15	1.52(3)
C1 -C2	1.51(3)	C14 -H14A	0.940
C1 -HC1A	0.945	C14 -H14B	0.944
C1 -HC1B	0.948	C15 -C16	1.48(4)

Distance(Å)		Distance(Å)	
C15 -H15A	0.946	C27 -C28B	1.531
C15 -H15B	0.953	C27 -C28C	1.535
C16 -H16A	0.956	C27 -H27A	0.950
C16 -H16B	0.953	C27 -H27B	0.950
C16 -H16C	0.940	C28A -H28A	0.950
N2 -C17	1.52(3)	C28A -H28B	0.950
N2 -C21	1.55(3)	C28A -H28C	0.950
N2 -C25	1.47(3)	C28B -H28D	0.950
N2 -C29	1.54(3)	C28B -H28E	0.950
C17 -C18	1.59(3)	C28B -H28F	0.950
C17 -H17A	1.014	C28C -H28G	0.950
C17 -H17B	0.959	C28C -H28H	0.950
C18 -C19	1.58(4)	C28C -H28J	0.950
C18 -H18A	0.959	C29 -C30	1.40(4)
C18 -H18B	0.951	C29 -H29A	0.965
C19 -C20	1.39(4)	C29 -H29B	0.955
C19 -H19A	0.954	C30 -C31	1.61(5)
C19 -H19B	0.945	C30 -H30A	0.940
C20 -H20A	0.949	C30 -H30B	0.946
C20 -H20B	0.945	C31 -C32	1.23(6)
C20 -H20C	0.939	C31 -H31A	0.938
C21 -C22	1.50(3)	C31 -H31B	0.938
C21 -H21A	0.993	C32 -H32A	0.955
C21 -H21B	0.923	C32 -H32B	0.946
C22 -C23	1.543	C32 -H32C	0.967
C22 -H22A	0.958		
C22 -H22B	0.949		
C23 -C24	1.501		
C23 -H23A	0.950		
C23 -H23B	0.950		
C24 -H24A	0.950		
C24 -H24B	0.950		
C24 -H24C	0.950		
C25 -C26	1.50(3)		
C25 -H25A	1.001		
C25 -H25B	0.930		
C26 -C27	1.525		
C26 -H26A	0.961		
C26 -H26B	0.947		
C27 -C28A	1.563		

Angle(°)			Angle(°)		
P1 -Pt -P2	90.8(2)	B23 -O3a -P3	124.4(14)		
P1 -Pt -P3	178.2(2)	B34 -O3b -P3	130.0(24)		
P1 -Pt -P4	88.9(2)	B41 -O4a -P4	133.2(15)		
P2 -Pt -P3	89.3(2)	B34 -O4b -P4	127.7(20)		
P2 -Pt -P4	178.0(2)	O2b -B12 -O1b	119.1(22)		
P3 -Pt -P4	90.9(2)	F12a -B12 -O1b	102.9(20)		
P4 -O24 -P2	137.1(9)	F12b -B12 -O1b	107.3(21)		
P3 -O13 -P1	135.7(8)	F12a -B12 -O2b	109.3(21)		
Pt -P1 -O1a	116.5(6)	F12b -B12 -O2b	113.8(22)		
Pt -P1 -O1b	116.9(6)	F12b -B12 -F12a	102.7(21)		
Pt -P1 -O13	111.6(5)	O3a -B23 -O2a	118.4(21)		
Pt -P2 -O2a	118.3(6)	F23a -B23 -O2a	110.8(21)		
Pt -P2 -O2b	117.3(6)	F23b -B23 -O2a	106.1(20)		
Pt -P2 -O24	109.6(5)	F23a -B23 -O3a	108.9(20)		
Pt -P3 -O3a	116.4(5)	F23b -B23 -O3a	105.2(20)		
Pt -P3 -O3b	116.9(6)	F23b -B23 -F23a	106.7(20)		
Pt -P3 -O13	109.7(5)	O4b -B34 -O3b	132.2(36)		
Pt -P4 -O4a	115.8(6)	F34a -B34 -O3b	100.7(31)		
Pt -P4 -O4b	115.5(5)	F34b -B34 -O3b	115.8(35)		
Pt -P4 -O24	110.4(5)	F34a -B34 -O4b	94.2(27)		
Pt -Pt -P1	90.6(1)	F34b -B34 -O4b	106.8(30)		
Pt -Pt -P2	91.4(1)	F34b -B34 -F34a	97.4(28)		
Pt -Pt -P3	91.3(1)	O4a -B41 -O1a	115.9(22)		
Pt -Pt -P4	90.6(1)	F41a -B41 -O1a	104.2(21)		
O1b -P1 -O1a	106.6(8)	F41b -B41 -O1a	107.9(22)		
O13 -P1 -O1a	100.5(7)	F41a -B41 -O4a	107.6(21)		
O13 -P1 -O1b	102.7(7)	F41b -B41 -O4a	111.1(22)		
O2b -P2 -O2a	107.3(8)	F41b -B41 -F41a	109.8(22)		
O24 -P2 -O2a	100.0(7)	C5 -N1 -C1	110.9(14)		
O24 -P2 -O2b	101.8(7)	C9 -N1 -C1	110.9(14)		
O3a -P3 -O13	101.8(7)	C13 -N1 -C1	108.5(15)		
O3b -P3 -O13	103.3(7)	C9 -N1 -C5	106.1(14)		
O3b -P3 -O3a	106.8(8)	C13 -N1 -C5	109.9(14)		
O4a -P4 -O24	102.1(7)	C13 -N1 -C9	110.4(14)		
O4b -P4 -O24	103.9(7)	C2 -C1 -N1	119.4(16)		
O4b -P4 -O4a	107.6(7)	HC1A -C1 -N1	106.6		
B41 -O1a -P1	130.9(15)	HC1B -C1 -N1	106.5		
B12 -O1b -P1	131.7(15)	HC1A -C1 -C2	107.2		
B23 -O2a -P2	122.7(14)	HC1B -C1 -C2	106.9		
B12 -O2b -P2	133.1(16)	HC1B -C1 -HC1A	110.1		



Angle(°)			Angle(°)				
C3	-C2	-C1	115.5(18)	HC8C	-C8	-HC8A	110.4
HC2A	-C2	-C1	108.3	HC8C	-C8	-HC8B	111.9
HC2B	-C2	-C1	108.1	C10	-C9	-N1	115.4(16)
HC2A	-C2	-C3	107.8	HC9A	-C9	-N1	107.9
HC2B	-C2	-C3	107.5	HC9B	-C9	-N1	108.3
HC2B	-C2	-HC2A	109.5	HC9A	-C9	-C10	107.4
C4	-C3	-C2	117.7(19)	HC9B	-C9	-C10	107.8
HC3A	-C3	-C2	107.6	HC9B	-C9	-HC9A	109.9
HC3B	-C3	-C2	107.2	C11	-C10	-C9	108.7(17)
HC3A	-C3	-C4	107.2	H10A	-C10	-C9	109.7
HC3B	-C3	-C4	106.9	H10B	-C10	-C9	109.9
HC3B	-C3	-HC3A	110.2	H10A	-C10	-C11	109.7
HC4A	-C4	-C3	109.0	H10B	-C10	-C11	109.2
HC4B	-C4	-C3	109.7	H10B	-C10	-H10A	109.6
HC4C	-C4	-C3	109.9	C12	-C11	-C10	109.5(19)
HC4B	-C4	-HC4A	109.1	H11A	-C11	-C10	110.3
HC4C	-C4	-HC4A	109.2	H11B	-C11	-C10	109.5
HC4C	-C4	-HC4B	109.9	H11A	-C11	-C12	109.7
C6	-C5	-N1	114.4(16)	H11B	-C11	-C12	108.1
HC5A	-C5	-N1	108.5	H11B	-C11	-H11A	109.8
HC5B	-C5	-N1	108.2	H12A	-C12	-C11	108.9
HC5A	-C5	-C6	108.5	H12B	-C12	-C11	107.6
HC5B	-C5	-C6	108.2	H12C	-C12	-C11	109.4
HC5B	-C5	-HC5A	109.1	H12B	-C12	-H12A	109.5
C7	-C6	-C5	109.0(18)	H12C	-C12	-H12A	111.4
HC6A	-C6	-C5	109.5	H12C	-C12	-H12B	110.0
HC6B	-C6	-C5	109.4	C14	-C13	-N1	118.4(17)
HC6A	-C6	-C7	109.5	H13A	-C13	-N1	106.8
HC6B	-C6	-C7	109.4	H13B	-C13	-N1	106.9
HC6B	-C6	-HC6A	110.1	H13A	-C13	-C14	107.4
C8	-C7	-C6	108.9(21)	H13B	-C13	-C14	107.4
HC7A	-C7	-C6	109.2	H13B	-C13	-H13A	109.8
HC7B	-C7	-C6	108.9	C15	-C14	-C13	115.4(18)
HC7A	-C7	-C8	110.6	H14A	-C14	-C13	107.7
HC7B	-C7	-C8	109.7	H14B	-C14	-C13	107.5
HC7B	-C7	-HC7A	109.5	H14A	-C14	-C15	108.0
HC8A	-C8	-C7	107.3	H14B	-C14	-C15	107.5
HC8B	-C8	-C7	108.3	H14B	-C14	-H14A	110.8
HC8C	-C8	-C7	109.3	C16	-C15	-C14	112.0(20)
HC8B	-C8	-HC8A	109.5	H15A	-C15	-C14	109.9

Angle(°)	Angle(°)
H15B -C15 -C14 109.3	C22 -C21 -N2 114.7(16)
H15A -C15 -C16 108.5	H21A -C21 -N2 104.9
H15B -C15 -C16 107.5	H21B -C21 -N2 110.3
H15B -C15 -H15A 109.6	H21A -C21 -C22 106.9
H16A -C16 -C15 109.2	H21B -C21 -C22 111.5
H16B -C16 -C15 108.9	H21B -C21 -H21A 108.1
H16C -C16 -C15 110.0	C23 -C22 -C21 101.8
H16B -C16 -H16A 108.8	H22A -C22 -C21 110.9
H16C -C16 -H16A 109.8	H22B -C22 -C21 114.3
H16C -C16 -H16B 110.1	H22A -C22 -C23 110.1
C21 -N2 -C17 103.3(15)	H22B -C22 -C23 110.6
C25 -N2 -C17 112.1(16)	H22B -C22 -H22A 108.9
C29 -N2 -C17 110.8(16)	C24 -C23 -C22 108.2
C25 -N2 -C21 111.0(16)	H23A -C23 -C22 110.3
C29 -N2 -C21 110.3(15)	H23B -C23 -C22 109.2
C29 -N2 -C25 109.2(16)	H23A -C23 -C24 109.8
C18 -C17 -N2 115.6(17)	H23B -C23 -C24 109.8
H17A -C17 -N2 111.2	H23B -C23 -H23A 109.5
H17B -C17 -N2 116.3	H24A -C24 -C23 109.5
H17A -C17 -C18 103.0	H24B -C24 -C23 109.5
H17B -C17 -C18 105.6	H24C -C24 -C23 109.5
H17B -C17 -H17A 103.7	H24B -C24 -H24A 109.5
C19 -C18 -C17 113.7(20)	H24C -C24 -H24A 109.5
H18A -C18 -C17 108.4	H24C -C24 -H24B 109.5
H18B -C18 -C17 106.7	C26 -C25 -N2 116.3(20)
H18A -C18 -C19 109.4	H25A -C25 -N2 108.3
H18B -C18 -C19 110.0	H25B -C25 -N2 112.2
H18B -C18 -H18A 108.6	H25A -C25 -C26 104.0
C20 -C19 -C18 105.3(23)	H25B -C25 -C26 108.5
H19A -C19 -C18 109.9	H25B -C25 -H25A 106.8
H19B -C19 -C18 110.0	C27 -C26 -C25 111.9
H19A -C19 -C20 110.8	H26A -C26 -C25 106.6
H19B -C19 -C20 111.2	H26B -C26 -C25 110.8
H19B -C19 -H19A 109.6	H26A -C26 -C27 108.9
H20A -C20 -C19 108.0	H26B -C26 -C27 109.8
H20B -C20 -C19 108.7	H26B -C26 -H26A 108.8
H20C -C20 -C19 108.7	C28A -C27 -C26 109.7
H20B -C20 -H20A 110.0	C28B -C27 -C26 109.7
H20C -C20 -H20A 110.5	C28C -C27 -C26 109.3
H20C -C20 -H20B 110.8	H27A -C27 -C26 109.1

Angle(°)				Angle(°)			
H27B	-C27	-C26	109.7	H31A	-C31	-C32	110.5
H27A	-C27	-C28A	109.4	H31B	-C31	-C32	111.5
H27B	-C27	-C28A	109.4	H31B	-C31	-H31A	111.6
H27B	-C27	-H27A	109.5	H32A	-C32	-C31	109.6
H28A	-C28A	-C27	109.5	H32B	-C32	-C31	111.6
H28B	-C28A	-C27	109.5	H32C	-C32	-C31	110.1
H28C	-C28A	-C27	109.5	H32B	-C32	-H32A	109.4
H28B	-C28A	-H28A	109.5	H32C	-C32	-H32A	107.6
H28C	-C28A	-H28A	109.5	H32C	-C32	-H32B	108.4
H28C	-C28A	-H28B	109.5				
H28D	-C28A	-H28C	162.4				
H28F	-C28A	-H28C	120.9				
H28F	-C28A	-H28D	68.4				
H28D	-C28B	-C27	109.5				
H28E	-C28B	-C27	109.5				
H28F	-C28B	-C27	109.5				
H28E	-C28B	-H28D	109.5				
H28F	-C28B	-H28D	109.5				
H28F	-C28B	-H28E	109.5				
H28G	-C28C	-C27	109.5				
H28H	-C28C	-C27	109.5				
H28J	-C28C	-C27	109.5				
H28H	-C28C	-H28G	109.5				
H28J	-C28C	-H28G	109.5				
H28J	-C28C	-H28H	109.5				
C30	-C29	-N2	120.7(20)				
H29A	-C29	-N2	104.0				
H29B	-C29	-N2	105.1				
H29A	-C29	-C30	109.1				
H29B	-C29	-C30	109.4				
H29B	-C29	-H29A	107.9				
C31	-C30	-C29	109.6(24)				
H30A	-C30	-C29	108.3				
H30B	-C30	-C29	108.3				
H30A	-C30	-C31	110.0				
H30B	-C30	-C31	109.9				
H30B	-C30	-H30A	110.7				
C32	-C31	-C30	101.4(33)				
H31A	-C31	-C30	111.0				
H31B	-C31	-C30	110.4				

**Table A7** Observed and Calculated Structure Factors for  
Tetrakis(tetra-*n*-butylammonium) tetrakis(bis(difluoroborato)- $\mu$ -  
pyrophosphito)diplatinate(II)

The columns contain, in order,  $I$ ,  $10F_{\text{obs}}$ ,  $10F_{\text{calc}}$ , and  $10(F^2_{\text{obs}}-F^2_{\text{calc}})/\sigma F^2_{\text{obs}}$ . A minus sign preceding  $F_{\text{obs}}$  indicates that  $F^2_{\text{obs}}$  is negative.

Fluoroborated Pt:2 POP4.

Page 1

-17	0	1		7	681	555	33	7	497	371	24	12	490	461	6
				8	-174	10	-8								
				9	155	281	-17	-16	8	1		-15	5	1	
1	227	144	9	10	112	102	0								
3	275	69	21	11	249	127	15	2	-126	9	-3	1	325	290	6
5	374	311	7					3	-98	97	-4	2	115	14	4
7	572	450	19					4	-193	172	-18	3	376	322	9
9	318	214	9									4	271	133	20
				1	400	262	26	-15	0	1		5	364	253	19
				2	223	57	14					6	214	223	-1
				3	410	357	9	1	-215	13	-14	7	194	75	9
1	157	130	2	4	-107	118	-6	3	276	266	1	8	431	375	11
2	-177	56	-10	5	485	327	33	5	995	804	46	9	526	415	25
3	231	171	6	6	433	338	17	7	974	816	38	10	284	257	3
4	150	171	-1	7	88	94	0	9	514	485	5	11	528	439	19
5	360	145	29	8	422	301	25	11	87	100	0				
6	492	378	22	9	-95	124	-7	13	251	221	2	-15	6	1	
7	117	54	2	10	169	177	0								
8	333	297	6	11	263	235	4	-15	1	1		1	-119	159	-11
9	-175	24	-9					1	230	166	8	2	106	186	-6
								2	-309	39	-33	3	251	181	9
								3	214	215	0	4	333	210	18
								4	559	388	42	5	410	300	22
								5	211	251	-5	6	-181	72	-10
								6	933	798	44	7	507	455	11
								7	-147	32	-6	8	297	183	15
								8	667	567	29	9	470	438	6
								9	-60	97	-4	10	456	325	24
								10	217	233	-2	11	276	159	16
								11	385	223	30				
								12	80	47	1	-15	7	1	
								13	224	154	7	1	121	40	3
												2	136	34	5
												3	151	82	4
												4	396	261	25
												5	77	86	0
												6	546	458	19
												7	-199	49	-11
												8	614	506	25
												9	258	162	10
												10	344	307	5
												-15	8	1	
												1	95	38	2
												2	288	85	21
												3	298	152	20
												4	-233	37	-15
												5	276	328	-8
												6	-186	16	-8
												7	518	412	21
												8	-66	38	-1
												-15	9	1	
												1	209	235	-3
												2	-81	53	-2
												3	140	231	-9
												4	212	206	0
												5	68	58	0
												6	377	218	27
												7	126	5	4
												-14	0	1	
												2	341	261	16
												4	780	625	36
												6	951	906	12
												8	740	653	19
												10	429	391	6
												12	0	169	-5
												14	474	482	-1
												-14	1	1	
												1	98	38	2
												2	187	160	3



Fluoroborated Pt2 POP4.

Page 3

10	113	21	3	12	416	294	26					1	449	365	15
11	371	312	11	13	664	637	8	-12	7	1		2	141	11	5
				14	596	582	4					3	414	333	13
-13	10	1		15	261	185	10	1	83	68	0	4	73	129	-3
				16	426	336	20	2	-165	73	-10	5	-180	54	-10
1	191	175	1					3	530	508	6	6	97	98	0
2	468	441	6	-12	3	1		4	-117	21	-4	7	-121	127	-7
3	-98	153	-8					5	813	765	17	8	-176	83	-10
4	34	195	-10	1	446	351	26	6	-158	13	-8				
5	184	210	-3	2	720	717	1	7	828	795	11	-12	13	1	
6	138	20	6	3	348	286	14	8	127	77	3				
7	430	225	37	4	457	446	3	9	376	350	6	1	-166	18	-7
8	223	186	3	5	338	309	6	10	97	136	-3	2	184	193	0
9	108	32	3	6	192	39	15	11	-46	42	-1	3	-42	213	-12
10	420	340	14	7	352	366	-3	12	79	48	1	4	66	61	0
				8	564	519	14	13	418	314	20	5	389	290	15
-13	11	1		9	458	372	21	14	-105	76	-4				
				10	844	895	-18					-11	0	1	
1	440	452	-2	11	-137	156	-14	-12	8	1		1	307	287	4
2	65	93	-1	12	854	848	2	1	-138	76	-8	3	983	947	16
3	466	380	16	13	267	275	-1	2	172	192	-2	5	676	608	20
4	-164	66	-10	14	527	507	13	3	101	147	-3	7	532	528	1
5	49	124	-4	15	347	262	15	4	481	516	-9	9	284	235	6
6	92	15	-2	16	-178	8	-9	5	-80	1	-2	11	247	277	-4
7	-82	85	4					6	772	701	23	13	1026	984	11
8	89	18	1	-12	4	1		7	115	68	2	15	973	958	3
								8	526	497	7	17	389	469	-11
-13	12	1		1	626	602	8	9	-120	108	-9				
				2	-190	111	-16	10	-202	101	-15	-11	1	1	
1	9	118	-3	3	449	395	15	11	184	191	0	1	809	763	19
2	507	372	24	4	257	185	14	12	348	241	19	2	659	631	11
3	133	53	3	5	305	280	5	13	216	127	10	3	359	233	30
4	277	194	10	6	-186	66	-15					4	692	669	9
5	134	153	-1	7	357	285	18	-12	9	1		5	40	28	0
				8	101	135	-2	1	-148	162	-14	6	556	543	4
-12	0	1		9	816	767	17	2	240	315	-12	7	565	513	18
				10	-122	211	-17	3	135	236	-11	8	561	567	-2
2	616	600	6	11	1001	976	9	4	-143	158	-17	9	440	474	-10
4	603	511	24	12	-174	13	-9	5	473	468	1	10	-184	84	-14
6	417	416	0	13	606	638	-9	6	-153	137	-13	11	690	586	37
8	460	414	9	14	88	77	0	7	505	461	10	12	645	631	4
10	429	235	32	15	189	126	6	8	232	267	-5	13	416	315	22
12	523	521	0					9	295	171	18	14	890	908	-6
14	885	900	-3	-12	5	1		10	449	396	12	15	217	135	8
16	695	688	1					11	-124	152	-10	16	628	630	0
				1	215	19	16	12	321	287	6	17	-89	101	-5
-12	1	1		2	371	293	21								
				3	-98	116	-8	-12	10	1		-11	2	1	
1	330	375	-11	4	147	90	5	1	524	515	2	1	671	704	-13
2	358	366	-2	5	362	414	-13	2	-161	121	-11	2	948	871	34
3	585	487	35	6	163	65	9	3	309	317	-1	3	630	582	18
4	109	79	2	7	323	316	1	4	201	228	-3	4	505	442	21
5	524	432	30	8	467	445	6	5	292	30	26	5	422	358	18
6	-133	145	-15	9	172	127	5	6	356	280	13	6	458	443	5
7	592	558	11	10	754	704	17	7	257	218	5	7	655	637	7
8	318	252	13	11	-90	64	-3	8	181	242	-6	8	603	624	-7
9	511	466	13	12	668	577	28	9	499	412	20	9	632	585	16
10	433	373	15	13	261	126	17	10	232	114	12	10	900	892	3
11	-194	55	-13	14	154	233	-9	11	478	452	6	11	79	141	-4
12	244	355	-21	15	276	270	0					12	644	688	-15
13	767	732	11					-12	11	1		13	604	546	17
14	206	210	0	-12	6	1		1	161	138	1	14	440	436	1
15	788	770	5					2	556	459	23	15	641	618	7
16	92	53	1	1	328	301	5	3	-185	90	-11	16	112	22	3
				2	-172	184	-25	4	107	204	-8	17	297	226	11
-12	2	1		3	-93	16	-3	5	-105	66	-5				
				4	709	628	28	6	-161	19	-7	-11	3	1	
1	710	603	38	5	-113	2	-4	7	280	85	17	1	1477	1424	23
2	576	520	19	6	756	760	-1	8	350	298	8	2	680	676	1
3	371	363	2	7	-81	175	-12	9	174	38	7	3	655	595	23
4	392	355	9	8	592	526	20	10	539	416	28	4	345	333	3
5	72	178	-10	9	433	385	12					5	209	154	8
6	550	475	24	10	114	42	3	-12	12	1		6	387	217	42
7	283	287	0	11	282	299	-3					7	556	576	-7
8	580	498	26	12	171	103	5								
9	591	548	13	13	393	236	32								
10	390	407	-4	14	423	369	10								
11	731	708	8	15	-92	122	-6								









Fluoroborated Pt2 POP4.				Page 7												
7	735	701	9	13	338	280	14	6	592	544	21	4	749	733	6	
8	389	327	10	14	457	577	-38	7	857	859	0	5	-95	24	-3	
9	918	814	31	15	313	246	13	8	508	550	-16	6	437	387	14	
10	-207	50	-11	16	555	619	-19	9	947	928	9	7	335	329	1	
11	517	514	0	17	427	421	1	10	139	96	4	8	206	185	3	
12	335	185	22	18	200	132	6	11	605	610	-1	9	498	470	8	
13	-160	170	-12	19	408	370	8	12	409	493	-24	10	374	312	13	
	-8	13	1		-7	2	1	13	-40	62	-2	11	354	297	11	
1	-157	132	-13	1	507	412	39	14	581	573	2	12	542	563	-5	
2	-33	183	-9	2	114	136	-3	15	339	309	6	13	-118	45	-4	
3	274	209	10	3	1812	1808	2	16	-162	119	-13	14	505	472	7	
4	-163	159	-15	4	71	222	-23	17	535	551	-3	15	344	174	21	
5	489	369	26	5	699	790	-50	18	-195	17	-9	16	496	345	29	
6	347	286	11	6	1596	1719	-65		-7	6	1		-7	10	1	
7	459	317	26	7	398	438	-14	1	1516	1439	36	1	267	241	4	
8	646	538	26	8	909	997	-49	2	731	744	-6	2	357	330	6	
9	161	47	6	9	558	583	-11	3	601	687	-39	3	336	380	-10	
10	430	392	6	10	1044	1120	-39	4	239	216	4	4	133	137	0	
11	221	263	-4	11	654	693	-17	5	970	936	17	5	108	63	3	
	-8	14	1	12	448	530	-26	6	487	498	-4	6	489	460	8	
1	115	83	1	13	310	340	-7	7	335	359	-7	7	143	184	-4	
2	377	241	23	14	37	71	-1	8	619	585	13	8	966	884	31	
3	-119	33	-3	15	616	733	-42	9	126	166	-4	9	220	211	1	
4	488	346	31	16	543	543	0	10	518	509	2	10	600	605	-1	
5	146	89	3	17	481	439	11	11	539	548	-3	11	145	103	3	
6	502	369	27	18	621	657	-9	12	-235	205	-34	12	-105	199	-14	
7	286	195	12		-7	3	1	13	967	984	-6	13	268	248	2	
8	219	103	9	1	1508	1552	-24	14	-183	79	-11	14	203	139	6	
9	-41	161	-7	2	45	22	0	15	480	596	-30	15	157	161	0	
10	295	186	13	3	319	341	-7	16	269	155	14		-7	11	1	
	-8	15	1	4	1027	1086	-34		-7	111	251	-18				
1	257	258	0	5	844	860	-8	1	320	353	-8	1	311	405	-20	
2	-126	71	-5	6	261	147	25	2	1692	1700	-3	2	-233	58	-22	
3	379	330	8	7	1764	1785	-10	3	223	191	7	3	-188	79	-13	
4	-176	0	-8	8	395	398	0	4	1461	1460	0	4	-198	37	-13	
5	410	355	10	9	1371	1472	-52	5	514	547	-12	5	570	535	11	
6	104	21	2	10	769	795	-12	6	871	933	-30	6	386	354	7	
7	208	218	0	11	776	840	-29	7	356	284	20	7	1077	993	31	
	-8	16	1	12	96	149	-5	8	102	204	-12	8	147	236	-9	
1	205	200	0	13	-29	208	-16	9	181	149	4	9	962	912	17	
2	292	278	1	14	358	356	0	10	436	453	-5	10	-217	159	-20	
3	-252	64	-15	15	414	404	2	11	214	49	16	11	468	455	3	
	-7	0	1	16	544	437	29	12	1001	994	2	12	183	49	8	
1	1303	1274	16	17	741	729	3	13	-94	125	-6	13	281	76	20	
2	2486	2493	-2	18	189	223	-3	14	1015	1025	-3	14	-40	28	0	
3	2217	2226	-2		-7	4	1	15	-43	3	0		-7	12	1	
4	850	897	-18	1	186	148	6	16	504	556	-12	1	215	187	4	
5	370	307	14	2	802	787	8	17	110	43	2	2	148	179	-3	
6	735	817	-28	3	216	108	21		-7	8	1	3	-159	61	-10	
7	391	451	-13	4	493	480	5	1	1211	1198	6	4	324	223	18	
8	727	727	0	5	114	46	6	2	-97	97	-7	5	357	313	9	
9	363	265	13	6	1329	1311	9	3	1510	1545	-16	6	718	674	13	
10	-52	137	-4	7	467	534	-27	4	143	245	-17	7	430	384	9	
	-7	1	1	8	1171	1221	-25	5	1166	1152	6	8	931	907	7	
1	90	101	-1	9	473	454	6	6	182	149	5	9	111	170	-4	
2	1612	1651	-21	10	1087	1113	-12	7	462	454	2	10	587	586	0	
3	49	73	-1	11	210	285	-16	8	185	178	0	11	98	134	-2	
4	2236	2368	-59	12	467	453	4	9	422	314	27	12	216	248	-3	
5	573	561	5	13	409	321	22	10	243	200	6	13	266	176	10	
6	918	1077	-97	14	145	126	2	11	736	736	0		-7	13	1	
7	327	366	-13	15	217	89	13	12	-104	155	-10	1	207	242	-5	
8	238	312	-24	16	665	621	13	13	960	942	6	2	301	226	11	
9	547	607	-28	17	103	136	-2	14	-88	64	-3	3	181	9	10	
10	506	573	-27	18	682	716	-9	15	656	680	-6	4	428	339	19	
11	348	302	12		-7	5	1	16	246	123	13	5	168	161	0	
12	687	705	-7	1	1279	1279	0		-7	9	1	6	258	322	-9	
				2	335	369	-10	1	263	350	-20	7	632	559	18	
				3	248	219	6	2	980	965	6	8	376	223	25	
				4	572	540	14	3	119	225	-13	9	488	456	6	
				5	543	517	11					10	257	150	12	
												11	370	260	18	

Fluoroborated Pt2 POP4.

12	288	310	-3	8	252	284	-8	1	539	554	-6	-6	10	1	
-7	14	1		9	1023	1124	-56	2	1462	1459	1				
1	212	238	-3	10	1038	1082	-23	3	466	462	1	1	452	530	-25
2	136	177	-3	11	769	826	-26	4	834	876	-23	2	638	617	7
3	403	354	9	12	537	631	-37	5	-32	28	-1	3	79	98	-1
4	163	62	6	13	118	132	-1	6	633	634	0	4	470	343	37
5	429	369	12	14	516	578	-20	7	616	615	0	5	366	368	0
6	346	135	34	15	497	504	-2	8	-74	20	-3	6	-61	72	-3
7	226	200	3	16	461	510	-13	9	836	803	15	7	1030	980	19
8	416	270	25	17	570	636	-19	10	501	480	6	8	227	199	4
9	-88	68	-3	18	64	166	-7	11	8	176	-12	9	687	674	4
10	-217	45	-14	19	541	567	-6	12	856	892	-14	10	280	232	8
-7	15	1		-6	3	1		13	-201	132	-19	11	244	318	-12
1	-121	82	-5	1	86	278	-42	14	748	742	2	12	287	293	0
2	398	340	10	2	-127	16	-10	15	74	161	-6	13	-213	5	-12
3	-8	70	-1	3	552	616	-33	16	317	331	-2	14	195	150	4
4	374	368	0	4	829	816	7	17	329	265	11	15	392	342	10
5	123	22	3	5	-106	119	-13	-6	7	1		-6	11	1	
6	303	256	6	6	2246	2427	-81	1	1884	1876	3	1	-147	53	-8
7	154	41	5	7	-105	51	-7	2	202	208	-1	2	295	308	-2
8	-145	28	-5	8	1830	1927	-47	3	1416	1428	-4	3	69	74	0
-7	16	1		9	798	790	3	4	-167	53	-13	4	575	468	32
1	327	293	5	10	1551	1628	-38	5	1127	1161	-17	5	-77	133	-9
2	-106	116	-5	11	826	840	-6	6	109	35	5	6	745	798	-19
3	400	322	13	12	324	335	-3	7	218	236	-4	7	156	81	6
4	-188	38	-8	13	169	228	-8	8	138	27	8	8	1098	1060	13
5	254	260	0	14	307	251	11	9	466	431	11	9	233	278	-7
6	-54	129	-4	15	176	310	-23	10	-270	73	-28	10	543	571	-7
-6	0	1		16	597	597	0	11	918	899	7	11	300	95	27
2	2061	2222	-79	17	178	249	-8	12	214	279	-9	12	260	173	11
4	2746	2964	-71	18	700	704	-1	13	1178	1163	6	13	134	9	5
6	1524	1648	-54	-6	4	1		14	-144	192	-16	14	301	214	12
8	514	447	21	1	987	990	-2	15	615	629	-4	-6	12	1	
10	799	905	-42	2	387	365	7	16	248	18	17	1	295	349	-11
12	740	795	-19	3	417	482	-26	17	397	237	26	2	349	281	17
14	390	473	-17	4	129	124	0	-6	8	1		3	-77	4	-2
16	423	502	-15	5	1406	1521	-64	1	442	367	23	4	208	273	-10
18	-141	8	-4	6	584	583	0	2	1317	1353	-17	5	549	576	-8
-6	1	1		7	1637	1636	0	3	255	130	22	6	249	280	-4
1	1454	1454	0	8	665	625	18	4	1492	1419	33	7	929	864	21
2	524	598	-36	9	1454	1557	-52	5	240	318	-21	8	187	208	-2
3	2669	2752	-33	10	339	374	-10	6	822	761	26	9	708	704	1
4	762	772	-6	11	821	851	-13	7	181	218	-6	10	64	17	1
5	2075	2089	-6	12	-81	38	-3	8	68	9	1	11	398	298	20
6	364	417	-21	13	66	140	-6	9	186	226	-6	12	284	126	19
7	650	730	-42	14	97	155	-5	10	752	777	-8	13	-63	11	0
8	445	514	-30	15	343	380	-8	11	329	356	-5	14	376	225	18
9	385	475	-36	16	-129	85	-7	12	1037	1039	0	-6	13	1	
10	265	391	-36	17	601	660	-16	13	82	256	-17	1	447	448	0
11	690	855	-81	18	-286	95	-22	14	771	787	-5	2	-15	224	-14
12	301	283	4	-6	5	1		15	-110	18	-3	3	526	452	18
13	349	433	-24	1	600	621	-9	16	432	405	5	4	-192	61	-13
14	287	198	17	2	727	794	-36	17	-119	123	-7	5	469	416	12
15	725	753	-10	3	775	715	30	-6	9	1		6	552	476	20
16	308	331	-5	4	-36	16	0	1	658	689	-12	7	105	215	-11
17	309	277	6	5	810	804	3	2	-127	152	-15	8	540	489	12
18	490	422	17	6	1050	1036	7	3	907	899	3	9	53	12	0
19	-67	159	-8	7	299	252	11	4	259	180	13	10	249	229	2
-6	2	1		8	1155	1218	-17	5	862	850	4	11	306	231	10
1	824	858	-20	9	335	312	6	6	369	363	1	12	88	73	0
2	711	820	-67	10	903	978	-36	7	-93	221	-20	-6	14	1	
3	409	455	-19	11	279	338	-12	8	642	630	4	1	208	145	6
4	1616	1718	-56	12	281	287	-1	9	393	335	13	2	578	558	5
5	1727	1776	-25	13	715	686	11	10	378	331	10	3	-233	141	-19
6	871	972	-60	14	85	130	-3	11	638	627	3	4	479	432	9
7	974	1009	-20	15	268	212	9	12	-138	216	-18	5	144	14	5
				16	455	391	14	13	695	603	26	6	383	288	19
				17	-50	17	0	14	-325	3	-27	7	247	234	1
				18	529	538	-1	15	349	331	3	8	193	0	10
				-6	6	1		16	343	305	6				



Fluoroborated Pt2 POP4.

Page 10

1	131	79	2	13	336	347	-2	4	997	1033	-20	1	621	656	-13
2	651	630	5	14	676	690	-5	5	954	913	21	2	660	729	-28
3	-169	39	-7	15	664	652	4	6	253	227	6	3	639	619	7
4	433	391	8	16	-106	267	-26	7	804	826	-10	4	657	688	-11
5	-178	60	-9	17	624	625	0	8	579	596	-7	5	1263	1269	-2
6	-64	172	-8	18	197	54	11	9	863	880	-7	6	597	536	19
7	-251	0	-18	19	372	442	-12	10	1373	1372	0	7	862	806	21
8	323	81	28					11	-44	128	-6	8	280	271	1
9	-201	136	-16	-4	3	1		12	1152	1078	28	9	649	645	1
10	296	221	9					13	325	274	9	10	318	225	15
	-5	16	1	1	118	98	2	14	657	532	35	11	553	431	30
1	426	388	7	2	1456	1550	-57	15	313	297	2	12	403	327	14
2	-167	18	-7	3	601	525	38	16	120	176	-3	13	63	84	0
3	387	371	3	4	1387	1522	-83	17	396	295	18	14	-78	84	-3
4	177	130	4	5	656	581	38	18	291	106	18	15	606	485	25
5	107	169	-4	6	2288	2401	-50					16	48	30	0
6	75	136	-3	7	304	271	9	-4	7	1					
7	-114	25	-3	8	1934	2030	-46	1	1614	1618	-2				
8	181	205	-1	9	660	626	15	2	247	299	-14	-4	11	1	
	-5	17	1	10	1094	1147	-27	3	1668	1643	-12	1	212	101	13
1	165	170	0	11	312	340	-7	4	73	150	-9	2	-99	95	-6
2	114	236	-9	12	141	45	7	5	642	607	15	3	-69	144	-10
3	-172	58	-7	13	374	369	1	6	295	350	-16	4	780	796	-6
4	234	170	5	14	545	603	-19	7	420	438	-5	5	127	137	0
	-4	0	1	15	323	295	5	8	206	245	-8	6	1008	986	8
2	337	72	60	16	678	654	7	9	1186	1236	-22	7	535	417	29
4	3030	2914	34	17	-207	108	-15	10	-99	11	-3	8	830	867	-11
6	1590	1586	1	18	613	604	2	11	1503	1404	39	9	-38	13	0
8	1266	1307	-17	19	168	172	0	12	432	397	7	10	404	360	9
10	1861	1917	-20					13	1144	1014	45	11	77	120	-2
12	1177	1288	-42	-4	4	1		14	439	363	17	12	-114	96	-6
14	875	876	0	1	844	897	-33	15	543	436	23	13	107	8	3
16	332	349	-3	2	299	156	35	16	-84	105	-5	14	422	338	14
18	-70	101	-3	3	680	692	-6	17	185	27	8	15	-186	102	-10
	-4	1	1	4	187	159	5	18	-18	141	-4				
1	1546	1646	-62	5	1610	1643	-17					-4	12	1	
2	290	273	5	6	194	208	-2	-4	8	1		1	-104	266	-25
3	2986	3113	-47	7	2013	2026	-5	1	318	329	-3	2	490	447	11
4	1074	1111	-24	8	327	304	6	2	1485	1566	-40	3	543	476	18
5	1585	1693	-62	9	1529	1602	-36	3	-120	22	-7	4	317	332	-3
6	1355	1404	-30	10	301	358	-17	4	703	770	-31	5	690	686	1
7	524	491	15	11	557	469	30	5	363	345	5	6	81	29	1
8	1047	1117	-42	12	23	131	-6	6	544	587	-16	7	813	823	-3
9	1222	1356	-77	13	-95	235	-21	7	708	604	39	8	199	162	4
10	400	393	2	14	184	86	8	8	186	275	-16	9	331	297	6
11	1518	1538	-9	15	425	432	-1	9	247	329	-17	10	148	69	4
12	187	129	9	16	292	186	14	10	1124	1040	33	11	-170	112	-12
13	915	1004	-42	17	535	535	0	11	462	439	5	12	110	98	0
14	32	188	-12	18	-194	95	-12	12	1277	1127	54	13	174	138	2
15	563	620	-18	19	544	434	21	13	432	368	12	14	189	247	-5
16	452	381	18					14	760	625	37				
17	230	159	7	-4	5	1		15	-32	47	-1	-4	13	1	
18	217	324	-17	1	1242	1218	13	16	211	212	0	1	666	694	-8
19	201	259	-7	2	351	283	20	17	-84	103	-4	2	-155	0	-7
	-4	2	1	3	394	426	-13					3	826	833	-2
1	939	895	28	4	455	554	-44	-4	9	1		4	507	433	18
2	676	724	-29	5	472	428	17	1	1030	1113	-40	5	299	386	-17
3	1023	1000	-15	6	1485	1515	-18	2	147	96	5	6	435	435	0
4	1866	1907	-21	7	101	110	0	3	688	780	-39	7	61	55	0
5	2244	2282	-17	8	1126	1140	-7	4	906	907	0	8	357	248	18
6	90	4	4	9	292	440	-42	5	817	846	-12	9	299	124	24
7	1841	1987	-75	10	1046	1066	-9	6	905	892	5	10	153	118	2
8	594	579	7	11	691	722	-12	7	602	608	-2	11	325	222	15
9	1466	1574	-58	12	-112	14	-4	8	816	786	11	12	-192	3	-9
10	914	976	-33	13	708	646	21	9	250	224	4	13	419	322	15
11	424	435	-3	14	111	314	-23	10	301	346	-9				
12	1075	1088	-6	15	333	260	12	11	834	714	38	-4	14	1	
				16	358	309	10	12	372	311	12	1	-148	83	-7
				17	-84	72	-3	13	693	583	28	2	869	900	-9
				18	469	432	6	14	336	113	27	3	125	69	3
								15	124	199	-5	4	702	692	3
								16	371	362	1	5	121	100	1
												6	290	211	11
												7	286	208	12
												8	229	51	16











Fluoroborated Pt2 POP4.

5	641	664	-10						13	611	665	-16	3	324	257	19
6	-58	60	-3	0	295	81	19		14	-146	115	-10	4	329	218	25
7	546	541	1	1	-72	87	-3		15	847	946	-33	5	515	528	-4
8	280	154	25						16	146	86	3	6	1030	1107	-36
9	281	271	2	1	0	1			17	493	578	-18	7	52	129	-5
10	352	426	-20						18	-52	65	-1	8	934	999	-28
11	104	59	2	1	5294	5017	58						9	145	44	6
12	257	251	1	3	2179	1999	84		1	4	1		10	914	860	19
13	362	395	-7	5	712	660	29						11	394	192	32
14	-176	22	-9	7	1680	1505	86		0	2206	2171	15	12	576	585	-2
				9	1672	1636	17		1	1052	1147	-60	13	-165	20	-8
0	13	1		11	1377	1386	-4		2	2744	2674	35	14	279	215	8
				13	790	849	-23		3	69	215	-18	15	119	243	-10
1	651	653	0	15	-86	93	-5		4	2669	2631	14	16	342	249	13
2	316	328	-3	17	312	270	6		5	347	331	4	17	-252	156	-20
3	430	415	5	19	400	493	-18		6	2562	2488	28				
4	623	588	14						7	143	196	-7	1	8	1	
5	-113	71	-7	1	1	1			8	1282	1211	32				
6	436	476	-12						9	130	190	-8	0	626	567	24
7	237	236	0	0	5194	4944	54		10	261	42	28	1	1973	1998	-10
8	374	301	19	1	42	4	1		11	-99	203	-17	2	-124	216	-28
9	539	520	6	2	2298	2005	130		12	391	379	2	3	1265	1289	-11
10	236	234	0	3	707	686	13		13	-157	174	-17	4	1220	1225	-2
11	543	523	6	4	952	699	141		14	834	922	-28	5	134	164	-3
12	134	135	0	5	498	460	16		15	156	41	5	6	553	489	21
13	192	251	-8	6	235	186	10		16	645	749	-28	7	892	900	-3
				7	693	655	19		17	316	108	20	8	403	369	9
				8	1412	1392	10		18	318	417	-13	9	1013	1046	-12
0	14	1		9	-70	14	-2						10	-234	15	-15
				10	1422	1408	6		1	5	1		11	642	640	0
0	598	559	11	11	161	158	0						12	286	289	0
1	122	157	-3	12	1057	1104	-21		0	983	866	63	13	584	565	4
2	595	557	14	13	262	374	-20		1	1028	1042	-8	14	217	199	1
3	484	441	15	14	298	233	11		2	1387	1424	-21	15	-243	36	-14
4	170	246	-13	15	371	371	0		3	2621	2631	-3	16	223	73	10
5	194	182	1	16	165	173	0		4	187	10	17	17	340	272	8
6	-156	26	-10	17	295	279	2		5	1921	1847	33				
7	295	254	8	18	362	369	-1		6	853	888	-17	1	9	1	
8	568	518	17	19	-205	26	-9		7	1283	1229	26				
9	135	205	-7						8	649	697	-19	0	908	939	-14
10	535	631	-28	1	2	1			9	441	438	0	1	571	620	-19
11	133	127	0						10	123	116	0	2	1175	1279	-52
12	448	419	7	0	151	178	-6		11	-182	2	-11	3	725	715	4
				0	1421	1414	4		12	388	334	12	4	397	484	-25
				1	1482	1391	54		13	374	416	-8	5	1023	1022	0
				2	1156	1071	52		14	-157	147	-11	6	390	429	-9
1	503	435	21	3	2909	2634	97		15	669	723	-14	7	935	951	-6
2	-86	82	-5	4	299	229	17		16	-299	75	-21	8	890	905	-5
3	353	293	15	5	942	789	79		17	509	531	-4	9	298	246	9
4	-185	11	-14	6	460	337	40		18	216	287	-7	10	851	769	26
5	150	83	6	7	468	610	34						11	-149	216	-18
6	132	55	5	8	604	633	-12		1	6	1		12	554	619	-16
7	309	270	8	9	250	294	-9						13	560	590	-6
8	-57	58	-2	10	939	924	6		0	-134	172	-22	14	415	421	-1
9	624	551	24	11	640	624	5		1	1926	2057	-64	15	420	358	10
10	82	135	-3	12	252	193	8		2	626	668	-19	16	-100	3	-2
				13	610	686	-23		3	698	749	-24				
				14	62	106	-2		4	892	947	-28	1	10	1	
				15	589	670	-22		5	378	364	4				
0	431	313	20	16	-161	215	-21		6	467	492	-8	0	235	201	7
1	40	51	0	17	196	298	-12		7	916	886	13	1	391	395	-1
2	284	227	10	18	231	311	-9		8	210	188	3	2	777	899	-51
3	74	162	-7	19					9	778	797	-7	3	489	518	-9
4	142	117	2						10	119	95	2	4	1168	1226	-24
5	286	283	0						11	465	480	-3	5	175	236	-8
6	298	138	27	0	1772	1580	100		12	177	21	9	6	959	963	-1
7	314	204	18	1	2011	2094	-42		13	398	402	0	7	573	616	-12
8	345	299	9	2	1201	1312	-72		14	417	422	0	8	653	559	27
				3	1808	1756	26		15	-231	35	-13	9	496	518	-5
				4	827	933	-63		16	441	482	-7	10	132	24	4
1	226	180	6	5	3104	2885	73		17	421	402	3	11	425	460	-7
2	-125	144	-12	6	278	402	-36		18	-178	194	-12	12	571	638	-15
3	-181	80	-13	7	1302	1207	48						13	332	428	-16
4	391	369	5	8	437	387	16		1	7	1		14	353	538	-31
5	-86	17	-2	9	418	439	-6						15	164	222	-4
6	470	412	14	10	210	183	4		0	1683	1614	33				
				11	850	768	33		1	24	51	0	1	11	1	
0	18	1		12	275	308	-6		2	1921	1984	-29				

Fluoroborated Pt2 POP4.

0	-87	49	-3	9	-159	105	-8	16	145	220	-8	6	767	770	-1
1	656	617	14	10	539	540	0	17	244	335	-14	7	197	165	4
2	92	237	-18					18	335	307	4	8	1002	955	19
3	885	905	-8	1	16	1						9	-100	68	-5
4	271	229	8					2	3	1		10	819	740	28
5	744	778	-12	0	84	15	1					11	-184	154	-19
6	354	385	-7	1	292	247	7	0	285	176	27	12	451	515	-15
7	655	534	35	2	-178	83	-10	1	2221	2143	36	13	284	299	-2
8	331	274	10	3	-108	136	-8	2	2783	2563	82	14	250	27	17
9	243	106	14	4	192	225	-4	3	1289	1342	-32	15	389	487	-21
10	-90	112	-5	5	224	3	14	4	3121	2838	93	16	309	347	-5
11	38	241	-14	6	257	231	3	5	-25	112	-6	17	321	342	-2
12	-149	128	-9	7	-106	208	-11	6	2353	2093	102				
13	483	590	-21	8	-143	55	-5	7	581	630	-22	2	7	1	
14	226	144	7					8	314	277	9				
15	344	410	-8	1	17	1		9	580	590	-4	0	246	292	-12
				0	95	168	-4	10	509	496	4	1	1551	1537	7
1	12	1		1	86	120	-1	11	121	141	-2	2	439	510	-26
0	96	85	0	2	-227	134	-16	12	526	530	-1	3	817	889	-36
1	358	297	14	3	278	258	2	13	-109	98	-6	4	186	192	0
2	452	468	-4	4	-113	18	-3	14	573	726	-45	5	463	409	17
3	223	206	2	5	358	354	0	15	-133	75	-6	6	341	323	5
4	492	518	-7	6	162	24	6	16	465	587	-28	7	1013	985	12
5	55	177	-9					17	131	48	4	8	298	184	19
6	485	442	11	2	0	1		18	160	255	-10	9	905	929	-9
7	78	35	1									10	-121	96	-8
8	278	369	-15	0	2759	2605	61	2	4	1		11	441	510	-17
9	436	358	16	2	2798	2668	50	0	770	755	8	12	219	141	8
10	-139	44	-5	4	2416	2330	36	1	1674	1729	-30	13	250	329	-12
11	315	346	-4	6	1491	1423	37	2	390	348	14	14	-169	186	-17
12	160	321	-17	8	2553	2531	8	3	3157	3028	43	15	79	183	-6
13	-242	69	-12	10	1234	1245	-5	4	376	235	37	16	168	212	-3
14	459	398	9	12	809	889	-32	5	3113	2998	38	17	354	417	-10
				14	334	284	11	6	24	2	0				
				16	-126	180	-13	7	1509	1476	15	2	8	1	
				18	230	420	-25	8	238	281	-10	0	1537	1531	2
								9	359	346	3	1	176	356	-47
0	689	713	-7	2	1	1		10	261	78	28	2	1128	1145	-8
1	184	194	-1					11	418	413	1	3	477	458	6
2	443	395	11	0	1489	1564	-50	12	132	188	-5	4	-89	161	-15
3	451	449	0	1	2650	2603	19	13	510	576	-17	5	816	843	-11
4	-234	96	-22	2	215	233	-5	14	-150	91	-8	6	787	847	-26
5	324	275	8	3	1542	1555	-7	15	733	791	-17	7	532	516	4
6	-276	144	-27	4	623	575	25	16	308	179	15	8	904	879	9
7	446	386	13	5	118	140	-3	17	455	490	-7	9	247	190	8
8	518	535	-4	6	698	676	11	18	71	129	-2	10	731	768	-12
9	217	320	-14	7	1366	1369	-1					11	107	111	0
10	595	611	-3	8	158	125	4	2	5	1		12	508	581	-18
11	-52	39	-1	9	1662	1655	3	0	268	170	22	13	246	353	-15
12	324	326	0	10	422	442	-6	1	1153	1136	9	14	-258	155	-24
13	251	237	1	11	1088	1114	-11	2	2421	2553	-56	15	-125	29	-3
				12	158	126	3	3	1196	1249	-30	16	-192	198	-16
				13	186	249	-10	4	2592	2497	36				
				14	152	307	-23	5	1149	1053	48	2	9	1	
				15	138	10	6	6	1790	1749	18	0	1000	1054	-25
				16	181	283	-15	7	569	516	18	1	1507	1530	-10
				17	179	307	-18	8	463	480	-5	2	721	728	-2
				18	-76	85	-3	9	742	739	1	3	539	580	-15
								10	118	108	1	4	813	882	-31
				2	2	1		11	359	285	15	5	374	434	-20
				0	2609	2420	77	12	362	367	-1	6	667	696	-10
				1	940	908	22	13	-136	237	-22	7	770	727	15
				2	578	598	-11	14	642	662	-6	8	611	608	0
				3	545	420	57	15	-256	181	-23	9	726	704	7
				4	314	195	29	16	576	617	-9	10	-179	10	-8
				5	2129	2114	6	17	316	278	4	11	666	691	-7
				6	288	375	-28	18	308	265	4	12	493	565	-17
				7	406	488	-32					13	362	509	-27
				8	1165	1167	-1	2	6	1		14	414	448	-6
				9	413	334	23					15	53	101	-1
				10	938	960	-10	0	1443	1445	-1	16	353	226	16
				11	509	515	-1	1	321	322	0				
				12	220	225	0	2	1361	1431	-38	2	10	1	
				13	454	488	-9	3	1590	1609	-9				
				14	-123	19	-5	4	543	617	-33	0	448	589	-46
				15	425	516	-22	5	607	651	-18	1	967	970	-1

Fluoroborated Pt2 POP4.

2	995	1034	-17	10	563	591	-5	4	2448	2179	107	16	270	261	1	
3	987	1084	-42	11	-253	11	-13	5	204	73	24	17	-37	334	-26	
4	146	50	6					6	1045	1014	17					
5	788	804	-6		2	15	1	7	810	812	0		3	6	1	
6	565	441	35					8	359	281	22					
7	719	726	-2	0	-158	129	-10	9	937	954	-8	0	203	245	-8	
8	582	657	-21	1	323	358	-6	10	447	419	9	1	1198	1301	-59	
9	198	244	-5	2	120	18	4	11	277	306	-6	2	1343	1311	17	
10	92	346	-28	3	108	86	1	12	215	363	-28	3	511	546	-14	
11	540	513	6	4	161	16	7	13	98	77	1	4	1205	1265	-31	
12	431	474	-9	5	-209	53	-12	14	361	462	-26	5	613	601	5	
13	582	653	-16	6	84	10	1	15	-74	87	-3	6	427	506	-26	
14	297	250	6	7	298	338	-6	16	167	253	-9	7	727	714	5	
15	399	390	1	8	207	62	8	17	115	282	-19	8	156	135	2	
				9	364	496	-21	18	82	80	0	9	814	883	-28	
	2	11	1	10	-178	74	-7					10	461	530	-18	
								3	3	1		11	466	476	-2	
0	374	358	3		2	16	1	0	2334	2291	19	12	159	169	-1	
1	500	549	-14		0	302	306	0	1	914	962	-30	13	314	253	8
2	541	585	-14		1	-76	69	-2	2	1416	1308	61	14	412	461	-11
3	341	294	11		2	274	244	3	3	3071	2937	46	15	230	304	-9
4	774	782	-3		3	47	144	-4	4	849	719	69	16	293	363	-9
5	121	263	-18		4	-46	41	-1	5	2459	2457	0	17	327	375	-6
6	633	624	2		5	144	213	-6	6	-149	4	-12				
7	426	385	11		6	-174	86	-8	7	780	837	-29				
8	281	291	-1		7	-190	76	-9	8	480	619	-57	0	1313	1441	-70
9	-183	84	-11		8	138	306	-18	9	243	215	6	1	280	187	19
10	107	147	-3						10	246	245	0	2	1248	1400	-84
11	-177	30	-9		2	17	1		11	333	320	3	3	380	402	-6
12	454	586	-29		0	-123	90	-6	12	168	10	10	4	292	328	-9
13	120	137	-1		1	157	173	-1	13	464	529	-18	5	52	41	0
14	429	478	-7		2	309	232	10	14	-184	70	-11	6	778	686	39
					3	-171	82	-9	15	358	519	-33	7	381	408	-7
	2	12	1		4	259	313	-7	16	-94	1	-2	8	880	887	-2
0	368	329	8		5	-226	20	-13	17	268	277	-1	9	181	197	-2
1	237	276	-6						18	-149	138	-10	10	628	698	-21
2	-153	147	-14		3	0	1						11	-77	67	-3
3	360	438	-16		1	1745	1670	42	3	4	1		12	305	446	-30
4	75	5	1		3	1402	1306	57	0	1003	807	109	13	-260	65	-18
5	390	383	1		5	1687	1676	5	1	248	110	26	14	-57	133	-6
6	-87	124	-7		7	2366	2377	-4	2	2690	2470	82	15	-264	158	-21
7	457	426	7		9	1962	2040	-35	3	1083	1053	17	16	156	335	-18
8	377	289	18		11	1015	1096	-36	4	2420	2236	73				
9	-74	87	-3		13	206	164	5	5	525	591	-29				
10	404	317	15		15	-177	8	-9	6	1897	1847	22	0	626	688	-27
11	119	182	-4		17	198	332	-17	7	84	108	-2	1	1335	1430	-47
12	146	147	0						8	397	424	-8	2	199	196	0
13	369	439	-10		3	1	1		9	-96	84	-6	3	313	358	-12
					0	1134	942	124	10	331	233	24	4	322	310	3
	2	13	1		1	257	309	-17	11	212	273	-11	5	417	410	1
0	134	77	3		2	597	639	-24	12	612	632	-6	6	482	468	4
1	421	411	2		3	1663	1533	70	13	282	232	8	7	963	942	8
2	327	355	-6		4	337	377	-15	14	554	670	-31	8	542	554	-3
3	151	168	-1		5	1096	1052	26	15	96	203	-9	9	713	723	-3
4	309	234	13		6	1293	1268	13	16	445	505	-12	10	-98	13	-3
5	221	142	9		7	143	169	-4	17	-67	139	-5	11	640	658	-5
6	392	326	13		8	1858	1886	-12	18	162	190	-2	12	347	371	-4
7	396	390	1		9	271	184	19					13	292	205	11
8	272	310	-5		10	1249	1276	-13	3	5	1		14	-169	103	-9
9	548	593	-10		11	123	77	4	0	839	914	-45	15	142	120	1
10	373	66	32		12	231	289	-10	1	1251	1307	-33	16	-223	34	-10
11	381	408	-4		13	183	251	-10	2	209	245	-7				
12	86	230	-9		14	167	114	5	3	2412	2451	-16				
					15	199	232	-5	4	175	27	16	0	1320	1424	-51
	2	14	1		16	232	251	-2	5	1729	1765	-17	1	1308	1351	-19
0	745	745	0		17	-175	111	-10	6	877	785	43	2	913	925	-5
1	174	236	-8		18	213	386	-23	7	840	840	0	3	627	686	-24
2	350	309	8						8	528	484	15	4	150	121	3
3	-157	184	-17		3	2	1		9	158	160	0	5	577	651	-26
4	252	2	20						10	666	657	3	6	600	693	-32
5	313	210	15		0	400	476	-35	11	497	571	-21	7	604	622	-6
6	259	355	-14		1	1094	1050	29	12	286	419	-24	8	659	759	-33
7	26	201	-10		2	698	578	64	13	441	475	-7	9	203	147	6
8	584	534	11		3	1250	1183	40	14	-35	179	-8	10	531	550	-5
9	146	113	2						15	483	671	-44	11	299	300	0





Fluoroborated Pt2 POP4.

11	362	203	25	5	439	441	0	8	943	1033	-43	5	643	724	-34	
12	250	209	5	6	159	298	-14	9	181	266	-16	6	843	882	-17	
13	203	257	-5	7	418	463	-8	10	412	488	-21	7	463	520	-17	
14	253	111	12	8	-120	16	-3	11	450	462	-3	8	754	803	-18	
				9	404	324	13	12	90	18	2	9	177	37	9	
	5	10	1	10	227	100	6	13	428	542	-30	10	339	381	-9	
0	782	816	-13					14	83	73	0	11	304	381	-13	
1	423	389	9		5	15	1	15	185	251	-7	12	349	322	4	
2	1015	997	7		0	488	500	-2	16	110	193	-6	13	328	342	-2
3	-201	74	-16		1	-185	112	-12	17	-9	67	-1	14	303	197	13
4	961	1059	-39		2	96	229	-10					15	143	135	0
5	-258	44	-22		3	-134	5	-5	6	3	1					
6	398	393	1		4	143	212	-6	0	1005	980	14				
7	267	275	-1		5	177	113	4	1	336	102	56	0	137	58	7
8	-179	71	-10		6	455	339	20	2	1399	1374	13	1	573	614	-17
9	85	235	-14		7	97	46	2	3	884	815	36	2	286	230	14
10	-92	244	-17		8	241	302	-7	4	1579	1602	-11	3	240	315	-18
11	311	182	16						5	310	342	-9	4	161	58	9
12	342	409	-10		5	16	1		6	670	694	-11	5	749	803	-23
13	99	19	2		0	207	220	-1	7	173	226	-9	6	594	586	2
14	-52	274	-15		1	313	337	-4	8	255	287	-7	7	764	797	-12
					2	242	279	-4	9	220	309	-20	8	285	294	-1
	5	11	1		3	267	68	17	10	579	657	-26	9	716	739	-7
0	-85	72	-4		4	219	132	7	11	-186	132	-16	10	-72	8	-1
1	756	765	-3		5	-179	113	-10	12	600	707	-32	11	287	387	-20
2	188	149	4		6	-211	41	-11	13	151	16	5	12	-69	111	-4
3	866	876	-3						14	442	466	-5	13	-94	44	-3
4	-101	174	-14		5	17	1		15	20	28	0	14	-106	7	-2
5	707	727	-6						16	186	164	2	15	-77	211	-11
6	-102	79	-4		0	222	261	-4								
7	-103	260	-20		1	397	425	-4	6	4	1		6	8	1	
8	-144	8	-5		2	193	143	3								
9	205	244	-5						0	496	508	-5	0	945	989	-21
10	-59	71	-2		6	0	1		1	2059	2052	3	1	432	480	-17
11	362	335	4						2	333	225	28	2	-60	114	-7
12	-273	4	-15		0	176	81	14	3	1695	1662	16	3	198	192	1
13	163	316	-16		2	126	145	-3	4	-56	101	-6	4	397	354	11
					4	808	745	33	5	845	826	9	5	-82	73	-4
	5	12	1		6	2047	1991	24	6	497	465	11	6	776	842	-25
0	458	505	-12		8	1592	1675	-39	7	98	39	3	7	337	303	6
1	193	155	-4		10	735	814	-31	8	210	242	-5	8	577	668	-28
2	517	581	-17		12	108	33	3	9	518	551	-11	9	168	152	1
3	187	168	2		14	-47	100	-3	10	-77	106	-5	10	579	581	0
4	551	590	-11		16	194	343	-22	11	850	937	-31	11	118	134	-1
5	238	315	-11						12	214	114	8	12	-189	162	-17
6	525	477	11		6	1	1		13	497	633	-33	13	-124	130	-7
7	168	260	-10						14	306	19	24	14	135	192	-4
8	-178	1	-8		0	715	699	9	15	337	352	-2	15	137	139	0
9	188	142	3		1	195	57	21	16	-235	64	-13				
10	100	205	-7		2	656	657	0					6	9	1	
11	-78	62	-2		3	384	471	-35	6	5	1		0	574	683	-44
12	119	254	-11		4	588	643	-26	0	1017	1035	-9	1	338	409	-19
					5	1328	1307	11	1	44	53	0	2	759	809	-21
	5	13	1		6	-27	93	-4	2	1548	1489	29	3	155	123	3
0	531	503	7		7	1178	1187	-4	3	348	402	-17	4	448	482	-9
1	174	259	-10		8	157	134	3	4	871	810	29	5	459	456	0
2	130	164	-2		9	1177	1248	-33	5	435	435	0	6	-105	105	-8
3	439	400	10		10	200	235	-6	6	621	633	-5	7	679	711	-10
4	258	305	-7		11	329	306	5	7	660	625	13	8	296	354	-12
5	447	451	0		12	237	265	-4	8	-132	34	-7	9	377	443	-15
6	410	438	-6		13	194	50	11	9	526	525	0	10	307	237	11
7	189	224	-3		14	288	250	5	10	598	646	-14	11	168	272	-12
8	209	365	-22		15	-46	186	-10	11	352	460	-24	12	160	251	-9
9	61	67	0		16	-226	127	-15	12	648	619	8	13	-46	52	-1
10	166	243	-8		17	303	303	0	13	-105	9	-2	14	81	196	-6
11	-106	173	-8						14	328	494	-30				
					6	2	1		15	283	156	15	6	10	1	
					0	1122	1215	-57	16	-133	157	-9				
	5	14	1		1	1045	1065	-12					0	309	351	-11
0	-30	104	-3		2	800	821	-11	6	6	1		1	730	762	-13
1	384	382	0		3	1402	1337	34					2	177	80	9
2	124	97	1		4	449	347	36	0	1139	1178	-20	3	988	1089	-41
3	39	42	0		5	457	464	-2	1	251	295	-10	4	226	142	11
4	274	288	-1		6	552	536	6	2	213	138	14	5	301	356	-9
					7	273	269	0	3	626	645	-8	6	-203	168	-19
									4	691	718	-11	7	-57	98	-3















Fluoroborated Pt2 POP4.

Page 27

1 179 15 8 17 5 1

0 170 109 3

---

---

**Chapter 3**

Design of the Positron Annihilation Mass Spectrometer

---

---

Robert J. Sweeney, Jesse L. Beauchamp



## Introduction

The positron,<sup>1-3</sup> or antielectron  $e^+$ , is a particle with mass identical to an electron but charge opposite in polarity and equal in magnitude. A positron and an electron annihilate, or convert to photons, each other at a rate proportional to the square of the overlap between their wave functions. Nevertheless, positronium (Ps), an "atom" composed of an electron and a positron, exists. The two low-energy forms of Ps are para-Ps, with particle spins antiparallel, and ortho-Ps, with parallel spins. Ps is formed in a 3:1 ratio of triplet o-Ps and singlet p-Ps. The lifetime of each species in vacuum because of annihilation is 125 psec for p-Ps and 140 nsec for o-Ps. The difference in these lifetimes reflects the influence of conservation of total spin angular momentum on the annihilation products. p-Ps annihilates into two 512 keV photons at  $180^\circ$  to one another while o-Ps produces three photons with a combined energy of 1.02 MeV.

p-Ps must produce at least two photons in annihilation to obey the conservation of linear momentum. The energy of each of the two photons equals the rest mass of the electron (or positron). o-Ps has nonzero spin angular momentum, so a minimum of three photons are produced in its annihilation. If only two photons were emitted, the vector sum of their intrinsic angular momenta could be either two or zero units, but not one. The energies and relative directions of the photons must ensure conservation of linear momentum.

The creation of the third photon in o-Ps's annihilation effectively involves an extra step and increases the lifetime. Similarly, annihilation of p-Ps into four photons, which is allowed, is even slower; a negligible fraction of Ps atoms experience this process.

In general, the annihilation of an electron and a positron of opposite spin into two photons proceeds at a rate  $\lambda_p$

$$\lambda_p = (\tau_p^0)^{-1} = 4\pi r_0^2 c \Psi(0)$$

$r_0$  = the classical radius of the electron

$\Psi(0)$  = the wave function of the electron at the positron

Positronium may be thought of as a very light isotope of the hydrogen atom in which the replacement of a positron for a proton in the nucleus makes the reduced mass one-half that of the hydrogen atom, or  $m_e/2$ . Consequently, the atomic radius increases from 0.53 Å to 1.06 Å and the ionization potential (IP) is halved from 13.6 eV to 6.8 eV, which limits the chemical options open to positrons. For example, the low IP of Ps prevents thermal (near zero kinetic energy) positrons from being able to oxidize most common organic species, since organics usually have IPs above 7 eV.



Energetic positrons are able to oxidize molecules if their kinetic energy falls within the Ore gap, i.e., if the positron kinetic energy  $E_+$  is between  $IP(R)$  and  $IP(R) - IP(Ps)$ .

Above  $IP(R)$ , the positron creates a "spur" or trail of free electrons and ionized molecules in its path until  $E_+$  falls below  $IP(R)$ .



Below  $IP(R) - IP(Ps)$ ,  $Ps$  formation is thermodynamically unfavorable and annihilation must result from some long-term association between the positron and a substrate. This may result in either a 1:1 positron attachment complex (PAC) in which the positron occupies a wave function within a molecule or a cluster of molecules about one positron.

In the gas phase at relatively low pressures, clustering is unlikely.<sup>4</sup> With low-kinetic-energy positrons, oxidation reactions are not possible. The only feasible reaction path involves PAC formation. Because of the limited expected lifetimes of such species (ca. 1 nsec), they are not available for direct study. Data collected from positron experiments are generally refer to only properties of the annihilation photons, e.g., their angular and temporal distributions.<sup>5, 6</sup>

The positron affinities  $A_+$  and the corresponding positronic wave functions for various atoms and molecules have been calculated. Schraeder's<sup>7</sup> calculations help in qualitatively describing tendencies in positron-molecule bonding. The positron affinities for the hydrogen atom and the second row elements Li through F, (Table 1) show that none of the free atoms should bind positrons.

Table 1. Critical charges for the attachment of positrons to free atoms.

<u>ATOM</u>	<u>A<sub>+</sub> (eV)</u>	<u>CRITICAL CHARGE</u>
H	-1.20	0.145
Li	-1.51	0.280
Be	-1.83	0.269
B	-3.22	0.359
C	-4.54	0.415
N	-6.46	0.494
O	-8.48	0.561
F	-11.05	0.640

In fact, the interaction becomes more repulsive as one goes right in a periodic series. This trend is expected; as nuclear shielding and polarizability decrease, the positron "feels" more of the repulsive nuclear potential.

Anions have favorable interactions with a positron because the long-distance potential is attractive. The amount of anionic charge an atom must possess in order to bind a positron is therefore greater than one electronic charge.<sup>7</sup> (Table 1)

In a molecule, the critical charge may be acquired through polarization of electronic molecular orbitals toward the atom on which the positron is localized. Larger, delocalized molecules therefore provide the polarizability required for a stable positronic complex. Since F, O, N and C have high critical charges, positrons in

organic structures are expected to localize about hydrogen atoms. Positron attachment, not surprisingly, behaves oppositely to electron attachment, which is favored by electronegative elements.

Positronic wave functions calculated for monosubstituted benzenes display trends that can be extrapolated to other organic systems.<sup>7</sup> In eight substituted benzenes investigated, the positron consistently localizes on a hydrogen atom. The positron also stays within the molecular plane, not in the  $\pi$  system. By localizing in the  $\sigma$  framework, the positron can interact with both lobes of the  $\pi$  system, polarizing them toward itself and gaining stabilization.

Calculations predict that benzene itself will not bind a positron. Possibly such a highly symmetric molecule cannot provide a unique site for positron binding that is available in the monosubstituted cases. With the positron delocalized over six protons, the electron density that each could polarize toward itself would be one-sixth that in a monosubstituted benzene. A highly delocalized positron cannot create an attractive center for binding. Thus we have another interesting contrast between positron and electron binding: While the most stable electron wave functions are nodeless and delocalized, positrons prefer wave functions that are localized and therefore have nodes. Calculations of the positronic wave functions for fluorobenzene<sup>7</sup> demonstrate that the most stable orbital has four nodes. The nodeless wave function lies much higher in energy.

Positrons in molecular complexes annihilate those electrons with which they have the greatest overlap. In the case of monosubstituted benzenes, electrons in  $\sigma$ -type MOs localized near the para-hydrogen atom are the most likely candidates for annihilation. The annihilation of a C-H  $\sigma$ -bonding electron leaves a cation with a very low-lying hole. This electronically excited cation undergoes rapid internal conversion to produce a vibrationally excited molecular cation in its ground electronic state which may fragment, as in electron impact mass spectrometry. This presents the possibility of using positron attachment as an ionization technique in mass spectrometry.

An important difference between positron attachment mass spectrometry (PAMS) and more conventional ionization methods is the potential selectivity; theory hints that positron attachment may depend strongly on molecular symmetry properties. For example, attachment may require the presence of a symmetry-unique proton. This criterion excludes PAC formation with such common atmospheric constituents as dioxygen, dinitrogen, carbon dioxide, water and argon. PAMS of atmospheric gas would therefore show only trace components.

Within molecules that do attach positrons, further selectivity may exist in the annihilation of specific electrons. In the case of the monosubstituted benzenes, electrons occupying C-H  $\sigma$ -type molecular orbitals should be annihilated at a much faster rate than other types.

Before such theories are evaluated, positron attachment must be demonstrated and relative rates of PAC annihilation determined for a series of molecules. The first report of low-energy positron attachment<sup>8</sup> concentrated on a series of alkanes, but there was no means of determining the reaction products or identifying the kinetic energy of the attaching positrons. Nevertheless, this study established the existence of the bound positron. Trapped positrons within a vacuum system were exposed to controlled amounts of alkanes and the positrons' lifetimes to annihilation measured by detection of the gamma photons emitted. Annihilation rates per unit pressure remained nearly constant from  $10^{-8}$  to  $10^{-6}$  torr of alkane, discounting clustering as a mechanism for the observed annihilation. Annihilation rates increased with carbon number from butane up, but began to level off at nonane. This effect is rationalized by assuming that the lifetime of the PAC to dissociation increases with the carbon number of the alkane. Dissociation of the PAC occurs faster than annihilation for smaller alkanes, but around C<sub>9</sub> the two rates are approximately equal. Once dissociation lifetimes are significantly longer than annihilation lifetimes, the quenching rate has reached its upper limit. Certainly, similar studies with other chemical species are of great interest.

## Mass Spectrometer Design

The design of a positron annihilation mass spectrometer (see Figure 1) may be subdivided into three divisions:

1. The production of a slow positron beam;
2. The promotion of positron attachment reactions;
3. The determination of reaction product distributions.

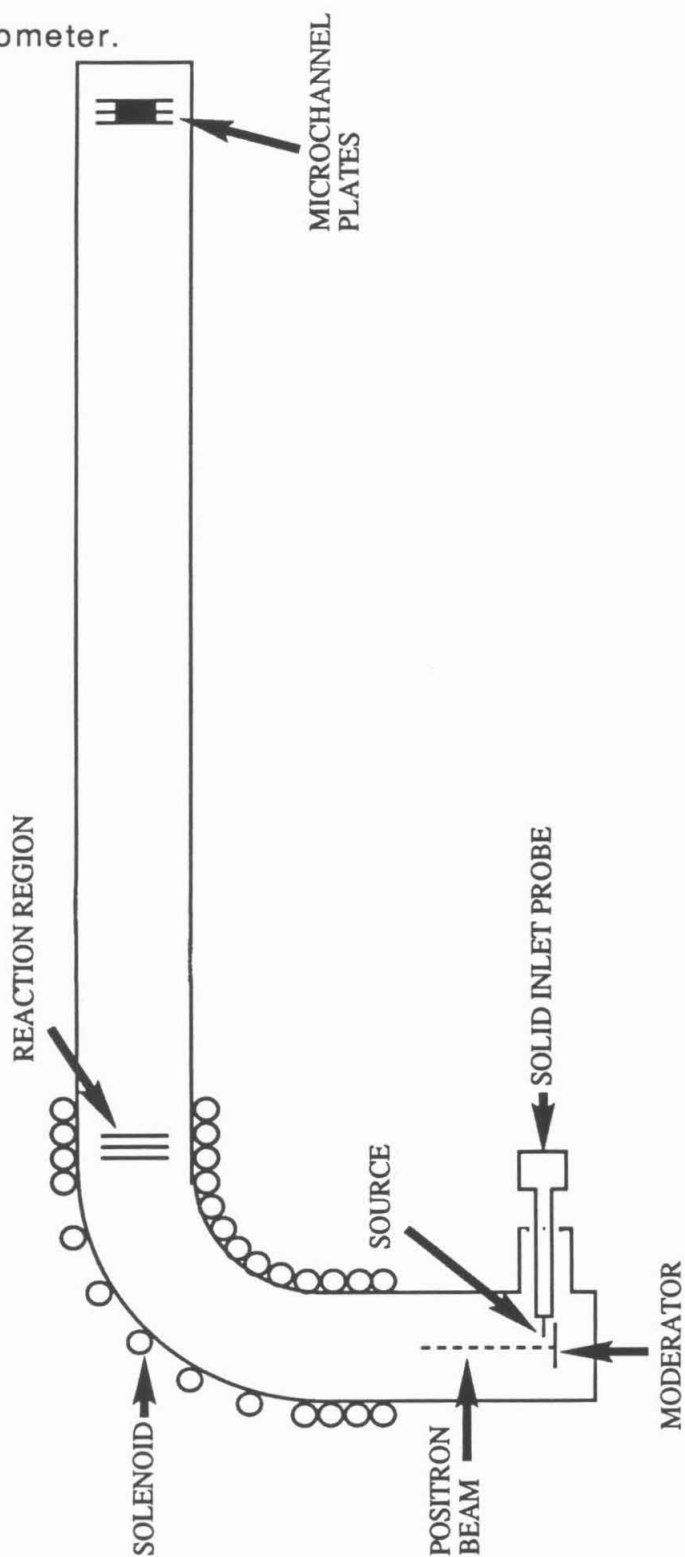
### The slow positron beam

When first created through nuclear decay, positrons possess very high kinetic energies (0.5 to 1.9 MeV<sup>9</sup>), but positrons must be slowed down to lower energies for this experiment. The deceleration of energetic positrons by moderator foils has been studied extensively, as has the production of slow positron beams.<sup>9, 10</sup> Moderators are customarily metals, metal oxides or sulfides that have a negative positron work function. In analogy to electrons, the positron work function is the energy required to remove a positron from a material. Substances with negative positron work functions spontaneously emit low-energy positrons normal to their surface. Energetic positrons penetrate the surface and emerge with efficiencies up to  $10^{-3}$  and kinetic energies below 6 eV.

Many moderator geometries have been investigated, the simplest being the backscattering and transmission geometries. Tungsten foil moderators in the backscattering geometry have been



**Figure 1.** A schematic diagram of the Positron Annihilation Mass Spectrometer.



used in the creation of slow positron beams.<sup>10</sup> This moderator provided beams of  $1200 \text{ e}^+ \text{ s}^{-1}$  from a  $700 \mu\text{Ci } ^{22}\text{Na}$  source, with an overall efficiency of  $4.7 \times 10^{-5}$ . Positron kinetic-energy distributions from tungsten moderators maximize at 4 eV, with a spread of 1.5 eV.

The PAMS instrument will use a 100 mCi  $^{58}\text{Co}$  positron source.  $^{58}\text{Co}$  produces 0.15  $\text{e}^+$  per annihilation event and has a lifetime of 70 days, and emitted positrons initially have 470 keV kinetic energy. The positron source, electroplated onto a copper needle, is introduced into the vacuum chamber on a solid inlet probe. The probe is sealed to vacuum with teflon V-rings.

Tungsten foil is held between stainless steel plates attached to a flange at the end of the vacuum chamber. Electrical feedthroughs in the flange allow biasing of the moderator to vary the kinetic energy of the emitted positron beam. A rough estimate of the positron current delivered by a 100mCi source ( $3.7 \times 10^{10}$  disintegrations  $\text{s}^{-1} \text{ Ci}^{-1}$ ) with moderator efficiency of  $10^{-4}$  (reasonable for tungsten) is  $3.7 \times 10^5 \text{ e}^+ \text{ s}^{-1}$ .

Moderated positrons are guided around a  $90^\circ$  bend by a solenoidal field in an effort to prevent nonmoderated positrons and gamma rays from reaching the detector. The curvature of the small (200 Gauss) magnetic field will not cause moderated positrons to move off-center more than a few millimeters, while energetic particles and photons should pass through the field into the vacuum chamber walls. The slow positron beam is then guided into the reaction region where attachment takes place.

## The attachment process

The forces involved in electron attachment reactions with neutral molecules at long distances should also apply to positron attachment, and extensive analogies between the two will serve as a basis for the following treatment of positron attachment.

Initial electron-neutral interactions are dominated by the charge-dipole coulombic attraction. At short distances, detailed molecular potentials become more important since the charged particle no longer feels the average charge distribution. Instead, a vibrationally excited attachment complex forms, and the analogy between positronic and electronic processes is no longer valid. Upon formation of an electron attachment product, both the electron's kinetic energy and the electron attachment energy are randomly channeled into the ion's vibrational modes. If this energy is sufficiently large, anion formation may be accompanied by rapid dissociation of the molecular anion into charged and neutral fragments. Dissociation may also take the form of electron ejection with regeneration of the starting materials. Alternatively, the excited anion may be stabilized by transferring some of its energy to other molecules through collisions. If the anion possesses many vibrational degrees of freedom, the energy may be distributed among many modes that do not promote dissociation. As expected, the cross section for nondissociative electron attachment reaches a maximum at zero electron kinetic energy.<sup>11</sup> This condition channels the least energy into modes that promote dissociation. Clearly, efficient PAC formation requires very low (effectively zero) energy positrons.

A reliable calculation of the ion current produced by annihilation requires some knowledge of the cross section for positron attachment. As this is not known, the cross section for dissociative electron attachment to  $\text{CCl}_4$ , which peaks strongly at zero energy, will be used as an example. Chutjian and Alajajian<sup>12</sup> approximate the cross section for low-energy, dissociative electron attachment to  $\text{CCl}_4$  by

$$\sigma(E) = NaE^{-1/2}\exp(-E^2/b^2)$$

$$N = 5.45 \times 10^{-14} \text{ cm}^2, \quad a = 0.117 \text{ eV}^{1/2}, \quad b = 0.005 \text{ eV},$$

where  $E$  is the kinetic energy of the attaching electron. This equation gives a cross section of  $300\text{\AA}^2$  at thermal energies.

From the attachment rate of a positron with velocity  $v$

$$R = N_0\sigma(v)v,$$

one may define a differential rate of attachment

$$dR = N_0\sigma(v)dv,$$

with  $N_0$  being the density of the attaching gas. The differential number of attachments ( $dN_a$ ) is this differential rate multiplied by the time spent at that velocity.

$$dN_a = N_0\sigma(v)dv [dx/dv] = N_0\sigma(v)dx$$

$$x = \text{position of positron}$$

This expression, when integrated, produces the theoretical number of attachments that each positron can experience as it changes

velocity over some distance, for example, a positron slowing from 5 to 0 eV over 0.25 cm. By reducing the integration limits to 0.07 and 0 eV to simplify the integral, one obtains

$$N_a = 12.3 \text{ torr}^{-1} \text{ positron}^{-1}.$$

With the estimated positron current of  $3.7 \times 10^5 \text{ e}^+ \text{ s}^{-1}$ , this allows  $4.6 \times 10^6$  attachments  $\text{s}^{-1} \text{ torr}^{-1}$ , or one annihilation per 200  $\mu\text{sec}$  at one millitorr pressure. A similar calculation with the cross section expression for  $\text{SF}_6$  gives one annihilation per 550  $\mu\text{sec}$ .

These estimates demonstrate the feasibility of collecting a full positron annihilation mass spectrum in a reasonable amount of time with the proposed source intensity.

A variation of Shmikk's reflectron device<sup>13</sup> creates the zero energy positrons necessary for attachment. Our version consists of two grids held parallel to each other and perpendicular to the positron's axis of motion. For a 5 eV positron beam, the first grid that the particles encounter is held at ground and the second at 10V. The electric field between the grids slows the positrons and effectively stops and turns them around in the middle. While turning around, the positrons have zero kinetic energy in the axis of motion, and it is during this time that attachment is most probable. The lifetime of a PAC because of annihilation being ca. 1 nsec, the ion will not have time to exit the reflectron before annihilation. This situation corresponds to the calculation above.

A reagent gas for attachment enters the reaction region through a hypodermic needle aimed toward the center of the two grids. The needle creates a high-pressure region where annihilation is most likely, without overwhelming the pumping capacity of the vacuum system. Pressures of one millitorr can be maintained in the reaction region while keeping the main chamber below  $10^{-5}$  torr.

### **Product distributions**

Following annihilation, the energetic molecular cation remaining may fragment into a number of neutral species and one smaller cation. Circuits triggered by the gamma rays produced in annihilation change voltages on the grids before the cation exits from the reaction region. The grids rapidly switch from 10V and ground to 100V and 105V, now pushing the cation away from the source region to an ion detector. The time that passes between detection of the annihilation photon and detection of the ion serves as the time-of-flight (TOF). From a TOF spectrum, a mass spectrum can be obtained using

$$\text{TOF} = d(2V)^{-1/2}(m/z)^{1/2}$$

$d$  = distance traveled,  $V$  = accelerating voltage,  $(m/z)$  = ion mass.

A standard method for the detection of gamma rays is the use of plastic scintillators. Certain plastics, such as poly(methylmethacrylate) or PMMA, are able to convert high-energy photons which pass through them into many lower-energy photons

( $\lambda=420$  nm). With the proper construction, PMMA sheets contain the low energy photons through internal reflectance, allowing their detection by a photomultiplier tube (PMT) connected to one end of the sheet.

In our case, a 5 mm thick Bicon PMMA cylinder wrapped around the vacuum chamber captures the photons. A lucite light pipe attached to the scintillator guides the 420 nm photons to the face of an EMI photomultiplier tube. The PMT signal passes through an Amptek A101 amplifier, which discriminates against false signals caused by thermal emission of electrons in the PMT. The A101 outputs a rectangular 5V, 220 nsec pulse, which triggers the switching of grid voltages and begins timing the TOF.

The Bicon scintillator converts each 300 eV of a gamma ray photon into one 420 nm photon with an efficiency of 5%. This produces approximately 170 detectable photons per annihilation event (two photons at 512 keV each). A PMT quantum efficiency of 18% and gain of  $10^7$  create a pulse of 19 picocoulombs to the discriminator.

A chevron multichannel plate (MCP) detector records the arrival of the cation at the end of the flight tube. Microchannel plates act as electron multipliers, providing a gain of up to  $10^8$ . The MCP pulse triggers a second Amptek A101 amplifier/discriminator whose output stops the timing circuitry. This pulse also causes the computer to collect the TOF datum from the external electronics and to reset all devices for the next annihilation event.

The start (PMT) and stop (MCP) pulses open and close a gate through which passes the output from a 20 MHz clock. The clock pulses during the ion flight enter a Metrabyte MCN8 counting board, which talks directly to a computer. The number of clock pulses allowed to reach the counter provides the TOF, when multiplied by 50 nsec.



## Data Analysis

Two forms of data are extracted from the positron annihilation mass spectra: the internal energy of the molecular cation when formed and the relative positron annihilation rates for gaseous reagents.

### Cation internal energy

An expression for the total internal energy of the cation first formed by the annihilation event ( $E_{\text{int}}[\text{R}^+]$ ) is the sum of terms that require detailed knowledge of both the positron affinity of the attaching molecule and the identities of annihilated electrons.



$$E_{\text{int}}[\text{R}^+] = A_+ + \text{IP}' - \text{IP}$$

IP = first ionization energy of the molecule R

IP' = ionization energy of the molecular orbital occupied by the annihilated electron

Since IP is known through photoelectron spectroscopy (PES), three unknown energy terms remain in the energy expression.

The internal energy of molecular cations may be extracted from its fragmentation pattern with the use of photoelectron-photoion coincidence (PEPICO) breakdown curves. In PEPICO experiments, high-energy photons (of energy  $h\nu$ ) ionize a molecule and the resulting free electron and cation are analyzed. The cation detector is triggered only if the ejected electron possesses nearly zero kinetic energy. This indicates that the molecular cation, when

initially formed, had  $h\nu - IP$  internal energy. The energy disperses among the various vibrational and rotational modes of the cation and leads to fragmentation. The ionic product distributions from PEPICO experiments should match with the PAMS spectra of molecules when

$$E_{\text{int}}[R^+] = A_+ + IP' - IP = h\nu - IP, \text{ or}$$

$$h\nu = IP' + A_+.$$

Thus, comparison of the spectra from PAMS and PEPICO to determine  $h\nu$  reveals the value of  $IP' - A_+$ . This analysis assumes that the PAMS fragmentation pattern results from the selective annihilation of electrons from a single MO of the PAC, which may or may not apply.

The positron affinity must be positive if binding takes place, so an upper limit can be placed on  $IP'$ . If one assumes that the positron affinity takes on values similar to those for electron affinities, usually less than about 5 eV, one can also give  $IP'$  a lower bound of  $h\nu - 5$  eV.  $IP'$  should not be expected to correspond to a vertical or adiabatic transition in the PES spectrum, since the electronically excited molecular cation is formed from the PAC's distorted geometry.  $IP'$  therefore correlates with a high  $\nu$  vibronic peak in the PES ionization band.

All considered, the IP of the annihilated electron can be known within a range of perhaps 5 eV through this analysis, which allows one to distinguish between the HOMO, weakly and strongly bonding orbitals and core atomic orbitals. For example, if PAMS of ethylene yields an ion distribution of 80%  $C_2H_2^+$  and 20%  $C_2H_4^+$ ,  $h\nu$

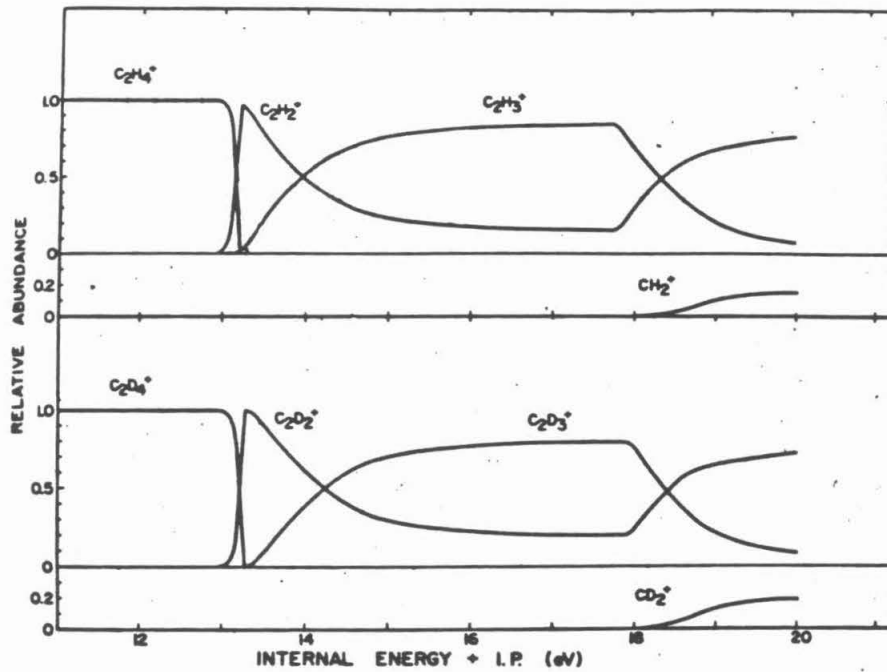
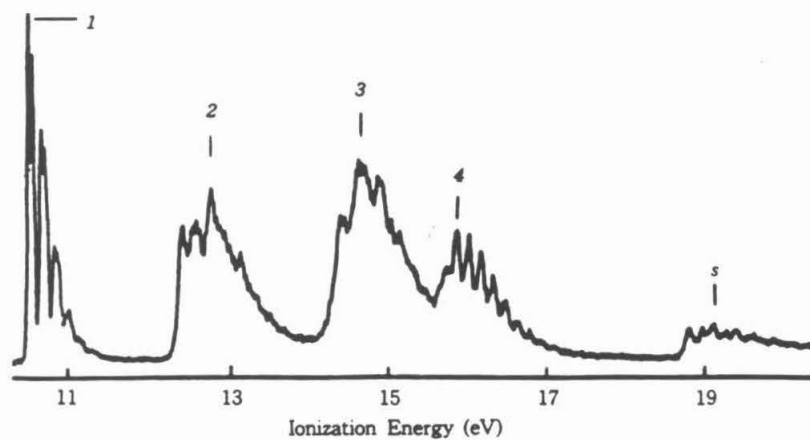
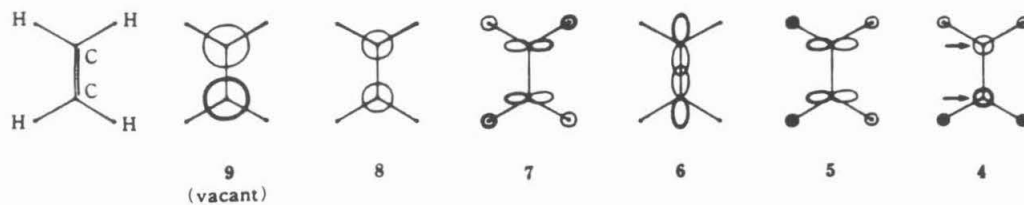
Figure 2. The PEPICO diagram for ethylene.<sup>14</sup>

Figure 3. The photoelectron spectrum for ethylene.<sup>15</sup>

Exptl. $I_p$ (eV)	SCF MO [6-31 G]		
	$-\epsilon$ (eV)	MO	Character
1	10.51	$1b_{1u}$ (8)	$\pi_{C=C}$
2	12.85	$1b_{1g}$ (7)	$\pi_{CH_2}^-$ (pseudo)
3	14.66	$3a_g$ (6)	$\sigma_{CC}$
4	15.87	$1b_{3u}$ (5)	$\pi_{CH_2}^+$ (pseudo)
19.1	21.20	$2b_{1u}$ (4)	$C_{2s}^-$



can be estimated from the PEPICO spectrum<sup>14</sup> (Figure 2) as 13.2 eV. IP' must then lie between 13.2 and 8.2 eV, which implicates  $\pi^-(C=C)$  or  $\pi(CH_2)$  electrons in the annihilation<sup>15</sup> (Figure 3).

### **Relative annihilation rates**

Competition experiments, in which two compounds of known relative concentration are exposed to the same positron beam, produce relative annihilation rates. The mass spectrum collected from the experiment is a weighted sum of the spectra from the individual PAMS experiments. A comparison of relative concentrations in the reaction region and peak heights from the TOF spectrum provide a quantitative evaluation of the relative affinity of each reagent for positrons. Many such experiments will develop a "positron reactivity ladder" from which theoretical predictions can be evaluated.

The annihilation rate is dependent on both the attachment cross section and the lifetime of the PAC with respect to dissociation back to the positron and neutral molecule. The lifetime of PACs with respect to annihilation is assumed relatively invariant, about 1 nsec. Dissociation is discouraged by the presence of many vibrational modes, which randomize the attachment energy. The lifetimes of larger, less rigid molecules should therefore be longer than those of smaller species. For very small molecules, the very short PAC dissociative lifetimes ( $\ll 1$  nsec) may prevent observation of annihilation and its products.

## Instrumental Details

The following section contains a detailed description of the positron annihilation mass spectrometer, which was designed but only partially constructed. Drawings of all parts are held by the Beauchamp group at Caltech.

### The Source Region

A 100 millicurie Co-58 radioactive source attached to a copper needle is introduced into the vacuum chamber via a solid inlet system. This inlet allows some motion of the source within the chamber, but most importantly makes it possible to rapidly position the radioactive source. Immediately after the seals are made about the inlet probe, lead shielding must be built around the source region. The source is ordered from New England Nuclear-Dupont in Massachusetts.

The Co-58 source emits positrons spontaneously, but they have an initial kinetic energy of around 500 keV, which is too high for attachment. A tungsten foil directly behind the source is used as a moderator. High-energy positrons entering the foil have a probability of about one in  $10^4$  of being spontaneously reemitted normal to the foil surface with low kinetic energy, about 5 eV. The moderator is attached to an aluminum plate connected to the moderator flange with aluminum stand-offs. There are four feedthroughs in the flange that allow biasing of the moderator. The moderator is constructed with EV parts.

The low energy positrons are guided around a 90° turn by a solenoidal field (100-200 Gauss) to lose nonmoderated particles, which go straight through the chamber walls. The solenoidal field leads to the reaction region. The solenoid has not been constructed at this time.

### **The Reaction Region**

The reaction region consists of four grids attached to an aluminum plate held from the detection flange with aluminum stand-offs. The reaction region is constructed with EV parts. The grids are Ni mesh from Buckbee-Mears. The four grids are parallel and perpendicular to the axis of the vacuum chamber. The grids, in order, are referred to as RET (retardation), P1, P2 and EXT (extraction). RET is closest to the source region; EXT is on the detection flange side. EXT should be grounded.

As the positrons encounter RET, they are slowed down if RET is not held at ground. The total electric field between P2 and RET should be large enough to stop and turn around the positrons between P1 and P2. When the positrons are turning around and have zero kinetic energy (or nearly so) is the time when we expect the attachment process to take place. Attachment, annihilation and detection of the emitted gamma ray should take place in effectively zero time, before the ion has time to escape the space between P1 and P2.

Once the gamma ray is detected with the scintillator, the electronics is triggered and very rapidly changes the biases on P1

and P2. This must also happen before the ion has time to move. The voltages between on P1 and P2 will now force the ion toward the EXT plate . The ions are then accelerated between P2 and EXT and speed toward the detector.

Typical bias voltages in the reaction region are: EXT(0,0), P2(-10,-100), P1(0,-105), where the two numbers refer to the normal and triggered biases, respectively, in volts. This example provides 100 eV ions with a potential kinetic energy spread of 5 eV. This limits the resolution of the mass spectrum, and the triggered P1-P2 difference should be minimized.

The target gas is introduced into the reaction region via a steel needle. It fits onto an adapter at the end of a copper tube that extends from the detector flange. On the outside of the flange, a Cajon adapter connects the tube to a simple, one-port inlet system with a leak valve. The target gas is aimed toward the center of the gap between P1 and P2, where the attachment is expected. There is currently no means of measuring the actual pressure in the reaction region; only the overall pressure of the vacuum chamber is known.

### **The Detector.**

The detector consists of two microchannel plates (MCPs) in a tandem, chevron configuration. The literature on MCPs is clear, and the background on their operation will not be given here. Our MCPs were purchased from the Varian Image Division. The MCP assembly, as received from Comstock, was of poor design and has been adapted. The major change is the introduction of separate assembly screws



and voltage feed screws. Also, a grounded faceplate/grid with a large opening has been introduced to accelerate the positive ions to keV energies before they strike the front MCP. This will increase their probability of detection. The faceplate is attached to the detector flange with aluminum stand-offs.

Resistors inside the vacuum chamber connected to the MCP assembly fill two functions; two limit the possible current passing through the MCPs and a third is part of a high-pass filter. The capacitor associated with the filter is outside the chamber. The resistors are of either  $10\text{M}\Omega$  or  $15\text{M}\Omega$ , from the Victoreen company. They are special glass-enclosed resistors that neither "leak" and cause noise nor have an appreciable vapor pressure.

The MCPs operate well without noticeable noise at applied voltages of at least 2300V. They are triggered by ions or electrons emitted by the ion gauge, and the gauge must be turned off when one is trying to detect ions. The ion gauge can, however, be used to "scrub" the MCPs. To scrub the plates, put about 1300V across them at  $<10^{-6}$  torr and turn on the ion gauge. The bombardment of ions cleans the plates and improves signal-to-noise. MCPs should be kept under vacuum if at all possible and if nothing else, away from humidity. MCP output is fed to an Amptek A101 preamplifier/discriminator. The best high-pass filter arrangement I could find for the signal coming off the MCP collector plate consists of: a  $10\text{M}\Omega$  resistor inside the vacuum chamber between the collector and the high-voltage input, an HV  $0.01\mu\text{F}$  capacitor outside

the flange after the feedthrough and a 10pF capacitor directly before the A101 input pin.

Eight high-voltage feedthroughs, identical to those on the moderator flange, are in the detector flange. These feedthroughs were cannibalized off an old Bendix TOF instrument. Connections between the feedthroughs and the MCP assembly and the reaction region are made with shielded coaxial cable obtained from the Electronics Shop. It has a very low vapor pressure. Pins and cables are attached by either golden Burndy pins from the Instrument Shop or custom-made connects (as on the moderator flange).

### **The Vacuum Chamber**

The vacuum chamber is constructed of nonmagnetic 304 steel with standard 4 5/8 Conflat flanges. The source region's five-way cross and the 90° elbow are standard products from MCB or Huntington. A six-inch Varian diffusion pump is attached to the main chamber through a 12-hour liquid nitrogen trap that usually lasts closer to 11 hours. Seals are made on both ends of the trap with O-rings. A roughing pump is connected to both the diff pump foreline and the source region.

A glass-enclosed ion gauge (also MCB or Huntington) with a one-inch diameter arm and a thermocouple gauge with a Varian 843 controller measure the chamber pressures. Another thermocouple gauge is on the diff pump foreline to measure the backing pressure. This gauge does not read true pressure and should be replaced.

Once the trap is filled, the system given overnight on the diff pump and the ion gauge degassed, the pressure should be down to  $1.5 \times 10^{-7}$ . Baking out the chamber will give an even lower background pressure. Be careful baking out with the MCPs.

## **The Computer**

The computer is an XT Clone with a hard disk and two floppy drives. The program that was going to be used to collect data is named PAMS and is adapted from Dave Dearden's PES program. It is written in Profort fortran. The various subroutines and Profort devices are in the PAMS directory. L.BAT is a batch file used to link all the various object files and libraries necessary to run PAMS successfully. PAMS has been through several hands before this incarnation and may seem cumbersome, but it works. As of now, it does not save data but it should not be difficult to correct this deficiency. The code listing for the main program and subroutines are attached, as are diskettes with all relevant software.

Data are collected by the computer through a Metrabyte MDB64 board in the body of the computer, which talks to the external Metrabyte MCN8 counter board (discussed under Electronics). The Metrabyte manual is relatively clear, and the Metrabyte people are willing to answer questions.

## The Electronics

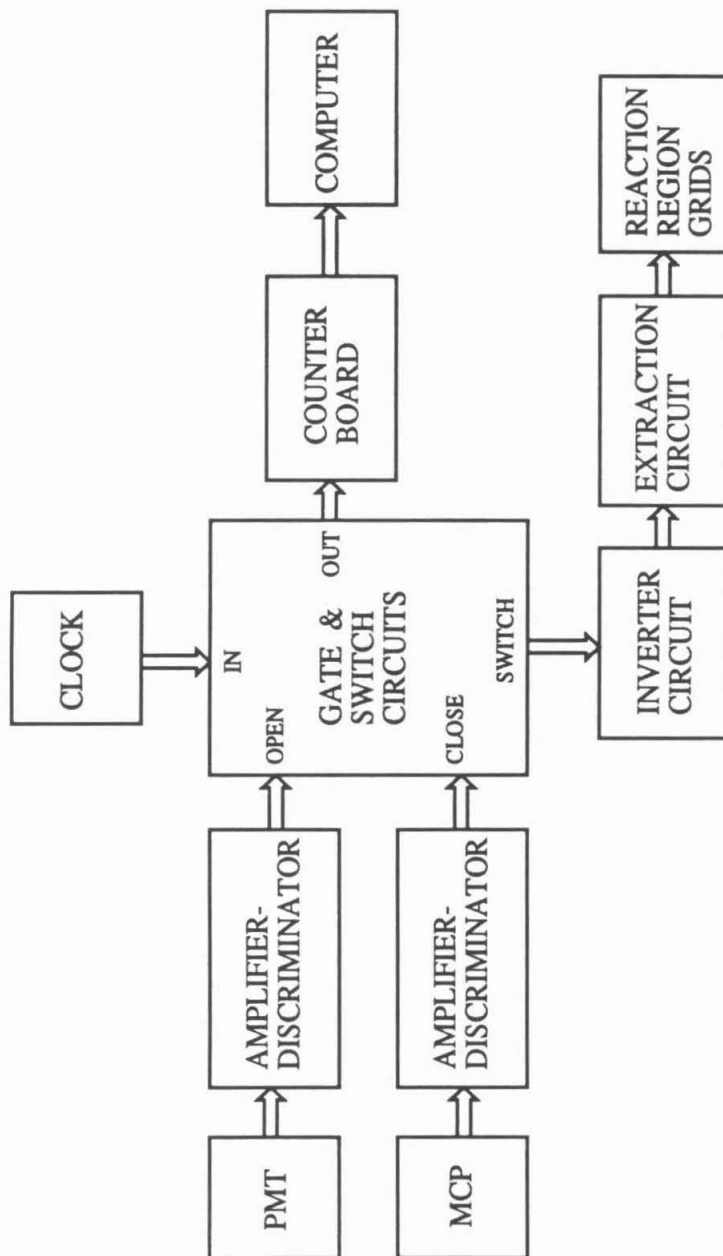
The electronics has main functions: detect annihilation events, switch the voltage on P1 and P2 and detect ions for a TOF analysis of their mass. The detection function will be discussed under Scintillator. (See flowchart, Figure 4.)

Once a gamma ray has been detected, the PMT PAD (see later) sends a 5V, 220 nsec pulse to the MCN8 BOX. The MCN8 box holds three circuits: the MCN8 board, the gate circuit (Figure 5) and an external clock. This box has three inputs: a 5V source power, the PMT input and the MCP input. The latter two come directly from the appropriate Amptek A101 Preamplifier Discriminator (PAD). The two outputs are 200  $\mu$ sec 5V pulses that are triggered by the rising edge of the PMT pulse. One output goes HI from ground to 5V and one goes LO from 5V to ground.

In the gate circuit, the PMT pulse also opens a gate that passes clock pulses through to a MCN8 counter. The clock is used to time the ion's flight down the tube and is on the same vectorboard as the rest of the circuit. Clock pulses are passed through the gate until a pulse is received from the MCP. This closes the gate. The MCP and PMT pulses are also fed into counters. The clock gate may also be closed by another pulse, from either the external clock or by a pulse from the MCN8 internal clocks.

The PAMS program proceeds as follows: Once the PMT pulse is received by its counter and read as a nonzero count by the computer, the computer looks at the MCP counter and waits for that pulse to

**Figure 4.** A flowchart describing the electronic controls of the Positron Annihilation Mass Spectrometer.



arrive. Once it is counted, the computer looks at the clock counter and records the number of clock pulses that made it to the counter. This number, multiplied by the amount of time between each pulse, provides the time of the ion's flight. Once the clock counter is read, all counters are zeroed and the sequence begins again. Thus, a TOF spectrum is collected.

The two output pulses from the MCN8 box are used to switch P1 and P2. One output (labeled SWITCH, Figure 6) passes through an inverter box (Figure 7), which switches polarity of the pulse and amplifies it with an op-amp. The inverter output passes to the extractor box. (Figure 8) The extractor box controls the voltage on P1 and P2 and is responsible for rapidly switching the voltages on the plates for as long as the input pulse lasts (i.e., 200 msec). Two trimpots (or variable resistors) in the extractor box allow one to vary the biases on P2 for maximizing resolution and signal. The extractor serves as a gate/voltage divider for another input, which may range up to about 300V. This voltage is approximately the triggered bias on P2 and therefore approximately the kinetic energy of the ion.

The PADs are Amptek A101 chips on Amptek circuitboards. The triggering threshold of the A101 is too low and must be raised by an added resistor, as described in the Amptek literature. Shielding of all inputs into the A101 is absolutely required.

Figure 5. The Gate circuit.

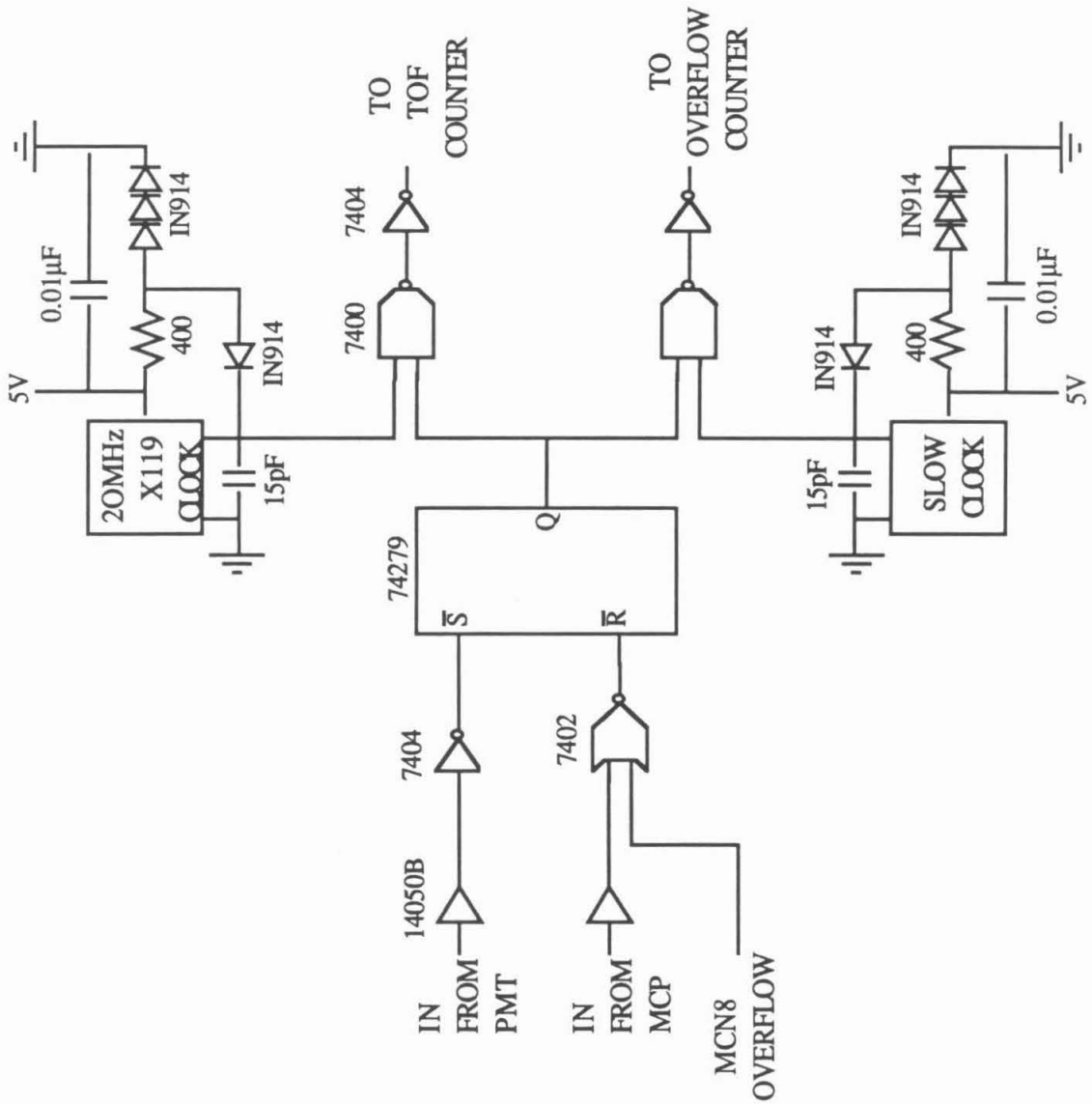
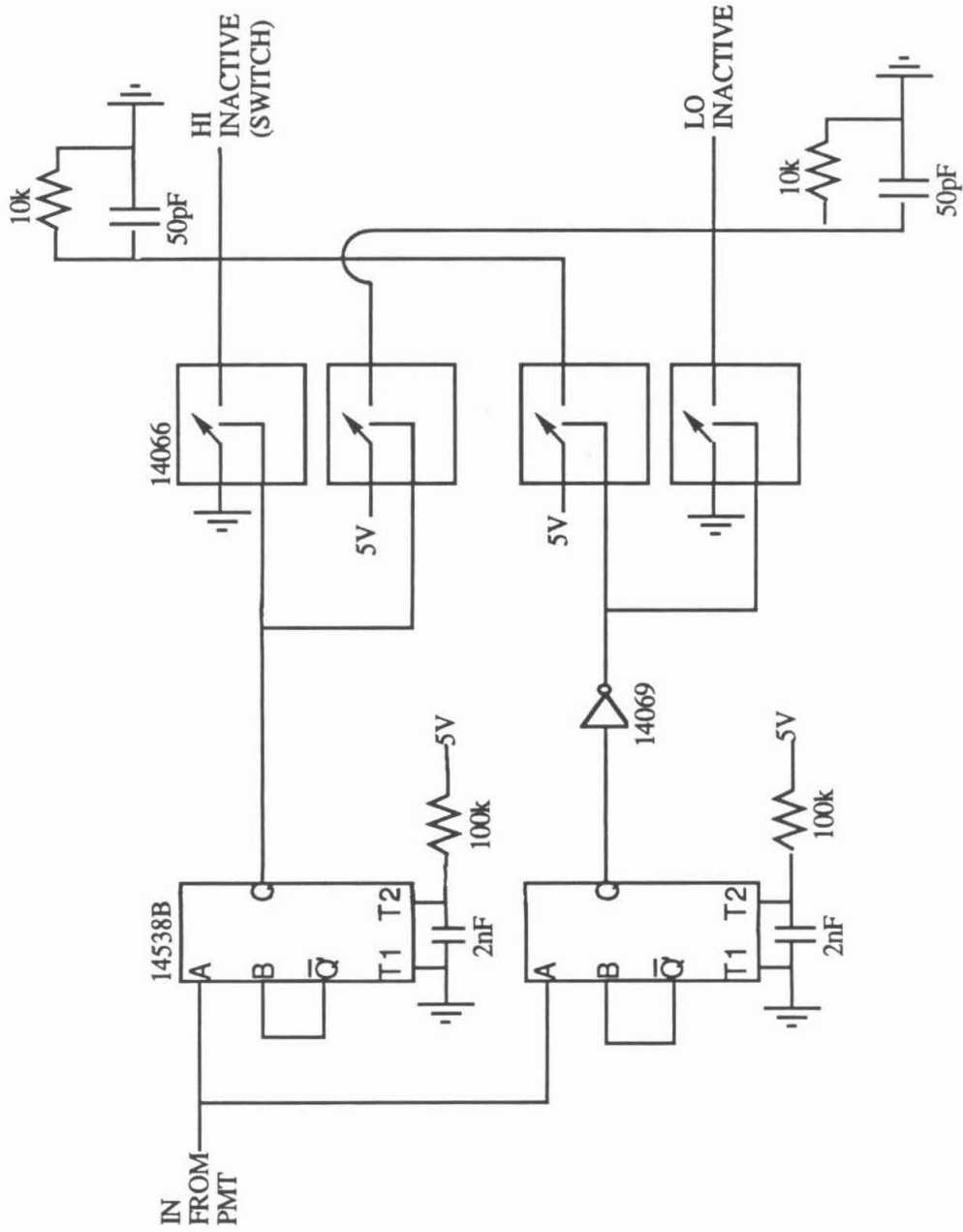
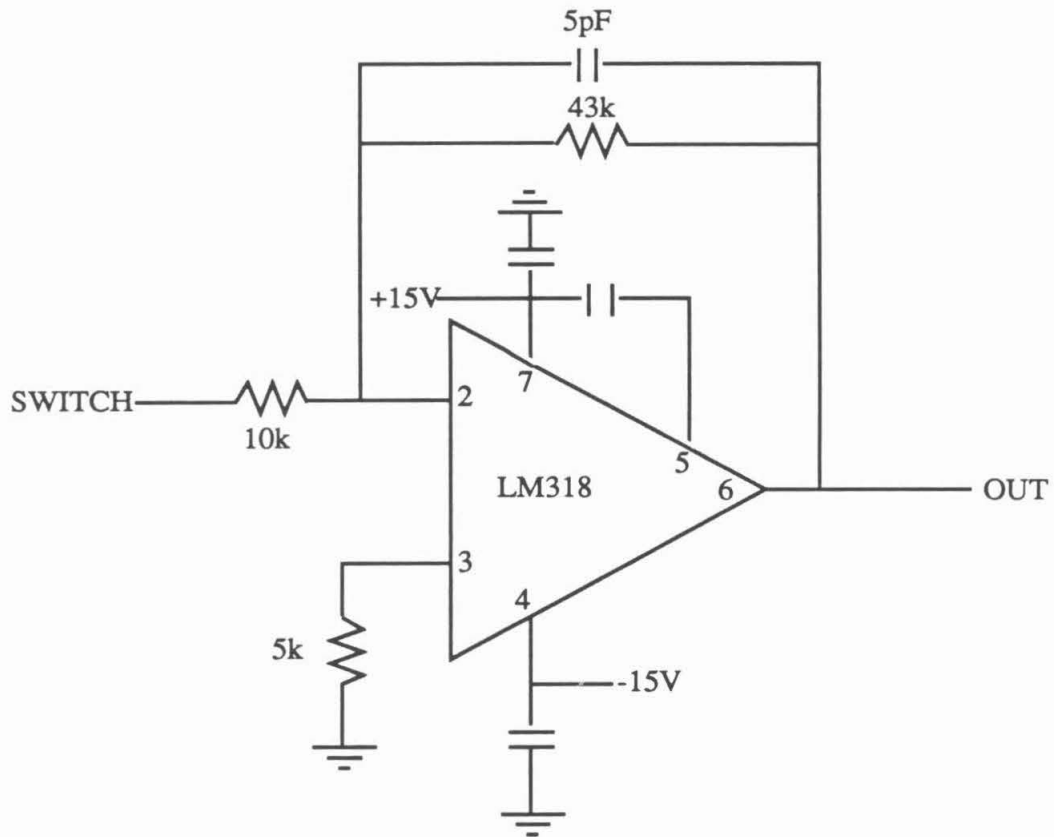


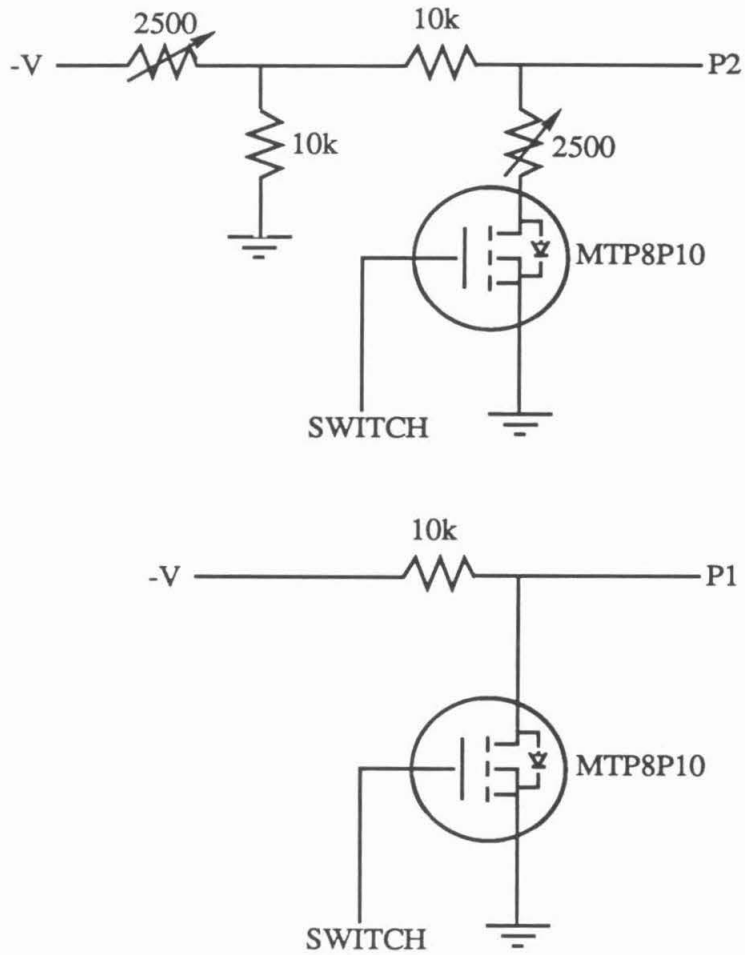
Figure 6. The Switch circuit.





**Figure 7.** The Inverter circuit.

Capacitors are  $0.1\mu\text{F}$

**Figure 8.** The Extract circuit.

For positive voltages, IRF731 or IRF732 take the place of the MTP8P10.

## The Scintillator

The gamma rays emitted during annihilation will pass through the vacuum chamber walls with high probability. Outside the chamber, a Bicron poly(methylmethacrylate) or PMMA scintillator will "collect" the photons. Scintillators are used for this purpose because as high-energy photons pass through them, they convert the photons to low-energy, visible photons, which are easily detected with a photomultiplier tube (PMT). The PMT output is passed into an Amptek A101 similarly to the MCP output.

The scintillator must be bent to wrap around the vacuum chamber. The literature or calls to Bicron will help with this. Once bent, the scintillator must be painted with high-reflectance paint supplied by Bicron, which we have. The lucite light pipe off the scintillator should not be glued directly to the PMT face, but glued to a second lucite light pipe that is already attached to the PMT housing. Bicron has supplied an optical glue for this task. It has two components; one should be in the refrigerator.

An old EMI 6256S PMT fits into the PMT housing and should be up to the job.

Of the positron annihilation mass spectrometer project, the following were completed in this work:

1. Design of general experimental scheme
2. Design and construction of vacuum chamber and internal components
3. Design, construction and testing of electronic circuits
4. Adaptation of software
5. Adaptation, testing and maximization of MCPs

To Be Completed:

1. Construction and testing of solenoid
2. Testing and maximization of scintillator and PMT
3. Demonstration of mass spectrum collection using an electron beam in the reaction region
4. Simulation of positron attachment with electrons originating from an electron beam in the source region
5. Construction of shielding
6. Positron attachment experiments
7. Data analysis

**References**

- (1) Goldanskii, V. I.; Firsov, V. G. *Annu. Rev. Phys.* **1971**, *22*, 209.
- (2) Ache, H. J. *Positronium and Muonium Chemistry*; Ache, H. J.; 1979; p. 1.
- (3) Ache, H. J. *Agnew. Chem. Internat. Edit.* **1972**, *11*, 179.
- (4) Rytso, K.; Rantapuska, K.; Hautajarvi, P. *Positron Annihilation*; Coleman, P. G.; 1982; p. 111.
- (5) McNutt, J. D.; Sharma, S. C. *Positronium and Muonium Chemistry*; Ache, H. J.; 1979; p. 137.
- (6) Graf, G.; Tsandel, E. D. H.; MacMahon, P. L.; Glass, J. C. *Positronium and Muonium Chemistry*; Ache, H. J.; 1979; p. 67.
- (7) Schrader, D. M. *Positronium and Muonium Chemistry*; Ache, H. J.; 1979; p. 203.
- (8) Surko, C. M.; Passner, A.; Leventhal, M.; Wysocki, F. J. *Phys. Rev. Lett.* **1988**, *61*, 1831.
- (9) Mills, A. P., Jr. *Positron Solid-State Physics*; 1983; pp 431 .
- (10) Britton, D. T.; Rice-Evans, P. C.; Evans, J. H. *Nucl. Inst. Meth. Phys. Res.* **1985**, *B12*, 426.
- (11) Woodin, R. L.; Foster, M. S.; Beauchamp, J. L. *J. Chem. Phys.* **1980**, *72*, 4223.
- (12) Chutjian, A.; Alajajian, S. H. *Phys. Rev. A* **1985**, *31*, 2885.

- (13) Karataev, V. I.; Mamyrin, B. A.; Shmikk, D. V. *Sov. Phys. Tech. Phys.* **1972**, *16*, 1177.
- (14) Stockbauer, R.; Inghram, M. G. *J. Chem. Phys.* **1975**, *62*, 4862.
- (15) Kimura, K. *Handbook of HeI Photoelectron Spectra of Fundamental Organic Molecules*; 1981; pp 57 .